Quantum quench phase diagrams of an *s*-wave BCS-BEC condensate

E. A. Yuzbashyan,[1] M. Dzero,[2] V. Gurarie,[3] and M. S. Foster[1,4]

[1]*Center for Materials Theory, Rutgers University, Piscataway, New Jersey 08854, USA*

[2]*Department of Physics, Kent State University, Kent, Ohio 44240, USA*

[3]*Department of Physics, University of Colorado, Boulder, Colorado 80309, USA*

[4]*Department of Physics and Astronomy, Rice University, Houston, Texas 7700, USA*

We study the dynamic response of an *s*-wave BCS-BEC (atomic-molecular) condensate to detuning quenches within the two-channel model beyond the weak-coupling BCS limit. At long times after the quench, the condensate ends up in one of three main asymptotic states (nonequilibrium phases), which are qualitatively similar to those in other fermionic condensates defined by a global complex order parameter. In phase I the amplitude of the order parameter vanishes as a power law, in phase II it goes to a nonzero constant, and in phase III it oscillates persistently. We construct exact quench phase diagrams that predict the asymptotic state (including the many-body wave function) depending on the initial and final detunings and on the Feshbach resonance width. Outside of the weak-coupling regime, both the mechanism and the time dependence of the relaxation of the amplitude of the order parameter in phases I and II are modified. Also, quenches from arbitrarily weak initial to sufficiently strong final coupling do not produce persistent oscillations in contrast to the behavior in the BCS regime. The most remarkable feature of coherent condensate dynamics in various fermion superfluids is an effective reduction in the number of dynamic degrees of freedom as the evolution time goes to infinity. As a result, the long-time dynamics can be fully described in terms of just a few new collective dynamical variables governed by the same Hamiltonian only with "renormalized" parameters. Combining this feature with the integrability of the underlying (e.g., the two-channel) model, we develop and consistently present a general method that explicitly obtains the exact asymptotic state of the system.

PACS number(s): 67.85.De, 34.90.+q, 74.40.Gh

I. INTRODUCTION

The problem of a superconductor driven out of equilibrium by a sudden perturbation goes back many decades. Early studies [1–6] addressed small deviations from equilibrium using linearized equations of motion. An important result was obtained by Volkov and Kogan [3], who discovered a power law oscillatory attenuation of the Bardeen-Cooper-Schriffer (BCS) order parameter for nonequilibrium initial conditions close to the superconducting ground state.

In the past decade it was realized that even large deviations from equilibrium are within the reach of appropriate theoretical methods. Recent studies, motivated by experiments in cold atomic fermions, focused on quantum quenches, nonequilibrium conditions created by a sudden change in the superconducting coupling strength. Barankov *et al.* [7], in a paper that set off a surge of modern research in this long-standing problem [8–24] in the context of quantum gases, found that for initial conditions close to the unstable normal state, the order parameter exhibits large anharmonic periodic oscillations.

Subsequently, Yuzbashyan *et al.* [16] developed an analytical method to predict the state of the system at large times based on the integrability of the underlying BCS model. This work extended Volkov and Kogan's result to large deviations from equilibrium and showed that the oscillation frequency is twice the *nonequilibrium* asymptotic value of the order parameter, a conclusion confirmed by recent terahertz pump pulse experiments in $Nb_{1-x}Ti_xN$ films [25,26]. Later studies [17,18] mapped out the full quantum quench "phase diagram" for weakly coupled *s*-wave BCS superconductors finding that three distinct regimes occur depending on the

strength of the quench: Volkov-and-Kogan-like behavior, persistent oscillations, and exponential vanishing of the order parameter. Most recent research [27–30] fueled by experimental breakthroughs [25,31,32] investigates nonadiabatic dynamics of *s*-wave BCS superconductors in response to fast electromagnetic perturbations. Closely related subjects developing in parallel are exciton dynamics [33], collective neutrino oscillations [34,35], quenched *p*-wave superfluids [36,37], etc.

Most existing work addressed the dynamics in the BCS regime and, in particular, quenches such that the interaction strength is weak both before and after the quench. This was so that the system always remains in the BCS regime, since the physics of the condensate beyond this regime was not sufficiently well understood. However, a superfluid made up of cold atoms can be as well quenched from the BCS to the Bose-Einstein condensation (BEC) regime or within the BEC regime. With few exceptions [23,36,37], these types of quenches are not adequately studied in the existing literature.

Our paper aims to close this gap and analyze all possible interaction quenches throughout the BCS-BEC crossover in a paired superfluid, including BCS-to-BEC, BEC-to-BCS, and BEC-to-BEC quenches. We fully determine the steady state of the system at large times after the quench: the asymptote of the order parameter, as well as the approach to the asymptote; the many-body wave function; and certain observables, such as the radio-frequency absorption spectrum and the momentum distribution. In the BCS limit, we recover previous results. Beyond this limit the dynamics is quantitatively and sometimes qualitatively different. For example, the power law in the Volkov-and-Kogan-like attenuation changes in the BEC regime, exponential vanishing is replaced with a power law, and persistent oscillations first change their form and then

disappear altogether after a certain threshold for quenches from any initial (e.g., arbitrarily weak) to sufficiently strong final coupling. We believe an experimental verification of the predictions of this work is within a reach of current experiments in cold atomic systems.

The long-time dynamics can be determined explicitly due to a remarkable reduction mechanism at work, so that at large times the system is governed by an effective interacting Hamiltonian with just a few classical collective spin or oscillator degrees of freedom. In a sense, the system "flows in time" to a much simpler Hamiltonian. This observation, combined with the integrability of the original Hamiltonian (see below), lead to a method originally proposed in Ref. [16] for obtaining the long-time asymptote (steady state) of integrable Hamiltonian dynamics in the continuum (thermodynamic) limit. Here we improve this method as well as provide its comprehensive and self-contained review including many previously unpublished results and steps. We do so in the context of the s-wave BCS (one channel) and inhomogeneous Dicke (two-channel) models, but with some modifications the same method also applies to all known integrable pairing models [38–44], such as $p + ip$ superfluids [36,37], integrable fermion or boson pairing models with nonuniform interactions [45,46], Gaudin magnets (central spin models), and potentially can be extended to a much broader class of integrable nonlinear equations.

The purpose of this paper is therefore twofold. First, it serves as an encyclopedia of quantitatively exact predictions, new and old, for the quench dynamics of real s-wave BCS-BEC condensates in two and three spatial dimensions. Readers primarily interested in this aspect of our work will find most of the relevant information in the Introduction, Sec. VII, and Conclusion. In particular, Sec. I D concisely summarizes our main results and provides a guide to other sections that contain further results and details. Our second goal is to develop and thoroughly review a method for determining the far-from-equilibrium dynamics in a certain class of integrable models. We refer readers interested in learning about the method to Sec. II. Also, from this viewpoint, Secs. III and IV should be considered as applications of our approach and Sec. V as a related development.

A major experimental breakthrough with ultracold atoms was achieved in 2004, when they were used to emulate s-wave superconductors with an interaction strength that can be varied at will [47,48]. The experimental control parameter is the detuning ω, the binding energy of a two-fermion bound state (molecule). This parameter determines the strength of the effective interaction between fermions and can be varied both slowly and abruptly with the help of a Feshbach resonance. Moreover, it is straightforward to make time-resolved measurements of the subsequent evolution of the system. Thus, cold atoms provide a natural platform to study quenches in superfluids and in a variety of other setups [49,50].

At large ω we have fermionic atoms with weak effective attraction that form a paired superfluid, an analog of the superconducting state of electrons in a metal. As ω is decreased, the atoms pair up into bosonic molecules which then Bose condense. It was argued for a long time that both the paired superfluid and the Bose-condensed molecules are in the same phase of the fermionic gas, named the BCS-BEC condensate [51,52]. As ω decreases, the strength of the

effective interaction (coupling) between fermions increases from weak to strong and the system undergoes a BCS-BEC crossover. At $\omega \gg 2\varepsilon_F$, where ε_F is the Fermi energy, the system is deep in the BCS regime, while at large negative ω it is deep in the BEC regime. It is not known how to recreate such a crossover in a conventional solid-state superconductor since the interaction strength cannot be easily adjusted.

In a quantum quench setup the system is prepared in the ground state at a detuning ω_i. At $t = 0$ the detuning is suddenly changed, $\omega_i \rightarrow \omega_f$. At $t > 0$ the system evolves with a new Hamiltonian $H(\omega_f)$. The main goal is to determine the state of the system at large times, $t \rightarrow \infty$.

A. Models and approximations

We consider two closely related models in this paper in both two and three dimensions. The first one is the well-known two-channel model that describes two species of fermionic atoms interacting via an s-wave Feshbach resonance

$$\hat{H}_{2\mathrm{ch}} = \sum_{\mathbf{p},\sigma=\uparrow,\downarrow} \epsilon_{\mathbf{p}} \hat{a}_{\mathbf{p}\sigma}^{\dagger} \hat{a}_{\mathbf{p}\sigma} + \sum_{\mathbf{q}} \left(\omega + \frac{q^2}{4m} \right) \hat{b}_{\mathbf{q}}^{\dagger} \hat{b}_{\mathbf{q}}$$
$$+ g \sum_{\mathbf{pq}} \left(\hat{b}_{\mathbf{q}}^{\dagger} \hat{a}_{\frac{\mathbf{q}}{2}+\mathbf{p},\uparrow} \hat{a}_{\frac{\mathbf{q}}{2}-\mathbf{p},\downarrow} + \hat{b}_{\mathbf{q}} \hat{a}_{\frac{\mathbf{q}}{2}-\mathbf{p},\downarrow}^{\dagger} \hat{a}_{\frac{\mathbf{q}}{2}+\mathbf{p},\uparrow}^{\dagger} \right). \quad (1.1)$$

It is convenient to think of the two types of fermions of mass m and energy $\epsilon_{\mathbf{p}} = p^2/2m$ as spin-up and spin-down, created and annihilated by operators $\hat{a}_{\mathbf{p}\sigma}^{\dagger}$ and $\hat{a}_{\mathbf{p}\sigma}$. The interaction term converts two fermions into a bosonic molecule and vice versa at a rate controlled by the parameter g. Molecules are created and annihilated by $\hat{b}_{\mathbf{q}}^{\dagger}$ and $\hat{b}_{\mathbf{q}}$ and have a binding energy ω. The parameter g is set by the type of atoms and the specifics of a particular Feshbach resonance and cannot be changed in a single experiment; ω can be varied at will by varying the magnitude of the magnetic field applied during the experiment. This model describes atoms in the BCS regime when ω is large, which undergo a crossover to the BEC regime as ω is decreased.

A parameter with dimensions of energy important for our analysis of this model is $g^2 \nu_F$, where ν_F is the bulk density of states (proportional to the total volume) at the Fermi energy ϵ_F. A well-known parameter,

$$\gamma = \frac{g^2 \nu_F}{\epsilon_F}, \quad (1.2)$$

controls whether the resonance is narrow $\gamma \ll 1$ or broad $\gamma \gg 1$. This parameter is the dimensionless atom-molecule interaction strength or, equivalently, the resonance width.

A very convenient feature of the narrow resonance is that, regardless of the regime of the system, controlled by ω, the system is adequately described with mean-field theory [53]. This is already clear from the form of the Hamiltonian: Small γ implies that interaction g is small.

Broad resonances, on the other hand, correspond to large g. Under those conditions it is possible to integrate out the molecules $\hat{b}_{\mathbf{q}}$ to arrive at a simpler Hamiltonian [53] describing fermions interacting via a short-range attractive interaction

with variable strength,

$$\hat{H}_{1\text{ch}} = \sum_{\mathbf{p},\sigma=\uparrow,\downarrow} \epsilon_{\mathbf{p}} \hat{a}^{\dagger}_{\mathbf{p}\sigma} \hat{a}_{\mathbf{p}\sigma}$$
$$-\frac{\lambda}{\nu_F} \sum_{\mathbf{p}\mathbf{p}'\mathbf{q}} \hat{a}^{\dagger}_{\frac{\mathbf{q}}{2}-\mathbf{p},\downarrow} \hat{a}^{\dagger}_{\frac{\mathbf{q}}{2}+\mathbf{p},\uparrow} \hat{a}_{\frac{\mathbf{q}}{2}+\mathbf{p}',\uparrow} \hat{a}_{\frac{\mathbf{q}}{2}-\mathbf{p}',\downarrow}, \quad (1.3)$$

where

$$\lambda = \frac{g^2 \nu_F}{\omega} = \frac{\gamma \varepsilon_F}{\omega}. \quad (1.4)$$

This is the single (one)-channel, or BCS, model, which is the second model we analyze in this paper. It also describes the BCS-BEC crossover as ω is decreased (λ is increased). However, while in the BCS and (to some extent) in the BEC regimes corresponding to large and small λ, respectively, mean-field theory holds in equilibrium, for the intermediate values of λ (neither large nor small) the mean-field theory is known to break down. A special value of λ in the middle of the regime unaccessible to the mean-field theory already in equilibrium is called the unitary point. It corresponds to the interaction strength where molecules are about to be formed. Noncondensed molecules play an important role in the description of the unitary point and its special properties are a subject of many studies in the literature [52,54].

Just as in earlier work on the far-from-equilibrium superconductivity, we analyze the quench dynamics in the mean-field approximation where no molecules are transferred into or out of the BCS-BEC condensate after the quench; i.e., the dynamics of the condensate is decoupled from the noncondensed modes. We analyze the validity of this approximation for nonequilibrium steady states produced by quenches in the two-channel model in Appendix A. We find that the situation is similar to that in equilibrium [53]. In the case of a broad Feshbach resonance, mean field is expected to hold for quenches where both initial and final detunings are far from the unitary point. A quench into the unitary point is a very interesting problem addressed by some publications before [55], but the method we employ here is not applicable to this case.

Nevertheless, a variety of quenches are still accessible to our description even when the resonance is broad, including BCS $\rightarrow$ BCS, BCS $\rightarrow$ BEC, BEC $\rightarrow$ BCS, and BEC $\rightarrow$ BEC, where BCS and BEC stand for the value of the interaction strength far weaker or far stronger than that at the unitary point. In the case of BCS-BEC superfluids formed with interactions generated by narrow Feshbach resonances, the mean-field theory treatment is valid even at the threshold of the formation of the bound state and throughout the BCS-BEC crossover. Here we consider quenches of the detuning ω for both narrow and broad resonances within the mean field. Note that in the case of the one-channel model we expect the mean field on the BEC side to be valid only in the far BEC limit where the ground state essentially consists of noninteracting Bose-condensed molecules [56].

In the mean-field treatment the condensate is described by the $\mathbf{q} = 0$ part of the Hamiltonian (1.1), which is decoupled from $\mathbf{q} \neq 0$ terms in this approximation. The Hamiltonian

therefore becomes

$$\hat{H}_{2\text{ch}} = \sum_{\mathbf{p}} 2\epsilon_{\mathbf{p}} \hat{s}^z_{\mathbf{p}} + \omega \hat{b}^{\dagger} \hat{b} + g \sum_{\mathbf{p}} (\hat{b}^{\dagger} \hat{s}^-_{\mathbf{p}} + \hat{s}^+_{\mathbf{p}} \hat{b}), \quad (1.5)$$

where

$$\hat{s}^-_{\mathbf{p}} = \hat{a}_{\mathbf{p}\uparrow} \hat{a}_{-\mathbf{p}\downarrow}, \quad \hat{s}^z_{\mathbf{p}} = \frac{1}{2}\big(\hat{a}^{\dagger}_{\mathbf{p}\uparrow} \hat{a}_{\mathbf{p}\uparrow} + \hat{a}^{\dagger}_{-\mathbf{p}\downarrow} \hat{a}_{-\mathbf{p}\downarrow} - 1\big) \quad (1.6)$$

are Anderson pseudospin-$\frac{1}{2}$ operators [1] and

$$\hat{b} = \hat{b}_{\mathbf{q}=0}.$$

Hamiltonian (1.5) is also known as inhomogeneous Dicke or Tavis-Cummings model. In a quantum quench problem we need to solve Heisenberg equations of motion for this Hamiltonian for given initial conditions

$$\frac{d\hat{\vec{s}}_{\mathbf{p}}}{dt} = \hat{\vec{B}}_{\mathbf{p}} \times \hat{\vec{s}}_{\mathbf{p}}, \quad \frac{d\hat{b}}{dt} = -i\omega \hat{b} - ig\hat{J}_{-},$$
$$\hat{\vec{J}} = \sum_{\mathbf{p}} \hat{\vec{s}}_{\mathbf{p}}, \quad \hat{\vec{B}}_{\mathbf{p}} = 2g\hat{\vec{b}} + 2\epsilon_{\mathbf{p}}\hat{\mathbf{z}}, \quad (1.7)$$

where $\hat{\vec{b}} = \hat{b}_x \hat{\mathbf{x}} + \hat{b}_y \hat{\mathbf{y}}$, $\hat{b}_x$, and $-\hat{b}_y$ are Hermitian and anti-Hermitian parts of the operator $\hat{b} = \hat{b}_x - i\hat{b}_y$, and $\hat{\mathbf{x}}, \hat{\mathbf{y}}, \hat{\mathbf{z}}$ are coordinate unit vectors.

The second step in the mean-field treatment of the two-channel model is to replace Heisenberg operator $\hat{b}(t)$ in the first equation of motion in Eq. (1.7) with its time-dependent quantum-mechanical average, $\hat{b}(t) \rightarrow \langle \hat{b}(t) \rangle \equiv b(t)$, which is expected to be exact in thermodynamic limit as long as the $\mathbf{q} = 0$ state is macroscopically occupied at all times. This replacement can be shown to be exact in equilibrium using the exact solution for the spectrum of the inhomogeneous Dicke model [38,57] and numerically for the time-dependent problem [58]. Upon this replacement equations of motion become linear in operators and taking their quantum-mechanical average, we obtain

$$\dot{\vec{s}}_{\mathbf{p}} = \vec{B}_{\mathbf{p}} \times \vec{s}_{\mathbf{p}}, \quad \dot{b} = -i\omega b - ig J_{-},$$
$$\vec{J} = \sum_{\mathbf{p}} \vec{s}_{\mathbf{p}}, \quad \vec{B}_{\mathbf{p}} = 2g\vec{b} + 2\epsilon_{\mathbf{p}}\hat{\mathbf{z}}, \quad (1.8)$$

where $\vec{s}_{\mathbf{p}} = \langle \hat{\vec{s}}_{\mathbf{p}} \rangle$. These are Hamiltonian equations of motion for a classical Hamiltonian,

$$H_{2\text{ch}} = \sum_{\mathbf{p}} 2\epsilon_{\mathbf{p}} s^z_{\mathbf{p}} + \omega \bar{b} b + g \sum_{\mathbf{p}} (\bar{b} s^-_{\mathbf{p}} + b s^+_{\mathbf{p}}), \quad (1.9)$$

which describes a set of angular momenta (classical spins or vectors) coupled to a harmonic oscillator. Here, $\bar{b}$ denotes the complex conjugate of b. These dynamical variables obey the Poisson brackets

$$\big\{s^a_{\mathbf{p}}, s^b_{\mathbf{k}}\big\} = -\varepsilon_{abc} \delta_{\mathbf{p}\mathbf{k}} s^c_{\mathbf{p}}, \quad \{b, \bar{b}\} = i, \quad (1.10)$$

where a, b, and c stand for spatial indicies x, y, and z.

Similar steps in the case of the single-channel model (1.3) lead to a classical spin Hamiltonian,

$$H_{1\text{ch}} = \sum_{\mathbf{p}} 2\epsilon_{\mathbf{p}} s^z_{\mathbf{p}} - \frac{\lambda}{\nu_F} \sum_{\mathbf{p},\mathbf{p}'} s^-_{\mathbf{p}} s^+_{\mathbf{p}'}, \quad (1.11)$$

together with the corresponding equations of motion.

An important characteristic of the system both in and out of equilibrium is the superfluid order parameter or the gap function defined in the two-channel model as

$$\Delta(t) = -g\langle\hat{b}(t)\rangle = -gb(t) \equiv \Delta_x(t) - i\Delta_y(t). \quad (1.12)$$

In the one-channel limit, this expression turns into

$$\Delta_{1\text{ch}}(t) = \frac{\lambda}{\nu_F}\sum_{\mathbf{p}}\langle\hat{a}_{\mathbf{p}\uparrow}(t)\hat{a}_{-\mathbf{p}\downarrow}(t)\rangle = \frac{\lambda}{\nu_F}\sum_{\mathbf{p}}s_{\mathbf{p}}^-. \quad (1.13)$$

The magnitude $|\Delta(t)|$ of the order parameter is known as the Higgs or amplitude mode for its similarity with the Higgs boson [20,59] and its time-dependent phase represents a Goldstone mode. Note, however, that out of equilibrium the gap function does not entirely determine the state of the system. It specifies the effective magnetic field acting on each spin according to Eq. (1.8), but there is still a certain freedom in how the spin moves in this field. For example, even for a constant field the spin can precess around it, making an arbitrary constant angle with its direction.

In the above models we took a free single-particle spectrum, $\varepsilon_{\mathbf{p}} = p^2/2m$, and labeled states with momenta $\mathbf{p}$. This choice is not essential for our analysis. We can as well consider an arbitrary spectrum ε_i. The pairing is then between pairs of time-reversed states [60,61]; see also the first two pages in Ref. [13] for more details. For example, in Hamiltonian (1.5) this results in relabeling $\hat{\vec{s}}_{\mathbf{p}} \rightarrow \hat{\vec{s}}_i$, $\hat{a}_{\mathbf{p}\uparrow}\hat{a}_{-\mathbf{p}\downarrow} \rightarrow \hat{a}_{i\uparrow}\hat{a}_{i\downarrow}$, $\hat{a}_{\mathbf{p}\uparrow}^\dagger\hat{a}_{\mathbf{p}\uparrow} \rightarrow \hat{a}_{i\uparrow}^\dagger\hat{a}_{i\uparrow}$, etc., where the state $|i\downarrow\rangle$ is the time-reversed counterpart of $|i\uparrow\rangle$. Our results below depend only on the density of the single-particle states $\nu(\varepsilon)$ in the continuum limit regardless of whether these states are characterized by momenta $\mathbf{p}$ or any other set of quantum numbers i.

B. Ground state

In the ground state

$$\Delta(t) = \Delta_0 e^{-2i\mu t}, \quad (1.14)$$

where the magnitude Δ_0 is time independent. Apart from an overall rotation about the z axis with frequency 2μ, the ground state is a static solution of the equations of motion that minimizes $H_{2\text{ch}}$. The minimum is achieved when each spin is directed against its effective magnetic field, i.e.,

$$s_{\mathbf{p}}^- = \frac{\Delta_0 e^{-2i\mu t}}{2E(\varepsilon_{\mathbf{p}};\Delta_0,\mu)}, \quad s_{\mathbf{p}}^z = -\frac{\varepsilon_{\mathbf{p}} - \mu}{2E(\varepsilon_{\mathbf{p}};\Delta_0,\mu)}, \quad (1.15)$$

where

$$E(\varepsilon;\Delta,\mu) \equiv \sqrt{(\varepsilon - \mu)^2 + \Delta^2}. \quad (1.16)$$

Note that the length of the spin $s_{\mathbf{p}} = 1/2$. This is because the ground state is a tensor product of single spin-$\frac{1}{2}$ wave functions and $\vec{s}_{\mathbf{p}} = \langle\hat{\vec{s}}_{\mathbf{p}}\rangle$.

The equation of motion (1.8) for b yields

$$|J_-| = \frac{(\omega - 2\mu)\Delta_0}{g^2}, \quad (1.17)$$

which implies a self-consistency equation for Δ_0

$$\frac{(\omega - 2\mu)}{g^2} = \sum_{\mathbf{p}}\frac{1}{2E(\varepsilon_{\mathbf{p}};\Delta_0,\mu)}. \quad (1.18)$$

Further, the Hamiltonian (1.9) conserves

$$n = \bar{b}b + \sum_{\mathbf{p}}\left(s_{\mathbf{p}}^z + \frac{1}{2}\right), \quad (1.19)$$

which is the average total number of bosons and fermion pairs. This number is related to Δ_0 and the chemical potential μ as

$$2n = \frac{2\Delta_0^2}{g^2} + \sum_{\mathbf{p}}\left[1 - \frac{\varepsilon_{\mathbf{p}} - \mu}{E(\varepsilon_{\mathbf{p}};\Delta_0,\mu)}\right]. \quad (1.20)$$

The Fermi energy ε_F is the chemical potential of the fermionic atoms at zero temperature in the absence of any interaction, when only fermions are present. It provides an overall energy scale and it is convenient to measure all energies in units of the Fermi energy. Thus, from now on, we set everywhere below

$$\varepsilon_F = 1. \quad (1.21)$$

Below we often switch from discrete to continuum (thermodynamic limit) formulations. In the former version, there are N discrete single-particle energy levels $\varepsilon_{\mathbf{p}}$ with certain degeneracy each. Any quantity $A_{\mathbf{p}}$ we consider in this paper depends on $\mathbf{p}$ only through $\varepsilon_{\mathbf{p}}$, $A_{\mathbf{p}} = A(\varepsilon_{\mathbf{p}})$. For example, all spins $\vec{s}_{\mathbf{p}}$ on a degenerate level $\varepsilon_{\mathbf{p}}$ are parallel at all times and effectively merge into a single vector. There are N such vectors, so we count N distinct classical spins.

In thermodynamic limit, energies $\varepsilon_{\mathbf{p}}$ form a continuum on the positive real axis, i.e., are described by a continuous variable ε with a density of states $\nu(\varepsilon)$ that depends on the dimensionality of the problem

$$\nu(\varepsilon) = \nu_F f(\varepsilon), \quad (1.22)$$

where ν_F is the *bulk* density of states (proportional to the system volume) at the Fermi energy, $f(\varepsilon) = 1$ in two dimensions (2D), and $f(\varepsilon) = \sqrt{\varepsilon}$ in 3D. Summations over $\mathbf{p}$ turn into integrations,

$$\sum_{\mathbf{p}} A_{\mathbf{p}} \rightarrow \nu_F\int_0^\infty A(\varepsilon)f(\varepsilon)d\varepsilon. \quad (1.23)$$

With only fermions present, the total particle number is

$$2n = \int_0^1 2\nu(\varepsilon)d\varepsilon = \frac{4}{d}\nu_F, \quad (1.24)$$

where $d = 2,3$ is the number of spatial dimensions. Interaction redistributes this number between fermions and bosons as in Eq. (1.20). Combining Eqs. (1.20) and (1.24) and taking the continuum limit, we obtain

$$\frac{4}{d} = \frac{2\Delta_0^2}{\gamma} + \int_0^\infty\left[1 - \frac{\varepsilon - \mu}{\sqrt{(\varepsilon - \mu)^2 + \Delta_0^2}}\right]f(\varepsilon)d\varepsilon, \quad (1.25)$$

where γ is the dimensionless resonance width defined in Eq. (1.2).

Similarly, Eq. (1.18) becomes in the thermodynamic limit

$$\frac{2\omega - 4\mu}{\gamma} = \int_0^{\varepsilon_\Lambda}\frac{f(\varepsilon)d\varepsilon}{\sqrt{(\varepsilon - \mu)^2 + \Delta_0^2}}, \quad (1.26)$$
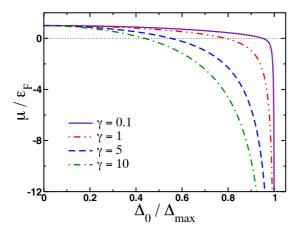
FIG. 1. (Color online) Ground-state chemical potential μ for the two-channel model in 3D in units of the Fermi energy ε_F as a function of the ground-state gap Δ_0 for various resonance width γ. $\mu(\Delta_0)$ is calculated from Eqs. (1.25) and (1.26). Note that in the two-channel model Δ_0 is bounded from above by Δ_{max}.

where ε_Λ is the high-energy cutoff. In 3D it can be eliminated by an additive renormalization of the detuning ω; see, e.g., Ref. [53]. This, however, does not affect our results for the quench dynamics as they depend on the difference between the initial and final values of the detuning.

Equations (1.25) and (1.26) contain two independent parameters not counting the cutoff. For example, we can choose γ and ω and determine μ and Δ_0 from these equations, or choose γ and Δ_0 and determine μ and ω etc.; see Fig. 1 for a plot of $\mu(\Delta_0)$ for various γ in 3D. Note also that $\Delta_0^2 = g^2 \bar{b}b$ is proportional to the number of bosons and is therefore limited by the total number of particles. Equation (1.25) implies

$$\Delta_0 \leqslant \sqrt{\frac{2\gamma}{d}} = \Delta_{max}. \qquad (1.27)$$

C. Quench setup and initial conditions

In a quantum quench setup we prepare the system in a ground state at a certain detuning ω_i; i.e., the initial state is

$$s_{\mathbf{p}}^-(t=0) = \frac{\Delta_{0i}}{2E(\varepsilon_{\mathbf{p}}; \Delta_{0i}, \mu_i)},$$
$$\qquad\qquad (1.28)$$
$$s_{\mathbf{p}}^z(t=0) = -\frac{\varepsilon_{\mathbf{p}} - \mu_i}{2E(\varepsilon_{\mathbf{p}}; \Delta_{0i}, \mu_i)},$$

where Δ_{0i}, μ_i are the ground-state values determined by Eqs. (1.25) and (1.26) with $\omega = \omega_i$. We then quench the detuning $\omega_i \rightarrow \omega_f$ and evolve the system with the two-channel Hamiltonian (1.9) starting from the initial state (1.28) at $t = 0$.

The state of the system is fully determined by the many-body wave function, which in the mean-field treatment is at all times a product state of the form

$$|\Psi(t)\rangle = |\psi(t)\rangle \otimes (\hat{b}^\dagger)^{n(t)}|0\rangle, \qquad (1.29)$$

where $n(t) = |b(t)|^2$ and $|\psi(t)\rangle$ is the fermionic part of the wave function:

$$|\psi(t)\rangle = \prod_{\mathbf{p}}[\bar{u}_{\mathbf{p}}(t) + \bar{v}_{\mathbf{p}}(t)\hat{a}_{\mathbf{p}\uparrow}^\dagger \hat{a}_{-\mathbf{p}\downarrow}^\dagger]|0\rangle. \qquad (1.30)$$

Bogoliubov amplitudes $u_{\mathbf{p}}(t), v_{\mathbf{p}}(t)$ obey the Bogoliubov de Gennes (BdG) equations

$$i\frac{\partial}{\partial t}\begin{pmatrix} u_{\mathbf{p}}(t) \\ v_{\mathbf{p}}(t) \end{pmatrix} = \begin{pmatrix} \epsilon_{\mathbf{p}} & \Delta(t) \\ \bar{\Delta}(t) & -\epsilon_{\mathbf{p}} \end{pmatrix}\begin{pmatrix} u_{\mathbf{p}}(t) \\ v_{\mathbf{p}}(t) \end{pmatrix}, \qquad (1.31)$$

with the normalization condition $|u_{\mathbf{p}}|^2 + |v_{\mathbf{p}}|^2 = 1$. Apart from an overall time-dependent phase (which is important for certain observables), these equations are equivalent to the classical spin equations of motion (1.8) and spins are related to the amplitudes as

$$\frac{s_{\mathbf{p}}^-}{s_{\mathbf{p}}} = 2u_{\mathbf{p}}\bar{v}_{\mathbf{p}}, \qquad \frac{s_{\mathbf{p}}^z}{s_{\mathbf{p}}} = |v_{\mathbf{p}}|^2 - |u_{\mathbf{p}}|^2, \qquad (1.32)$$

where $s_{\mathbf{p}}$ is the length of the spin. For quench initial conditions $s_{\mathbf{p}} = 1/2$, as explained below Eq. (1.16).

Each quench is uniquely characterized by three parameters: the resonance width $\gamma = g^2\nu_F$ and the initial ω_i and final ω_f values of the detuning in units of the Fermi energy. Indeed, ω_i and γ determine Δ_{0i} and μ_i and thus the initial condition, while the equations of motion (1.7) in the thermodynamic limit depend only on ω_f and γ. To see the latter, note that model parameters enter the equation of motion for spin $\vec{s}_{\mathbf{p}} \equiv \vec{s}(\varepsilon_{\mathbf{p}})$ only through $\Delta = -gb$, while the equation of motion for the bosonic field b can be equivalently written as

$$\dot{\Delta} = -i\omega_f\Delta + i\gamma\int_0^\infty s^-(\varepsilon)f(\varepsilon)d\varepsilon. \qquad (1.33)$$

Instead of ω_i, ω_f we find it more convenient to characterize the quench by Δ_{0i}, Δ_{0f}, the ground-state gaps corresponding to these values of the detuning. As discussed below Eq. (1.26), for a given γ, the detuning ω uniquely determines Δ_0 and vice versa. Note that Δ_{0f} has nothing to do with the time-dependent gap function $\Delta(t)$ and in particular with the large-time asymptote $\Delta(t \rightarrow \infty)$. Whenever $\Delta(t)$ goes to a constant at large times, we denote this constant Δ_∞.

D. Main results

Our main result is a complete description of the long-time dynamics of two- and one-channel models (1.9) and (1.11) in two and three spatial dimensions following a quench of the detuning $\omega_i \rightarrow \omega_f$ (coupling $\lambda_i \rightarrow \lambda_f$ in the one-channel model) in the thermodynamic limit. A key effect that makes such a description possible is a drastic reduction in the number of effective degrees of freedom as $t \rightarrow \infty$. It turns out that the large-time dynamics can be expressed in terms of just a few new collective spins plus the oscillator in the two-channel case that are governed by the same Hamiltonians (1.9) and (1.11) only with new effective parameters replacing $\varepsilon_{\mathbf{p}}$ and ω. The number of collective spins is $m = 0$, 1, or 2 and $m = -1$, 0, or 2 for one- and two-channel models, respectively, depending on the quench. The difference is due to the presence of the oscillator degree of freedom in the latter case. For example, $m = -1$ means that the effective large-time Hamiltonian H_{red} not only has no spins, but also the oscillator b is absent; i.e., $H_{red} = 0$. This reduction effect combined with integrability of classical Hamiltonians (1.9) and (1.11) allows us to determine the state of the system (its many-body wave function) at $t \rightarrow \infty$. We explain this method in detail in Sec. II. This section

provides a summary of main results obtained with the help of this method.

In Secs. III and IV, we construct exact quench phase diagrams shown in Figs. 2–5. Depending on the values of ω_i and ω_f either system reaches one of three distinct steady states labeled by I, II (including subregion II'), and III that can be thought about as nonequilibrium phases with second-order phase transition lines between them [$t \to \infty$ limit of the order parameter $\Delta(t)$ is continuous along lines separating different regions]. These steady states correspond to $m = 0$, 1, or 2 collective spins, respectively, for the one-channel model and to $m = -1$, 0, or 2 in the case of two channels.

Each point in the quench phase diagrams represents a particular quench specified by a pair of values $(\Delta_{0i}, \Delta_{0f})$. Here Δ_0 is the gap that the system would have in the ground state at detuning ω, which is a known function of ω. Values Δ_{0i} and Δ_{0f}—ground-state gaps for $\omega = \omega_i$ and ω_f, respectively—uniquely determine ω_i and ω_f at fixed resonance width γ. Note that Δ_{0f} is *not* the magnitude of the actual steady-state gap function $|\Delta(t)|$. Each quench $\omega_i \to \omega_f$ (or $\lambda_i \to \lambda_f$) therefore maps to a single point $(\Delta_{0i}, \Delta_{0f})$ and vise versa.

Steady states I, II, and III reached by the system at $t \to \infty$ can be described in terms of the superfluid order parameter $\Delta(t)$. In region I of phase diagrams in Figs. 2–5 the gap function vanishes at large times, $\Delta(t) \to 0$; see Fig. 6.

In region II (including subregion II') the magnitude of the order parameter asymptotes to a nonzero constant Δ_∞ as illustrated in Fig. 7,

$$\Delta(t) \to \Delta_\infty e^{-2i\mu_\infty t - 2i\varphi}, \qquad (1.34)$$

where $\Delta_\infty, \mu_\infty$ are functions of ω_i, ω_f (or, equivalently, of Δ_{0i} and Δ_{0f}), and γ to be determined below, and φ is a constant phase. Plots of Δ_∞ and μ_∞ as functions of Δ_{0f} for fixed Δ_{0i} are shown in Figs. 9, 18, and 19. The quantity μ_∞ plays the role of the out-of-equilibrium chemical potential. Subregions II and II' of region II correspond to $\mu_\infty > 0$ and $\mu_\infty < 0$, respectively.

In region III of quench phase diagrams the amplitude of the order parameter oscillates persistently at large times, as shown in Fig. 8,

$$\Delta(t) \to \sqrt{\Lambda^2(t) + h_1} e^{-i\Phi(t)}, \qquad (1.35)$$

where

$$\Lambda(t) = \Delta_+ \mathrm{dn}[\Delta_+(t - t_0), k'], \quad k' = \frac{\Delta_-}{\Delta_+}, \qquad (1.36)$$

where dn is the Jacobi elliptic function and t_0 is an integration constant. The magnitude of the order parameter oscillates periodically between $\Delta_b = (\Delta_-^2 + h_1)^{1/2}$ and $\Delta_a = (\Delta_+^2 + h_1)^{1/2}$. The phase contains linear and periodic parts [62],

$$\Phi(t) = 2\mu t - \int \frac{\kappa dt}{\Lambda^2(t) + h_1}. \qquad (1.37)$$

Constants h_1, Δ_+, Δ_-, μ, and κ are known functions of Δ_{0i}, Δ_{0f} (or ω_i, ω_f), and γ to be specified below; see also Figs. 9 and 10 and refer to Sec. II D 2 for more information about the periodic solution.

Previous studies of the BCS dynamics [3,7,16–19] were performed in the weak-coupling regime when both Δ_{0i} and
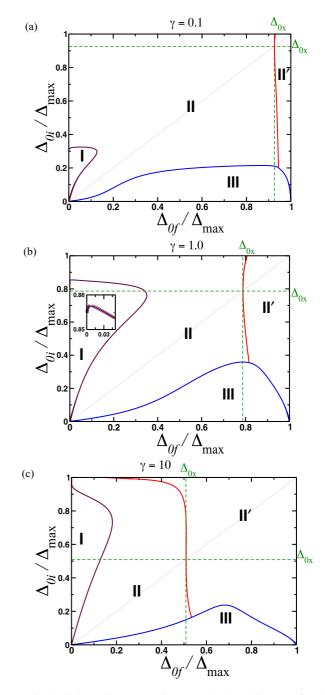

FIG. 2. (Color online) Detuning quench phase diagrams for the two-channel model (1.1) in 2D for an assortment of resonance widths γ. Each point represents a single quench labeled by Δ_{0i} (vertical axis) and Δ_{0f} (horizonal axis), pairing gaps the system would have in the ground state for initial and final detunings. At large times the system ends up in one of three steady states shown as regions I, II (including II'), and III. For quenches in region I the order parameter vanishes, $\Delta(t) \to 0$. In II $\Delta(t) \to \Delta_\infty e^{-2i\mu_\infty t - 2i\varphi}$ and in III $|\Delta(t)|$ oscillates persistently. Subregions II and II' differ in the sign of μ_∞ (out of equilibrium analog of the chemical potential): $\mu_\infty > 0$ in II and $\mu_\infty < 0$ in II'. The diagonal, $\Delta_{0i} = \Delta_{0f}$, is the no-quench line. To the left of it are strong-to-weak-coupling quenches; to the right are weak- to strong-coupling quenches. $\Delta_{\max} = \varepsilon_F \sqrt{\gamma}$ in 2D is the maximum possible ground-state gap and $\Delta_{0\times}$ is the ground-state gap corresponding to zero chemical potential; i.e., $\Delta_{0\times}$ is given by Eq. (1.25) for $\mu = 0$.
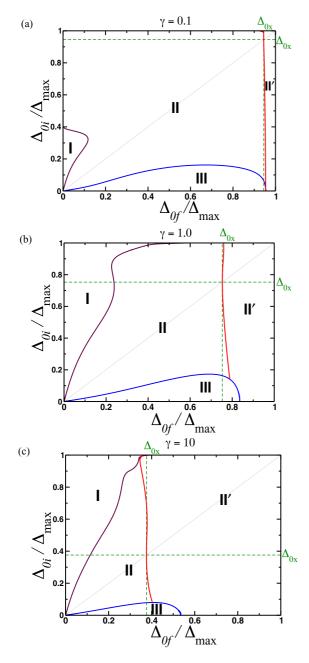
FIG. 3. (Color online) Same as Fig. 2 but in three spatial dimensions.

Δ_{0f} are much smaller than a characteristic high-energy scale (Fermi energy for cold gases and Debye energy for conventional superconductors). This limit corresponds to an infinitesimal vicinity of the origin $\Delta_{0i} = \Delta_{0f} = 0$ in our quench phase diagrams in Figs. 2–5. The weak-coupling limit is universal in that it is independent of the resonance width and dimensionality and thus is the same in all diagrams. Critical lines separating regions I from II and II from III are straight lines in this case coming out of the origin with slopes

$$\frac{\Delta_{0i}}{\Delta_{0f}} = e^{\pm \pi/2}. \tag{1.38}$$

Further, $h_1 = 0$ in Eq. (1.35) and Δ_∞, $\Delta_\pm$ take a simpler form given by Eqs. (3.27)–(3.29), and (3.31).
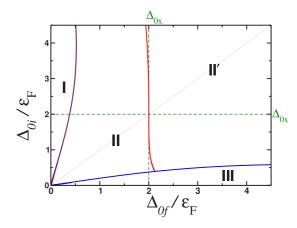

FIG. 4. (Color online) Interaction (λ) quench phase diagram for the one-channel model (1.11) in 2D. Otherwise same as Fig. 2.

There are several qualitatively new effects beyond the weak-coupling regime. At smaller resonance width $\gamma < \gamma_c = 16/\pi^2$, gapless region I terminates below Δ_{max} at $\Delta_{0i} = \gamma \pi/4$ along the vertical axis in 2D. This means that as initial coupling gets stronger (Δ_{0i} increases), even quenches to arbitrarily weak final coupling (small Δ_{0f}) do not result in vanishing $\Delta(t)$ at large times, in contrast to the weak-coupling regime, where quenches with sufficiently large Δ_{0f}/Δ_{0i} always do. The I-II critical line also displays an interesting backwards bending behavior for $\gamma < \gamma_c = 16/\pi^2$; see the inset in Fig. 2(b) and Eqs. (3.38) and (3.34).

Region III of persistent oscillations terminates at a threshold value of $\Delta_{0f} < \Delta_{max}$ in 3D, see Figs. 3 and 5. This means that even quenches from an infinitesimally weak initial coupling ($\lambda_i = 0+$ in the one-channel model, which corresponds to a vicinity of the normal state) to final couplings stronger than a certain threshold value produce no oscillations and $|\Delta(t)|$ instead goes to a constant. At finite but small initial gap Δ_{0i} (e.g., along the dashed line in Fig. 3) there is a
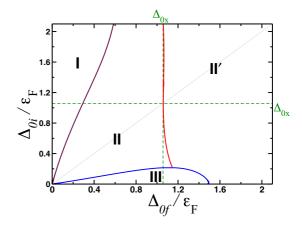

FIG. 5. (Color online) Interaction quench phase diagram for the one-channel model (1.11) in 3D (otherwise the same as Fig. 2). Consider, e.g., quenches from fixed infinitesimal coupling λ_i (small Δ_{0i}) to various final couplings λ_f. Increasing λ_f (Δ_{0f}) we move through gapless (I), gapped (II), then oscillating (III) steady states. As λ_f increases, further oscillations disappear and we again end up in a steady state characterized by constant asymptotic $|\Delta(t)|$ (II').
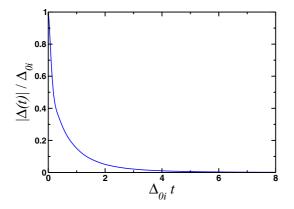
FIG. 6. (Color online) $|\Delta(t)|$ in region I for a 3D two-channel model, $\gamma = 1$, obtained from numerical evolution of $N = 5024$ spins following a detuning quench $\omega_i \rightarrow \omega_f$. Here $\Delta_{0i} = 0.27\Delta_{\max}$, $\Delta_{0f} = 4.30 \times 10^{-2}\Delta_{\max}$ [cf. Fig. 3(b)]. From these two values all other parameters obtain, e.g. $\mu_i = 0.90\varepsilon_F$ and $\omega_f - \omega_i = 1.97\varepsilon_F$.

reentrant behavior in both 2D and 3D as the final coupling (Δ_{0f}) increases when first there are no oscillations, then they appear, and then they disappear again. The threshold value of Δ_{0f} where the critical line separating regions II and
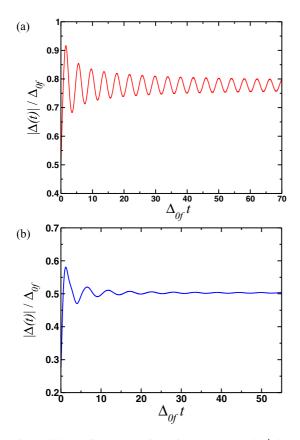

FIG. 7. (Color online) $|\Delta(t)|$ in regions II (top) and II' (bottom) for a 3D two-channel model, $\gamma = 1$, obtained from numerical evolution of $N = 5024$ spins after quenching the detuning ω. $\Delta_{0i} = 0.27\Delta_{\max}$, $\mu_i = 0.90\varepsilon_F$ in both panels (same as in Fig. 6). The final detuning corresponds to (a) $\Delta_{0f} = 0.56\Delta_{\max} = 2.07\Delta_{0i}$ and (b) $\Delta_{0f} = 0.97\Delta_{\max} = 3.59\Delta_{0i}$. See also Fig. 3(b).
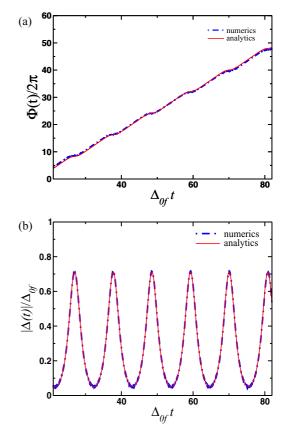

FIG. 8. (Color online) Amplitude (Higgs mode) and phase $\Phi(t)$ of the order parameter $\Delta(t)$ in region III of Fig. 3(c) after detuning quench from deep BCS to BEC in a 3D two-channel model for $\gamma = 10$. Numerical evolution with 5024 spins vs Eqs. (1.35) and (1.37). $\Delta_{0i} = 3.20 \times 10^{-3}\Delta_{\max}$, $\Delta_{0f} = 0.45\Delta_{\max}$, and $\delta\omega = -5.86\gamma$.

III terminates is given by Eq. (3.47) (plotted as a function of the resonance width in Fig. 22) and Eq. (4.18) for one- and two-channel models, respectively. For more details about quench diagrams, such as the shape of the critical lines, various thresholds and termination points, and values of parameters (e.g., Δ_∞, μ_∞, Δ_+, and Δ_-) characterizing asymptotic $\Delta(t)$, see Secs. III and IV.

The large-time asymptote of $\Delta(t)$ does not fully specify the steady state. One also needs to know the Bogoliubov amplitudes $u_{\mathbf{p}}(t \rightarrow \infty), v_{\mathbf{p}}(t \rightarrow \infty)$. We calculate them in Sec. II D in all three steady states. In terms of spin vectors, this translates into steady-state spin distribution. Even in regions I and II where $|\Delta(t)|$ goes to a constant, the steady state of the system is far from any equilibrium state. Time-independent $|\Delta(t)|$ means that in a frame that rotates around the z axis with frequency $2\mu_\infty$ the magnetic field $\vec{B}_{\mathbf{p}}$ that acts on spin $\vec{s}_{\mathbf{p}}$ in Eq. (1.7) is constant. In equilibrium $\vec{s}_{\mathbf{p}}$ aligns with $\vec{B}_{\mathbf{p}}$ or $-\vec{B}_{\mathbf{p}}$ (ground state). In steady states I and II it instead rotates around $\vec{B}_{\mathbf{p}}$, making a constant angle with it. Let $\theta_{\mathbf{p}}$ be the angle between $\vec{s}_{\mathbf{p}}$ and $-\vec{B}_{\mathbf{p}}$ (negative z axis in steady state I), so that in the ground state $\theta_{\mathbf{p}} = 0$. Out-of-equilibrium $\theta_{\mathbf{p}}$ determines the steady-state spin distribution function and is given by Eq. (3.11). This expression for $\cos\theta(\varepsilon_{\mathbf{p}})$ applies in all three steady states, but its interpretation in region III is slightly different and is explained below. A plot of the distribution
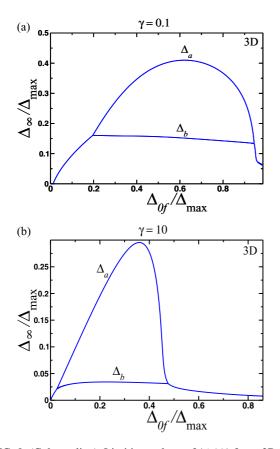
FIG. 9. (Color online) Limiting values of $|\Delta(t)|$ for a 3D two-channel model at large times after a detuning quench as functions of Δ_{0f} (or, equivalently, of final detuning ω_f) at fixed small $\Delta_{0i} = 0.05\Delta_{\max}$ (fixed initial detuning deep in the BCS regime). This corresponds to moving along a horizontal line (not shown) in Figs. 3(a) and 3(c) going through regions I, where $|\Delta(t)| \to 0$, II, where $|\Delta(t)| \to \Delta_\infty > 0$, III, where $|\Delta(t)|$ oscillates periodically between Δ_a and Δ_b, and into region II′, where again $|\Delta(t)| \to \Delta_\infty > 0$. Note that persistent oscillations appear and then disappear again as we decrease $\omega_f - \omega_i$ (i.e., increase Δ_{0f} at fixed Δ_{0i}). The same behavior is observed in the 3D one-channel model; see Fig. 5.

function $\cos\theta_{\mathbf{p}}$ is shown in Fig. 11. We explore the asymptotic states produced by detuning or interaction quenches in detail in Sec. II D. In Sec. VII we provide further insight into their physical nature and discuss their experimental signatures.

We perform detailed analysis of linearized equations of motion that goes much beyond previous work even in the weak-coupling regime and yields a range of new results. Small quenches of the detuning correspond to a small neighborhood of the diagonal in quench diagrams in Figs. 2–5; i.e., they fall within region II, where $|\Delta(t)| \to \Delta_\infty$ and Eq. (1.34) applies. We show that within linear approximation $\Delta_\infty = \Delta_{0f}$ and $\mu_\infty = \mu_f$; i.e., there are no corrections to these equations linear in the change of detuning or, equivalently, in $\delta\Delta_0 = \Delta_{0f} - \Delta_{0i}$. This is, in fact, a general result that has been overlooked by previous work; to first order in deviations from the ground state $\Delta(t)$ always asymptotes to its ground-state form for the Hamiltonian with which the system evolves at $t > 0$. Note, however, that when quadratic correction is taken into account one gets $\Delta_\infty < \Delta_{0f}$. For example, in the weak-
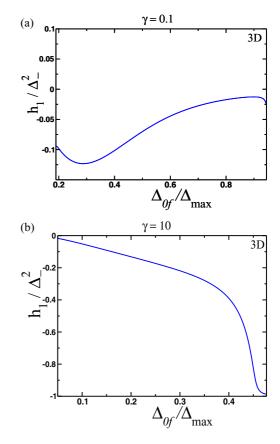

FIG. 10. (Color online) Parameter h_1 in Eq. (1.35) for asymptotic $|\Delta(t)|$ in phase III as a function of Δ_{0f} at fixed small $\Delta_{0i} = 0.05\Delta_{\max}$ (same as in Fig. 9). For quenches within the weak-coupling limit $h_1 = 0$, so nonzero h_1 quantifies deviations from this limit. Note that one must have $h_1 \geqslant -\Delta_-^2$, so that the expression under the square root in Eq. (1.35) is non-negative.

coupling regime we find

$$\Delta_\infty = \Delta_{0f} - \frac{(\delta\Delta_0)^2}{6\Delta_{0f}}. \tag{1.39}$$

We obtain an exact expression for $\Delta(t)$—Eqs. (5.35)–(5.37)—valid at all times and arbitrary coupling strength for both one- and two-channel models. In the weak-coupling regime this expression simplifies so that

$$|\Delta(t)| = \Delta_{0f} - 2\delta\Delta_0 \int_0^\infty \frac{dx}{\pi} \frac{\cos[2\Delta_0 t\cosh(\pi x/2)]}{1 + x^2}. \tag{1.40}$$

From here short- and long-time asymptotes follow. At short times the order parameter amplitude rises or falls sharply as

$$|\Delta(t)| = \Delta_{0i} + \frac{\delta\Delta_0}{|\ln(\Delta_0 t)|}. \tag{1.41}$$

The long-time behavior in the weak-coupling limit is

$$|\Delta(t)| = \Delta_{0f} - \frac{2\delta\Delta_0}{\pi^{3/2}} \frac{\cos(2\Delta_0 t + \pi/4)}{\sqrt{\Delta_0 t}}. \tag{1.42}$$

At stronger coupling in region II (but not II′) the long-time asymptote is still given by Eq. (1.42); only the coefficient in front of the second term on the right-hand side is more involved.
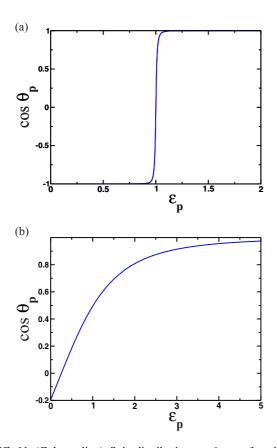
FIG. 11. (Color online) Spin distribution $\cos\theta_{\mathbf{p}}$ as a function of $\varepsilon_{\mathbf{p}}$ (in units of Fermi energy) at large times after the quench in a 3D two-channel model. In phases I and II, $-\cos\theta_{\mathbf{p}}/2$ is the projection of the spin $\vec{s}_{\mathbf{p}}$ onto its effective magnetic field (z axis in phase I) around which it precesses. In equilibrium $\cos\theta_{\mathbf{p}} = \pm 1$ (1 in the ground state) for all momenta and in phase I $\cos\theta_{\mathbf{p}} = -1$ and 1 correspond to doubly occupied and unoccupied states, respectively. Quench parameters are $\gamma = 1$ and (a) $\Delta_{0i} = 0.05\Delta_{\max}$, $\Delta_{0f} = 0.002\Delta_{\max}$ (BCS to deep BCS quench in phase I); (b) $\Delta_{0i} = 0.78\Delta_{\max}$, $\Delta_{0f} = 0.001\Delta_{\max}$ (BEC to deep BCS quench in phase I). In both cases $\mu_\infty \approx \varepsilon_F$. Note the Fermi-like shape of the distribution function in (a). Note that $\cos\theta_{\mathbf{p}} \to 1$ as $\varepsilon_{\mathbf{p}} \to \infty$, as it should, indicating that states at very high energies are empty.

Regions II and II$'$ differ in the sign of the phase frequency μ_∞, $\mu_\infty > 0$ in II and $\mu_\infty < 0$ in II$'$. We see below that frequency (Fourier) spectrum of quench dynamics in regions II and II$'$ is $E_\infty(\varepsilon_{\mathbf{p}}) = \sqrt{(\varepsilon_{\mathbf{p}} - \mu_\infty)^2 + \Delta_\infty^2}$, so that the Fourier transform of a dynamical quantity reads $\int_0^\infty A(\varepsilon) e^{-2iE_\infty(\varepsilon)t} d\varepsilon$. For $\mu_\infty > 0$ the phase has a stationary point on the integration path at $\varepsilon = \mu_\infty$, while for $\mu_\infty < 0$ it is absent. As a result, the long-time behavior in 3D in region II$'$ changes,

$$|\Delta(t)| = \Delta_{0f}\left[1 - c\frac{\delta\omega}{\gamma}\frac{\cos(2E_{\min}t + \pi/4)}{(2|\mu|t)^{3/2}}\right], \qquad (1.43)$$

where $E_{\min} = \sqrt{\mu^2 + \Delta_0^2}$, c is of order one, and $\delta\omega = \omega_f - \omega_i$. The same expression holds for the one-channel model after a replacement $\delta\omega/\gamma \to 1/\lambda_f - 1/\lambda_i$. Oscillation frequency $E_{\min}$ and $1/t^{3/2}$ decay are in agreement with Ref. [23] and reflect the fact that in the absence of a stationary point, the long-time asymptote is dominated by the end point of integration at

$\varepsilon = 0$, $E(0) = E_{\min}$, and the density of states in 3D vanishes as $\sqrt{\varepsilon}$ at small ε.

In 2D linear analysis yields a different approach to the asymptote in region II$'$

$$|\Delta(t)| = \Delta_{0f}\left[1 - \frac{\delta\omega}{\gamma}\frac{\sin(2E_{\min}t)}{|\mu|t\ln^2 t}\right], \qquad (1.44)$$

because of a constant density of states and $\ln\varepsilon$ divergence of the Fourier amplitude of $|\Delta(t)|$ at small ε (see below). We also determine the time-dependent phase of the order parameter $\Phi(t)$ in all cases corresponding to Eqs. (1.40)–(1.44), asymptotes of individual spins $\vec{s}_{\mathbf{p}}(t)$ as $t \to \infty$, and many other new results for the linearized dynamics in Sec. V.

Finally, we extend some of the above results for the long-time behavior of $|\Delta(t)|$ to the nonlinear regime, though, unlike the linear analysis, these results are not rigorous. In region II

$$|\Delta(t)| = \Delta_\infty + c'\frac{\cos(2\Delta_\infty t + \pi/4)}{\sqrt{\Delta_\infty t}}, \qquad (1.45)$$

where c' is a dimensionless coefficient. This answer holds for both one- and two-channel models in either dimension.

For region II$'$ we argue that the answer depends on dimensionality similarly to the linear analysis and

$$|\Delta(t)| = \Delta_\infty\left[1 - c_1\frac{\sin\left(2E_\infty^{\min}t\right)}{t\ln^2 t}\right] \quad \text{in 2D}, \qquad (1.46)$$

$$|\Delta(t)| = \Delta_\infty\left[1 - c_2\frac{\cos\left(2E_\infty^{\min}t + \pi/4\right)}{t^{3/2}}\right] \quad \text{in 3D}, \quad (1.47)$$

where $E_\infty^{\min} = \sqrt{\mu_\infty^2 + \Delta_\infty^2}$.

The approach to the gapless steady state (region I) is expected to be

$$|\Delta(t)| = \frac{c_4}{t\ln^r t} \quad \text{in 2D}, \qquad (1.48)$$

where $r = 1$ or $r = 2$, and

$$|\Delta(t)| = \frac{c_3}{t^{3/2}} \quad \text{in 3D}. \qquad (1.49)$$

We discuss these nonlinear large-time asymptotes in more detail in Sec. VI.

II. METHOD

Here we describe a method that allows one to determine the asymptotic state of the system at long times. Both the quantum (1.5) and classical (1.9) two-channel models are integrable meaning that there are as many nontrivial conservation laws as there are degrees of freedom. There is an exact Bethe ansatz-type solution for the quantum spectrum [38]. In the classical case integrability implies a formal inexplicit solution of the equations of motion in terms of certain multivariable special (hyperelliptic) functions [15] that can be helpful for understanding certain general features of the dynamics. Evaluating specific dynamical quantities of interest for realistic initial conditions with this solution is, however, roughly equivalent to just solving the equations of motion numerically. However, the latter could be as well done directly without the formal exact solution. This is a typical situation in the standard theory of nonlinear integrable systems.

Fortunately, it was realized that, at least for the BCS-type models, the large-time dynamics dramatically simplifies in the thermodynamic limit, so that the number of evolving degrees of freedom effectively drops to just a few spins. Building on this insight, Yuzbashyan *et al.* [16] were able to develop a method that goes beyond the standard theory and explicitly predicts the long-time dynamics in the thermodynamic limit.

The main idea of this method is as follows. First, we construct a special class of *reduced* solutions of the classical equations of motion for the two-channel model such that the dynamics reduces to that of just few effective spins. Then we choose a suitable reduced solution and fix its parameters so that its integrals of motion match those for a given quench in the thermodynamic limit. Reduced solutions have only few additional arbitrary constants and cannot generally satisfy all of the quench initial conditions (1.28). There are $2N + 2$ initial conditions (two angles per spin plus two initial conditions for the oscillator mode *b*) and only $N + 1$ correspond to the integrals of motion.

Next, exploiting the fact that for fixed $\Delta(t)$ BdG equations (1.31) are linear in the amplitudes $u_\mathbf{p}$ and $v_\mathbf{p}$, we derive the most general $t \rightarrow \infty$ asymptotic solution that has the same $\Delta(t)$ as the reduced one. It has the same integrals as the quench dynamics by construction and, in addition, $N + 1$ arbitrary independent constants to match the remaining initial conditions. We *conjecture* that the so-constructed asymptotic solution is the true large-time asymptote of the actual quench dynamics. To verify this *few spin conjecture* it is sufficient to show that the large-time asymptote of the actual $\Delta(t)$ matches that of the reduced (and therefore general asymptotic) solution. We do so numerically in the nonlinear case and analytically for infinitesimal quenches when the dynamics can be linearized.

We consider the two-channel model in this and the following sections and then obtain similar results for the one-channel (BCS) model in Sec. IV by taking the broad resonance, $\gamma \rightarrow \infty$, limit.

A. Integrability and Lax vector construction

An object called Lax vector plays a key role in our approach. It encodes all the information about the integrals of motion and turns out to be especially useful in analyzing the quench dynamics in the thermodynamic limit. The Lax vector is defined as

$$\vec{L}(u) = \sum_\mathbf{p} \frac{\vec{s}_\mathbf{p}}{u - \varepsilon_\mathbf{p}} - \frac{(\omega - 2\mu)}{g^2}\hat{\mathbf{z}} + \frac{2}{g^2}[(u - \mu)\hat{\mathbf{z}} - \vec{\Delta}],$$

(2.1)

where u is an auxiliary complex variable and $\vec{\Delta} \equiv \Delta_x\hat{\mathbf{x}} + \Delta_y\hat{\mathbf{y}}$. Poisson brackets of components of $\vec{L}(u)$ satisfy the following Gaudin algebra:

$$\{L^a(u), L^b(v)\} = \varepsilon_{abc}\frac{L^c(u) - L^c(v)}{u - v}.$$

(2.2)

This implies an important equality,

$$\{\vec{L}^2(u), \vec{L}^2(v)\} = 0.$$

(2.3)

Explicit evaluation of $\vec{L}^2(u)$ yields

$$\vec{L}^2(u) = \frac{(2u - \omega)}{g^4} + \frac{4\mathcal{H}_b}{\omega g^2} + \sum_\mathbf{p}\left[\frac{2\mathcal{H}_\mathbf{p}}{g^2(u - \varepsilon_\mathbf{p})} + \frac{s_\mathbf{p}^2}{(u - \varepsilon_\mathbf{p})^2}\right],$$

(2.4)

where

$$\mathcal{H}_\mathbf{p} = g^2 \sum_{\mathbf{q} \neq \mathbf{p}} \frac{\vec{s}_\mathbf{p} \cdot \vec{s}_\mathbf{q}}{(\epsilon_\mathbf{p} - \epsilon_\mathbf{q})} + (2\epsilon_\mathbf{p} - \omega)s_\mathbf{p}^z + g(\bar{b}s_\mathbf{p}^- + bs_\mathbf{p}^+),$$

$$\mathcal{H}_b = \bar{b}b + \sum_\mathbf{p} s_\mathbf{p}^z.$$

(2.5)

It follows from Eq. (2.3) that these spin Hamiltonians mutually Poisson commute, i.e.,

$$\{\mathcal{H}_\mathbf{p}, \mathcal{H}_{\mathbf{p}'}\} = \{\mathcal{H}_\mathbf{p}, \mathcal{H}_b\} = 0.$$

(2.6)

Moreover, the two-channel Hamiltonian (1.9) is

$$H_{2\text{ch}} = \omega\mathcal{H}_b + \sum_\mathbf{p} \mathcal{H}_\mathbf{p}.$$

(2.7)

This implies that $\mathcal{H}_\mathbf{p}$ and $\mathcal{H}_b$ are conserved by $H_{2\text{ch}}$ and establishes the integrability of the two-channel Hamiltonian. Note that $\vec{L}^2(u)$ is also conserved for any value of u and serves as a generator of the integrals of motion for the two-channel model. The same construction works in the quantum case as well; one only needs to promote classical dynamical variables to corresponding quantum operators and replace Poisson brackets with commutators.

Equations of motion can be conveniently and compactly written in terms of the Lax vector as

$$\dot{\vec{L}} = (-2\vec{\Delta} + 2u\hat{\mathbf{z}}) \times \vec{L}.$$

(2.8)

Comparing the residues at the poles at both sides of this equation, we see that it is equivalent to the equations of motion for spins (1.8).

The square of the Lax vector is of the form

$$\vec{L}^2(u) = \frac{Q_{2N+2}(u)}{g^4 \prod_{\varepsilon_\mathbf{p}}(u - \varepsilon_\mathbf{p})^2},$$

(2.9)

where N is the total number of distinct single-particle energies $\varepsilon_\mathbf{p}$, the product is similarly over nondegenerate values of $\varepsilon_\mathbf{p}$, and $Q_{2N+2}(u)$ is a polynomial in u of degree $2N + 2$. The roots of this *spectral* polynomial [or equivalently of $\vec{L}^2(u)$] play an important role in the further analysis of the asymptotic behavior. Note that since $\vec{L}^2(u)$ is conserved, so are its roots. They thus constitute a set of integrals of motion alternative to Eq. (2.5). Since $\vec{L}^2(u) \geqslant 0$ for real u, its roots come in complex conjugate pairs.

B. Reduced solutions

Let us look for special solutions of equations of motion (2.8) such that the Lax vector factorizes into time-dependent

and -independent parts,

$$\vec{L}^{\text{red}}(u) = \sum_{\mathbf{p}} \frac{\vec{\sigma}_{\mathbf{p}}}{u - \varepsilon_{\mathbf{p}}} - \frac{(\omega - 2\mu)}{g^2}\hat{\mathbf{z}} + \frac{2}{g^2}[(u - \mu)\hat{\mathbf{z}} - \vec{\Delta}]$$

$$= \left(1 + \sum_{\mathbf{p}} \frac{d_{\mathbf{p}}}{u - \epsilon_{\mathbf{p}}}\right)\vec{L}_m(u), \qquad (2.10)$$

where $\vec{\sigma}_{\mathbf{p}}$ (not to be confused with Pauli matrices) denote spins in this solution that can have arbitrary length to distinguish them from spins $\vec{s}_{\mathbf{p}}$ for the quench dynamics that have length 1/2. Further, $d_{\mathbf{p}}$ are time-independent constants to be determined later and $\vec{L}_m(u)$ is the Lax vector for an effective m-spin system,

$$\vec{L}_m(u) = \sum_{j=0}^{m-1} \frac{\vec{t}_j}{u - \eta_j} - \frac{(\omega' - 2\mu)}{g^2}\hat{\mathbf{z}} + \frac{2}{g^2}[(u - \mu)\hat{\mathbf{z}} - \vec{\Delta}].$$

$$(2.11)$$

Here $\vec{t}_j$ are new collective spin variables placed at new arbitrary "energy levels" η_j. Note that the bosonic field $\vec{b}$ and therefore $\vec{\Delta}$ are the same in the original and reduced models.

Substituting Eq. (2.10) into the equations of motion (2.8), we see that $\vec{L}_m(u)$ satisfies the same equation of motion. This means that variables $\vec{t}_j$ obey Bloch equations (1.8) with $\varepsilon_{\mathbf{p}} \to \eta_j$ and $\omega \to \omega'$, and are therefore governed by the same Hamiltonian,

$$H_{2\text{ch}}^{\text{red}} = \sum_{j=0}^{m-1} 2\eta_j t_j^z + \omega'\bar{b}b + g\sum_{j=0}^{m-1}(\bar{b}t_j^- + bt_j^+). \qquad (2.12)$$

We need at most $m = 1$ for analyzing the quench dynamics, so we are able solve the equations of motions for $\vec{t}_j$ directly.

Matching the residues at $u = \varepsilon_{\mathbf{p}}$ on both sides of Eq. (2.10), we express original spins in terms of $\vec{t}_j$

$$\vec{\sigma}_{\mathbf{p}} = d_{\mathbf{p}}\vec{L}_m(\varepsilon_j). \qquad (2.13)$$

Constants $d_{\mathbf{p}}$ are determined from the above equation using $\vec{\sigma}_{\mathbf{p}}^2 = \sigma_{\mathbf{p}}^2$, where $|\sigma_{\mathbf{p}}|$ is the length of spin $\vec{\sigma}_{\mathbf{p}}$. Note that $\sigma_{\mathbf{p}}$ can be of either sign (for future convenience). We have

$$d_{\mathbf{p}} = -\frac{\sigma_{\mathbf{p}}}{\sqrt{\vec{L}_m^2(\varepsilon_{\mathbf{p}})}}. \qquad (2.14)$$

It is important to note that $\sigma_{\mathbf{p}}$ are arbitrary constants at this point. We determine them later so that the integrals of motion for the reduced solution match those for quench dynamics.

To satisfy Eq. (2.10), we also need to match the residues at $u = \eta_k$ and the $u \to \infty$ asymptotic. This leads to the following $m + 1$ equations:

$$1 + \sum_{\mathbf{p}} \frac{d_{\mathbf{p}}}{\eta_k - \varepsilon_{\mathbf{p}}} = 0 \quad k = 0, \dots, m-1,$$

$$(2.15)$$

$$\omega = \omega' - 2\sum_{\mathbf{p}} d_{\mathbf{p}}.$$

Equations (2.15) constrain the coefficients of the spectral polynomial

$$Q_{2m+2}(u) = g^4\vec{L}_m^2(u)\prod_{k=0}^{m-1}(u - \eta_k)^2, \quad m \geqslant 0, \qquad (2.16)$$

of the m-spin system. Indeed, using Eq. (2.14), we can cast these constraints into the following form:

$$\sum_{\mathbf{p}} \frac{\sigma_{\mathbf{p}}\varepsilon_{\mathbf{p}}^{r-1}}{\sqrt{Q_{2m+2}(\varepsilon_{\mathbf{p}})}} = -\frac{\delta_{rm}}{g^2}, \quad r = 1, \dots, m,$$

$$(2.17)$$

$$\omega' = \omega + 2\sum_{k=0}^{m-1}\eta_k + \sum_{\mathbf{p}} \frac{2\sigma_{\mathbf{p}}g^2\varepsilon_{\mathbf{p}}^m}{\sqrt{Q_{2m+2}(\varepsilon_{\mathbf{p}})}}.$$

Here $m \geqslant 0$. These equations can be viewed as equations for determining the lengths of the collective spins $\vec{t}_j$.

We thus constructed a class of solutions such that the dynamics reduces to that of a smaller number of spins. These *few-spin solutions*, however, do not match the quench initial conditions, but, as we will see, the long-time asymptote of $\Delta(t)$ after the quench coincides with $\Delta(t)$ of an appropriately chosen few-spin solution. Specifically, $m = -1$, 0, and 1 are realized depending on the magnitude and the sign of the change in the detuning ω. Let us therefore consider these particular cases.

1. $m = -1$ spin solutions

$m = -1$ refers to the case when there are no collective spins and $b = 0$; i.e., the oscillator (which can be viewed as an infinite length limit of a spin) is effectively absent as well. In other words, $H_{\text{red}} = 0$ and $\vec{L}_m(u) = \frac{2u-\omega'}{g^2}\hat{\mathbf{z}}$. Equation (2.13) then implies that all spins in the reduced solution are along the z axis pointing in either a positive or a negative direction. It is convenient to redefine the sign of $\sigma_{\mathbf{p}}$ (only for $m = -1$) so that $\vec{\sigma}_{\mathbf{p}} = -\sigma_{\mathbf{p}}\hat{\mathbf{z}}$. We see directly from the equations of motion (1.8) that this configuration together with $b = 0$ is indeed a solution, a stationary one in the present case.

2. $m = 0$ spin solutions

In this case the reduced problem consists of a free classical oscillator as there are no collective spins; i.e., $H_{\text{red}} = \omega'\bar{b}b$. Equations of motion reduce to $\dot{b} = -i\omega'b$. Therefore,

$$\Delta(t) = -gb = ce^{-2i\mu t}, \qquad (2.18)$$

where c is a complex constant and we defined $\mu = \omega'/2$.

Expressions for the original spins follow from the reduced Lax vector

$$\vec{L}_m(u) = -\frac{2}{g^2}[\vec{\Delta} - (u - \mu)\hat{z}]. \qquad (2.19)$$

Equations (2.13) and (2.14) imply

$$\vec{\sigma}_{\mathbf{p}} = \frac{\sigma_{\mathbf{p}}}{E(\varepsilon_{\mathbf{p}};\Delta,\mu)}[\vec{\Delta} - (\varepsilon_{\mathbf{p}} - \mu)\hat{\mathbf{z}}], \qquad (2.20)$$

where $E(\varepsilon_{\mathbf{p}};\Delta,\mu) = \sqrt{(\varepsilon_{\mathbf{p}} - \mu)^2 + |\Delta|^2}$. We see that the ground state (1.15) is a one-spin solution with $c = \Delta_0$ and $\sigma_{\mathbf{p}} = 1/2$ (to minimize the energy). Excited states are also one-spin solutions with different parameters.

There is only one (last) constraint among Eqs. (2.17) for $m = 0$, which we recognize as a generalization of the gap equation (1.18).

3. *m = 1 spin solutions*

This example is substantially more involved than the previous two. Now there is one collective spin $\vec{t}$ coupled to an oscillator,

$$H_{\text{red}} = 2\eta t^z + \omega' \bar{b} b + g(\bar{b} t^- + b t^+), \qquad (2.21)$$

making the dynamics rather nontrivial. Our main goal presently is to derive a differential equation for $|\Delta(t)| = g|b(t)|$ and to relate its coefficients to the spectral polynomial $Q_4(u)$ of the reduced $m = 1$ problem given, in general, by Eq. (2.16).

H_{red} conserves $\bar{b} b + t^z$. It follows that t^z can be expressed through $|b|^2$ as $t^z = c_1 \Omega^2 + c_2$, where $c_{1,2}$ are constants and we introduced a notation

$$\Delta = \Omega e^{-i\Phi}. \qquad (2.22)$$

Equation (2.13) then implies that the *z* component of the original spins in the reduced solution can be similarly expressed through $|\Delta|$ as

$$\sigma_{\mathbf{p}}^z = a_{\mathbf{p}} \Omega^2 + b_{\mathbf{p}}. \qquad (2.23)$$

Note that constants $a_{\mathbf{p}}$ and $b_{\mathbf{p}}$ are inversely proportional to $\sqrt{\vec{L}_m^2(\varepsilon_{\mathbf{p}})}$ and therefore to $\sqrt{Q_4(\varepsilon_{\mathbf{p}})}$. It turns out that an efficient strategy to derive an equation for Ω and relate its coefficients to those of $Q_4(u)$ is somewhat indirect. First, we use equations of motion for $\vec{\sigma}_{\mathbf{p}}$ together with Eq. (2.23) to obtain an equation for Ω and expressions for $a_{\mathbf{p}}$ and $b_{\mathbf{p}}$. Identifying $\sqrt{Q_4(\varepsilon_{\mathbf{p}})}$ in the latter with the help of Eq. (2.14), we relate the coefficients.

Bloch equations (1.8) for spins in the reduced solution, $\vec{s}_p^{\text{red}} \equiv \vec{\sigma}_{\mathbf{p}}$, can be written as

$$\dot{\sigma}_{\mathbf{p}}^z = -i(\sigma_{\mathbf{p}}^- \bar{\Delta} - \sigma_{\mathbf{p}}^+ \Delta), \quad \dot{\sigma}_{\mathbf{p}}^- = -2i\sigma_{\mathbf{p}}^z \Delta - 2i\varepsilon_{\mathbf{p}} \sigma_{\mathbf{p}}^-. \qquad (2.24)$$

Substituting $\sigma_{\mathbf{p}}^z$ from Eq. (2.23) into the first equation, we obtain

$$\sigma_{\mathbf{p}}^- e^{i\Phi} - \sigma_{\mathbf{p}}^+ e^{-i\Phi} = 2i a_{\mathbf{p}} \dot{\Omega}. \qquad (2.25)$$

Multiplying the second equation in Eq. (2.24) by $e^{i\Phi}$ and adding the resulting equation to its complex conjugate, we get

$$\frac{d}{dt}(\sigma_{\mathbf{p}}^- e^{i\Phi} + \sigma_{\mathbf{p}}^+ e^{-i\Phi}) = 4 a_{\mathbf{p}} \varepsilon_{\mathbf{p}} \dot{\Omega} - 2 a_{\mathbf{p}} \dot{\Phi} \dot{\Omega}, \qquad (2.26)$$

where we also used Eq. (2.25). Integrating this and adding the result to Eq. (2.25), we obtain

$$\sigma_{\mathbf{p}}^- e^{i\Phi} = 2 a_{\mathbf{p}} \varepsilon_{\mathbf{p}} \Omega - a_{\mathbf{p}} A + i a_{\mathbf{p}} \dot{\Omega}, \qquad (2.27)$$

where $A = \int dt\, \dot{\Phi} \dot{\Omega}$. Equation (2.27) implies

$$|\sigma_{\mathbf{p}}^-|^2 = (2 a_{\mathbf{p}} \varepsilon_{\mathbf{p}} \Omega - a_{\mathbf{p}} A)^2 + a_{\mathbf{p}}^2 \dot{\Omega}^2. \qquad (2.28)$$

Equations (2.28) and (2.23) combined with the conservation of the length of the spin, $(\sigma_{\mathbf{p}}^z)^2 + |\sigma_{\mathbf{p}}^-|^2 = \sigma_{\mathbf{p}}^2$, yield a differential

equation for Ω

$$(a_{\mathbf{p}} \Omega^2 + b_{\mathbf{p}})^2 + (2 a_{\mathbf{p}} \varepsilon_{\mathbf{p}} \Omega - a_{\mathbf{p}} A + c_{\mathbf{p}})^2 + a_{\mathbf{p}}^2 \dot{\Omega}^2 = \sigma_{\mathbf{p}}^2. \qquad (2.29)$$

Dividing the last equation by $a_{\mathbf{p}}^2$ and rearranging, we obtain

$$\dot{\Omega}^2 + \Omega^4 + \Omega^2 \left(2\frac{b_{\mathbf{p}}}{a_{\mathbf{p}}} + 4\varepsilon_{\mathbf{p}}^2 \right) - 4\varepsilon_{\mathbf{p}} A \Omega + A^2$$
$$+ \frac{b_{\mathbf{p}}^2 - \sigma_{\mathbf{p}}^2}{a_{\mathbf{p}}^2} = 0. \qquad (2.30)$$

It turns out that A is a certain function of Ω. To see this, let $x_{\mathbf{p}}$ be a set of numbers such that $\sum_{\mathbf{p}} x_{\mathbf{p}} = 0$, multiply Eq. (2.30) by $x_{\mathbf{p}}$, and sum over $\mathbf{p}$. This yields

$$A = 2\mu\Omega + \frac{\kappa}{\Omega}, \qquad (2.31)$$

where μ and κ are arbitrary real constants. Substituting Eq. (2.31) into Eq. (2.30), we obtain

$$\dot{\Omega}^2 + \Omega^4 + 2\Omega^2 \left[\frac{b_{\mathbf{p}}}{a_{\mathbf{p}}} + 2\xi_{\mathbf{p}}^2 \right] + \frac{\kappa^2}{\Omega^2} + \frac{b_{\mathbf{p}}^2 - \sigma_{\mathbf{p}}^2}{a_{\mathbf{p}}^2} - 4\kappa\xi_{\mathbf{p}} = 0, \qquad (2.32)$$

where $\xi_{\mathbf{p}} = \varepsilon_{\mathbf{p}} - \mu$. Note that the same equation obtains in the reduced problem with $a_{\mathbf{p}} \to c_1$, $b_{\mathbf{p}} \to c_2$, etc. It follows that coefficients must be $\mathbf{p}$ independent; i.e.,

$$\frac{b_{\mathbf{p}}}{a_{\mathbf{p}}} + 2\xi_{\mathbf{p}}^2 = 2\rho, \quad \frac{b_{\mathbf{p}}^2 - \sigma_{\mathbf{p}}^2}{a_{\mathbf{p}}^2} - 4\kappa\xi_{\mathbf{p}} = 4\chi, \qquad (2.33)$$

where ρ and χ are $\mathbf{p}$-independent constants. We find

$$b_{\mathbf{p}} = -2(\xi_{\mathbf{p}}^2 - \rho) a_{\mathbf{p}},$$
$$a_{\mathbf{p}} = \frac{-\sigma_{\mathbf{p}}}{2\sqrt{(\xi_{\mathbf{p}}^2 - \rho)^2 - \kappa\xi_{\mathbf{p}} - \chi}}. \qquad (2.34)$$

As mentioned above $a_{\mathbf{p}}$ and $b_{\mathbf{p}}$ are inversely proportional to $\sqrt{Q_4(\varepsilon_{\mathbf{p}})}$. Equation (2.34) therefore implies

$$Q_4(u) = [(u - \mu)^2 - \rho]^2 - \kappa(u - \mu) - \chi, \qquad (2.35)$$

while the differential Eq. (2.32) for Ω reads

$$\dot{\Omega}^2 + \Omega^4 + 4\rho\Omega^2 + \frac{\kappa^2}{\Omega^2} + 4\chi = 0. \qquad (2.36)$$

This equation can be solved in terms of elliptic function. Let $w = \Omega^2$. We have

$$\dot{w}^2 + 4w^3 + 16\rho w^2 + 16\chi w + 4\kappa^2 \equiv \dot{w}^2 + 4P_3(w) = 0. \qquad (2.37)$$

Further, let $P_3(w) = (w - h_1)(w - h_2)(w - h_3)$, where $h_3 \geqslant h_2 \geqslant h_1$, and define

$$\omega = \Lambda^2 + h_1, \quad \Delta_+^2 = h_3 - h_1, \quad \Delta_-^2 = h_2 - h_1. \qquad (2.38)$$

We get

$$\dot{\Lambda}^2 = (\Delta_+^2 - \Lambda^2)(\Lambda^2 - \Delta_-^2), \qquad (2.39)$$

with the solution

$$\Lambda = \Delta_+ \mathrm{dn}[\Delta_+(t - t_0), k'], \quad k' = \frac{\Delta_-}{\Delta_+}, \qquad (2.40)$$

where dn is the Jacobi elliptic function and t_0 is an arbitrary integration constant.

It also follows from Eq. (2.31) and the definition of A below Eq. (2.27) that the phase of the order parameter is determined as

$$\dot{\Phi} = \frac{dA}{d\Omega} = 2\mu - \frac{\kappa}{\Lambda^2 + h_1}, \quad \Delta = \sqrt{\Lambda^2 + h_1}\, e^{-i\Phi}. \quad (2.41)$$

C. Matching integrals of motion

Given the quench initial conditions, we can evaluate all integrals of motion. This is equivalent to evaluating $\vec{L}^2(u)$ in the initial state as it is conserved and contains all the integrals as residues at $u = \varepsilon_{\mathbf{p}}$. It turns out that in the thermodynamic limit it is possible to find a reduced (few-spin) solution that has the same $\vec{L}^2(u)$, i.e., exactly the same integrals as the quench dynamics.

In the thermodynamic limit single-particle energies $\varepsilon_{\mathbf{p}}$ form a continuum on the positive real axis and $\vec{L}^2(u)$, therefore, has a continuum of poles at $u > 0$. Additionally, $\vec{L}^2(u)$ also has a continuum of roots along the $u > 0$ half line, as we show in Appendix B. Thus, $\sqrt{\vec{L}^2(u)}$ has a branch cut along $u > 0$ in the continuum limit. There can also be several *isolated* roots whose imaginary parts remain finite in this limit. Isolated roots play an important role in the dynamics; we determine them below and see that there are at most four such roots (two pairs of complex conjugate roots) for our quench problem.

Equation (2.10) implies

$$1 + \int d\varepsilon' \frac{d(\varepsilon')\nu(\varepsilon')}{u - \varepsilon'} = -z(u)\sqrt{\frac{\vec{L}^2(u)}{\vec{L}_m^2(u)}}, \quad z(u) = \pm 1, \quad (2.42)$$

where $\vec{L}^2(u)$ is evaluated for the quench initial conditions. Our task is to find the parameters for the reduced problem—$d(\varepsilon)$ and $\vec{L}_m^2(u)$—so that this equation holds. Then the reduced problem has the same integrals of motion as the quench dynamics.

Both sides of Eq. (2.42) have a branch cut along the positive real axis and tend to 1 as $u \to \infty$ for an appropriate choice of the sign $z(\infty)$. Further, provided that the isolated roots of $\vec{L}^2(u)$ coincide with the roots of $\vec{L}_m^2(u)$, there are no more branching points and both sides are analytic away from the shared branch cut at $u > 0$. If we further ensure that the left- and the right-hand sides of Eq. (2.42) have the same jump across the branch cut, then their difference is an entire function that vanishes at infinity. It is therefore identically zero by Liouville's theorem from complex analysis, and Eq. (2.42) holds.

To equate jumps across the branch cut, we take $u \to \varepsilon \pm i0$, apply the well-known formula $1/(x \pm i0) = \mathcal{P}(1/x) \mp i\pi\delta(x)$, and subtract one result from another. This fixes $d(\varepsilon)$,

$$d(\varepsilon) = -\frac{z(\varepsilon)}{2i\pi\nu(\varepsilon)} \frac{\sqrt{\vec{L}^2(\varepsilon_-)} - \sqrt{\vec{L}^2(\varepsilon_+)}}{\sqrt{\vec{L}_m^2(\varepsilon)}}, \quad (2.43)$$

where $\varepsilon_{\pm} = \varepsilon \pm i0$. According to expression (2.14) for $d_{\mathbf{p}} \equiv d(\varepsilon_{\mathbf{p}})$ this is equivalent to fixing the lengths of the spins, $|\sigma_{\mathbf{p}}| \equiv$

$|\sigma(\varepsilon_{\mathbf{p}})|$, in the few-spin solution so that

$$\sigma(\varepsilon) = z(\varepsilon) \frac{\sqrt{\vec{L}^2(\varepsilon_-)} - \sqrt{\vec{L}^2(\varepsilon_+)}}{2i\pi\nu(\varepsilon)}. \quad (2.44)$$

Thus, the few-spin solution with this $\sigma(\varepsilon)$ and $\vec{L}_m^2(u)$, whose roots are the same as the isolated roots of $\vec{L}^2(u)$, has the same integrals of motion as the quench problem.

D. Asymptotic solution for the quench dynamics

There are altogether $2(N + 1)$ initial conditions: two angles for each classical spin and two initial conditions for the oscillator. So far, we constructed a reduced m-spin solution that matches $N + 1$ integrals of motion. This satisfies $N + 1$ initial conditions. The dynamics of the reduced m-spin Hamiltonian contains $2(m + 1)$ constants, $m + 1$ of which (integrals of motion for H_{red}) are already fixed since we fixed $\vec{L}_m^2(u)$. The remaining $m + 1$ constants are not sufficient to match the remaining $N \to \infty$ initial conditions for the quench dynamics at finite m. This is resolved as follows. We use the known m-spin solution to derive a general asymptotic (i.e., valid at $t \to \infty$) solution of the equations of motion for spins $\vec{s}_{\mathbf{p}}$ with the same $\Delta(t)$ and the same integrals of motion as the m-spin solution. Integrals of motion therefore are those for the quench dynamics. In addition, this general solution contains the correct number $N + 1$ of independent constants. We therefore conjecture that this is the true solution for the quench dynamics at large times after the quench. By construction, to verify this *few-spin conjecture*, it is sufficient to show that the true asymptote of $\Delta(t)$ coincides with $\Delta(t)$ in the m-spin solution because given $\Delta(t)$ we obtain the most general asymptotic solution of equations of motion.

As discussed above Eq. (1.33), each quench is characterized by three parameters: the resonance width γ and the final ω_f and initial ω_i values of the detuning. We determine in the next section that $\vec{L}^2(u)$ for the quench dynamics can have zero, one, or two pairs of isolated complex roots for any γ depending on ω_i and ω_f. These, by construction, must also be all the roots of $\vec{L}_m^2(u)$, which has $m + 1$ pairs of complex conjugate roots according to Eq. (2.16). Cases relevant for the quench phase diagram are therefore $m = -1$, 0, and 1.

It is worthwhile to consider the $m = -1$ case separately in some detail to illustrate this procedure. Suppose $\vec{L}^2(u)$ evaluated for the quench initial condition has no complex (isolated) roots away from the real axis. Then there is an $m = -1$ spin solution constructed above that in the $N \to \infty$ limit has the same values of the integrals of motion as the spin dynamics. Spins in this solution are all along the z axis, $\vec{\sigma}_{\mathbf{p}} = -\sigma_{\mathbf{p}}\hat{z}$, and $\Delta(t) = -gb(t) = 0$. It is a particular solution of the equations of motion (1.8) such that $b(t) = 0$.

The general solution of the *spin part* of the equations of motion in Eq. (1.8) with $b(t) = 0$ is as follows: spins $\vec{s}_{\mathbf{p}}$ precess around the z axis (or equivalently around the reduced spins $\sigma_{\mathbf{p}}$) with frequencies $2\varepsilon_{\mathbf{p}}$, i.e.,

$$s_{\mathbf{p}}^z = \frac{\sigma_{\mathbf{p}}^z}{\sigma_{\mathbf{p}}} \frac{\cos\theta_{\mathbf{p}}}{2}, \quad s_{\mathbf{p}}^- = \frac{\sin\theta_{\mathbf{p}}}{2} e^{i\alpha_{\mathbf{p}}(t)}, \quad (2.45)$$

where $\theta_{\mathbf{p}}$ is the angle $\vec{s}_{\mathbf{p}}$ makes with $-\hat{\mathbf{z}}$ and $\alpha_{\mathbf{p}} = -2\varepsilon_{\mathbf{p}}t + \delta_{\mathbf{p}}$. Equivalently, this can be expressed as

$$\vec{s}_{\mathbf{p}} = \frac{\vec{\sigma}_{\mathbf{p}}}{\sigma_{\mathbf{p}}}\frac{\cos\theta_{\mathbf{p}}}{2} + \vec{s}_{\mathbf{p}}^{\perp}, \qquad (2.46)$$

where $\vec{s}_{\mathbf{p}}^{\perp}$ is the component transverse to $\vec{\sigma}_{\mathbf{p}}$, which rotates around $\vec{\sigma}_{\mathbf{p}}$ with frequency $2\varepsilon_{\mathbf{p}}$. Note that the length of spin $\vec{s}_{\mathbf{p}}$ is $1/2$, as it should be for the quench initial conditions.

This spin configuration has N additional constants $\delta_{\mathbf{p}}$, but it does not satisfy the equation of motion for $b(t)$ in Eq. (1.8) because $b(t) = 0$, while $J_{-}(t) = \sum_{\mathbf{p}} s_{\mathbf{p}}^{-} = \sum_{\mathbf{p}} f_{\mathbf{p}} e^{-2\varepsilon_{\mathbf{p}}t} \neq 0$, where $2f_{\mathbf{p}} = \sin\theta_{\mathbf{p}} e^{i\delta_{\mathbf{p}}}$. However, in the thermodynamic limit $J_{-}(t) = \int f(\varepsilon)\nu(\varepsilon)e^{-2\varepsilon t} \to 0$ as $t \to \infty$ and this solution becomes self-consistent.

Next we set $2\sigma_{\mathbf{p}} = \cos\theta_{\mathbf{p}}$ and substitute $\vec{s}_{\mathbf{p}} = \vec{\sigma}_{\mathbf{p}} + \vec{s}_{\mathbf{p}}^{\perp}$ into the Lax vector,

$$\vec{L}(u) = \vec{L}^{\text{red}}(u) + \sum_{\mathbf{p}} \frac{\vec{s}_{\mathbf{p}}^{\perp}}{u - \varepsilon_{\mathbf{p}}}. \qquad (2.47)$$

The second term vanishes by the Riemann-Lebesgue lemma (dephases) as $t \to \infty$ in the thermodynamic limit for u away from the real axis similarly to $J_{-}(t)$ and therefore $\vec{L}(u) \to \vec{L}^{\text{red}}(u)$. Constants $\sigma_{\mathbf{p}}$ are given by Eq. (2.44) to match the integrals of motion. Then the solution given by Eq. (2.45) with $2\sigma_{\mathbf{p}} = \cos\theta_{\mathbf{p}}$ has the same integrals of motion as the quench dynamics and the right number of additional constants to match the remaining initial conditions. As explained above, to verify that this is indeed the true asymptote of the quench dynamics, we only need to show that asymptotic $\Delta(t)$ coincides with $\Delta(t)$ of the $m = -1$ spin solution, i.e., that $\Delta(t) \to 0$ at large times after the quench whenever $\vec{L}^2(u)$ has no isolated complex roots (region I in quench phase diagrams above). We confirm this numerically; see, e.g., Figs. 5 and 12 and Refs. [16,18]. There is also a justification of this statement based on the general theory of integrable Hamiltonian dynamics. It works for both $m = -1$ and $m = 0$ and we present at the end of the $m = 0$ case below Eq. (2.65).

To summarize, if $\vec{L}^2(u)$ has no isolated complex roots for given (quench) initial conditions, then $\Delta(t) \to 0$ at large times in the thermodynamic limit and the steady-state spin configuration is

$$s_{\mathbf{p}}^z = -\frac{\cos\theta_{\mathbf{p}}}{2}, \quad s_{\mathbf{p}}^- = \frac{\sin\theta_{\mathbf{p}}}{2}e^{-2i\varepsilon_{\mathbf{p}}t + i\delta_{\mathbf{p}}}, \qquad (2.48)$$

where

$$\cos\theta(\varepsilon) = z(\varepsilon)\frac{\sqrt{\vec{L}^2(\varepsilon_-)} - \sqrt{\vec{L}^2(\varepsilon_+)}}{i\pi\nu(\varepsilon)}, \qquad (2.49)$$

and $\theta_{\mathbf{p}} \equiv \theta(\varepsilon_{\mathbf{p}})$. This expression evaluates explicitly for quench initial conditions; the answer is given by Eq. (3.11). The sign $z(\varepsilon) = \pm 1$ is fixed by requiring that $\cos\theta(\varepsilon)$ be smooth and spins $\vec{s}_{\mathbf{p}}$ point in the negative z direction at $\varepsilon_{\mathbf{p}} \to \infty$ (so that corresponding single-particles states be empty).

The logic for $m \geqslant 0$ is similar, but the calculation is a bit more involved. To derive the analog of Eq. (2.45), it is convenient to work with the BdG equations (1.31). In addition, there is an equation of motion for b in Eq. (1.8), which can be viewed as a self-consistency condition. In terms of $\Delta = -gb$
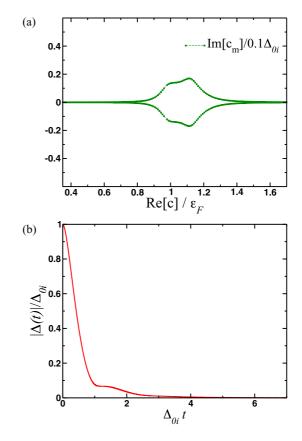

(a)

(b)

FIG. 12. (Color online) Order parameter $\Delta(t)$ vanishes whenever the square of the Lax vector $\vec{L}^2(u)$ has no isolated roots. Panel (a) shows real, Re[c], and imaginary, Im[c_m], parts of the roots c_m, and panel (b) shows the corresponding $|\Delta(t)|$ for a detuning quench in a 3D two-channel model with $\gamma = 0.1$ and $N = 1024$ spins. There are $N + 1$ pairs of complex conjugate continual roots whose imaginary parts scale as $1/N$ so that in the $N \to \infty$ limit they form a continuum on the real axis. Here $\Delta_{0i} = 0.34\Delta_{\text{max}}$, $\Delta_{0f} = 8.1 \times 10^{-3}\Delta_{\text{max}}$, $\mu_i = 0.91\varepsilon_F$, and $\delta\omega = 3.45\gamma$.

and Bogoliubov amplitudes it reads

$$\dot{\Delta} = -i\omega\Delta + ig^2\sum_{\mathbf{p}} 2s_{\mathbf{p}}u_{\mathbf{p}}\bar{v}_{\mathbf{p}}. \qquad (2.50)$$

The reduced m-spin solution is a particular solution $(U_{\mathbf{p}}, V_{\mathbf{p}})$ of the BdG equations that also satisfies the above self-consistency condition (with $s_{\mathbf{p}} \to \sigma_{\mathbf{p}}$). It is straightforward to check that $(\bar{V}_{\mathbf{p}}, -U_{\mathbf{p}})$ is also a solution of the BdG equations with the same $\Delta(t)$. Since for any fixed $\Delta(t)$ these equations are linear in the amplitudes, their most general normalized solution with this $\Delta(t)$ is a linear combination of these two independent solutions,

$$\begin{pmatrix} u_{\mathbf{p}} \\ v_{\mathbf{p}} \end{pmatrix} = \cos\frac{\theta_{\mathbf{p}}}{2}\begin{pmatrix} U_{\mathbf{p}} \\ V_{\mathbf{p}} \end{pmatrix} + \sin\frac{\theta_{\mathbf{p}}}{2}\begin{pmatrix} \bar{V}_{\mathbf{p}} \\ -U_{\mathbf{p}} \end{pmatrix}. \qquad (2.51)$$

The coefficients are made real by dropping an unimportant overall time-independent phase and including the relative phase into the common phase of $U_{\mathbf{p}}$ and $V_{\mathbf{p}}$. At this point $\theta_{\mathbf{p}}$ is an arbitrary angle. This solution does not generally satisfy the self-consistency condition (2.50) at finite t, but, as we see below, becomes self-consistent as $t \to \infty$.

Let us now determine the spins corresponding to this solution. Equation (2.51) implies

$$|v_{\mathbf{p}}|^2 - |u_{\mathbf{p}}|^2 = (|V_{\mathbf{p}}|^2 - |U_{\mathbf{p}}|^2)\cos\theta_{\mathbf{p}}$$
$$- \sin\theta_{\mathbf{p}}(\bar{U}_{\mathbf{p}}\bar{V}_{\mathbf{p}} + U_{\mathbf{p}}V_{\mathbf{p}}), \qquad (2.52)$$

$$u_{\mathbf{p}}\bar{v}_{\mathbf{p}} = U_{\mathbf{p}}\bar{V}_{\mathbf{p}}\cos\theta_{\mathbf{p}} + \frac{\sin\theta_{\mathbf{p}}}{2}(\bar{V}_{\mathbf{p}}^2 - U_{\mathbf{p}}^2).$$

True spins $\vec{s}_{\mathbf{p}}$ are related to $u_{\mathbf{p}}$, $v_{\mathbf{p}}$ through Eq. (1.32) with $s_{\mathbf{p}} = 1/2$. Spins $\vec{\sigma}_{\mathbf{p}}$ are similarly related to $U_{\mathbf{p}}, V_{\mathbf{p}}$. Let

$$U_{\mathbf{p}} = |U_{\mathbf{p}}| \exp\left[i\frac{\alpha_{\mathbf{p}} - \phi_{\mathbf{p}}}{2}\right],$$
$$(2.53)$$
$$V_{\mathbf{p}} = |V_{\mathbf{p}}| \exp\left[i\frac{\alpha_{\mathbf{p}} + \phi_{\mathbf{p}}}{2}\right].$$

We can express the absolute values of the amplitudes and their relative phase through the spin components

$$|V_{\mathbf{p}}|^2 = \frac{1}{2} + \frac{\sigma_{\mathbf{p}}^z}{2\sigma_{\mathbf{p}}}, \quad |U_{\mathbf{p}}|^2 = \frac{1}{2} - \frac{\sigma_{\mathbf{p}}^z}{2\sigma_{\mathbf{p}}}, \quad e^{-i\phi_{\mathbf{p}}} = \frac{\sigma_{\mathbf{p}}^-}{|\sigma_{\mathbf{p}}^-|},$$
$$(2.54)$$

while their common phase $\alpha_{\mathbf{p}}$ needs to be determined separately from the BdG equations.

We obtain in this notation

$$s_{\mathbf{p}}^z = \frac{\sigma_{\mathbf{p}}^z}{\sigma_{\mathbf{p}}}\frac{\cos\theta_{\mathbf{p}}}{2} - \frac{|\sigma_{\mathbf{p}}^-|}{\sigma_{\mathbf{p}}}\frac{\sin\theta_{\mathbf{p}}}{2}\cos\alpha_{\mathbf{p}},$$
$$(2.55)$$
$$s_{\mathbf{p}}^- = \frac{\sigma_{\mathbf{p}}^-}{\sigma_{\mathbf{p}}}\frac{\cos\theta_{\mathbf{p}}}{2} + \frac{\sin\theta_{\mathbf{p}}}{2}e^{-i\phi_{\mathbf{p}}}\left(\frac{\sigma_{\mathbf{p}}^z}{\sigma_{\mathbf{p}}}\cos\alpha_{\mathbf{p}} - i\sin\alpha_{\mathbf{p}}\right).$$

Note that $\sigma_{\mathbf{p}}^z/\sigma_{\mathbf{p}}$ and $\sigma_{\mathbf{p}}^-/\sigma_{\mathbf{p}}$ are components of the unit vector along the spin in the reduced solution $\vec{\sigma}_{\mathbf{p}}$. Geometrically, Eq. (2.55) says that $\vec{s}_{\mathbf{p}}$ makes a constant angle $\theta_{\mathbf{p}}$ (or $\pi - \theta_{\mathbf{p}}$ for negative $\sigma_{\mathbf{p}}$) with $\vec{\sigma}_{\mathbf{p}}$ and rotates around it with an angular velocity $\dot{\alpha}_{\mathbf{p}}$,

$$\vec{s}_{\mathbf{p}} = \frac{\vec{\sigma}_{\mathbf{p}}}{\sigma_{\mathbf{p}}}\frac{\cos\theta_{\mathbf{p}}}{2} + \vec{s}_{\mathbf{p}}^\perp. \qquad (2.56)$$

To see this, consider a body set of axis for $\vec{\sigma}_{\mathbf{p}}$. Take z' along $\vec{\sigma}_{\mathbf{p}}$, x' axis along the intersection of the zz' plane with the plane perpendicular to $\vec{\sigma}_{\mathbf{p}}$, and y' normal to $x'z'$ to form a right-handed coordinate system as usual. Then $\alpha_{\mathbf{p}}$ is the angle between $\vec{s}_{\mathbf{p}}^\perp$ and the x' axis and Eq. (2.55) follows.

The contribution of the second terms on the right-hand side of Eqs. (2.55) and (2.56) (terms containing $\alpha_{\mathbf{p}}$) to $\vec{L}(u)$ at u away from the real axis and to $J_-(t)$ vanishes (dephases) at large times at least for $m = 0$ and 1 in the thermodynamic limit, the same as in the $m = -1$ case considered above. For this to be true it is sufficient that $\alpha_{\mathbf{p}}$ contain a dispersing linear in t term, i.e.,

$$\alpha_{\mathbf{p}} = -2e_{\mathbf{p}}t + F_{\mathbf{p}}(t), \qquad (2.57)$$

where $e_{\mathbf{p}}$ is a continuous nonconstant function of $\varepsilon_{\mathbf{p}}$ and $F_{\mathbf{p}}(t)$ is a bounded function of t. Note that for $m = -1$, $e_{\mathbf{p}} = \varepsilon_{\mathbf{p}}$ and $F_{\mathbf{p}}(t) = \delta_{\mathbf{p}} = $ const.

To derive the asymptotic state, we follow the same procedure as for $m = -1$ above. We set $2\sigma_{\mathbf{p}} = \cos\theta_{\mathbf{p}}$, where $\cos\theta_{\mathbf{p}} \equiv \cos\theta(\varepsilon_{\mathbf{p}})$ is given by Eq. (2.49). Then $\vec{L}(u) \to$

$\vec{L}^{\text{red}}(u)$, $\Delta(t)$ is described by this m-spin solution at large times and satisfies the self-consistency condition (2.50), and the asymptotic spin configuration (2.55) and the m-spin problem have the same integrals of motion as the quench dynamics. The remaining $N + 1$ constants required to match the initial conditions are in $\alpha_{\mathbf{p}}$ (see below) and in the phase of $\Delta(t)$.

To determine $\alpha_{\mathbf{p}}$, rewrite the BdG equations as

$$i\partial_t(\ln U_{\mathbf{p}}) = \varepsilon_{\mathbf{p}} + \Delta\frac{V_{\mathbf{p}}}{U_{\mathbf{p}}}, \quad i\partial_t(\ln V_{\mathbf{p}}) = -\varepsilon_{\mathbf{p}} + \bar{\Delta}\frac{U_{\mathbf{p}}}{V_{\mathbf{p}}}.$$
$$(2.58)$$

Adding these equations and using Eqs. (2.53) and (2.54), we get, after some algebra,

$$\dot{\alpha}_{\mathbf{p}} = -\frac{\sigma_{\mathbf{p}}(\bar{\Delta}\sigma_{\mathbf{p}}^- + \Delta\sigma_{\mathbf{p}}^+)}{|\sigma_{\mathbf{p}}^-|^2}. \qquad (2.59)$$

1. $m = 0$

Suppose $\vec{L}^2(u)$ has a single pair of isolated complex roots at $u = \mu_\infty \pm i\Delta_\infty$. The 0-spin expression (2.18) for $\Delta(t)$ reads

$$\Delta(t) = \Delta_\infty e^{-2i\mu_\infty t - 2i\varphi}. \qquad (2.60)$$

The notation Δ_∞ and μ_∞ anticipates that this is also the long-time asymptote for the quench dynamics. Equation (2.20) implies

$$\frac{\sigma_{\mathbf{p}}^-}{\sigma_{\mathbf{p}}} = \frac{\Delta(t)}{E_{\mathbf{p}}^\infty}, \quad \frac{\sigma_{\mathbf{p}}^z}{\sigma_{\mathbf{p}}} = -\frac{\xi_p}{E_{\mathbf{p}}^\infty}, \qquad (2.61)$$

where $E_{\mathbf{p}}^\infty = E(\varepsilon_{\mathbf{p}}; \Delta_\infty, \mu_\infty) = \sqrt{(\varepsilon_{\mathbf{p}} - \mu_\infty)^2 + \Delta_\infty^2}$ and $\xi_{\mathbf{p}} = \varepsilon_{\mathbf{p}} - \mu_\infty$.

Equation (2.59) obtains $\dot{\alpha}_{\mathbf{p}} = -2E_{\mathbf{p}}^\infty$. We see that $\alpha_{\mathbf{p}}$ is of the form (2.57) and therefore the large-time asymptote of $\Delta(t)$ according to the few-spin conjecture is given by Eq. (2.60). The asymptotic spin configuration is then Eq. (2.55) with $\cos\theta_{\mathbf{p}} \equiv \cos\theta(\varepsilon_{\mathbf{p}})$ given by Eq. (2.49). Explicitly, using Eq. (2.61) and $\alpha_{\mathbf{p}} = -2E_{\mathbf{p}}^\infty t - \delta_{\mathbf{p}}$, we obtain

$$s_{\mathbf{p}}^z = -\frac{\xi_{\mathbf{p}}}{2E_{\mathbf{p}}^\infty}\cos\theta_{\mathbf{p}} - \frac{\Delta_\infty}{2E_{\mathbf{p}}^\infty}\sin\theta_{\mathbf{p}}\cos(2E_{\mathbf{p}}^\infty t + \delta_{\mathbf{p}}),$$

$$s_{\mathbf{p}}^- e^{2i\mu_\infty t + 2i\varphi} = \frac{\Delta_\infty}{2E_{\mathbf{p}}^\infty}\cos\theta_{\mathbf{p}} - \frac{\sin\theta_{\mathbf{p}}}{2}e^{2iE_{\mathbf{p}}^\infty t + i\delta_{\mathbf{p}}} \qquad (2.62)$$
$$- \left(\frac{\xi_p}{E_{\mathbf{p}}^\infty} - 1\right)\frac{\sin\theta_{\mathbf{p}}}{2}\cos(2E_{\mathbf{p}}^\infty t + \delta_{\mathbf{p}}).$$

In a reference frame rotating with frequency $2\mu_\infty$ around z axis, $\Delta(t) \to \Delta_\infty$ meaning that magnetic field acting on spin $\vec{s}_{\mathbf{p}}$ is time independent. In this frame $\vec{s}_{\mathbf{p}}$ rotates around the field or, equivalently, around the reduced spin $\vec{\sigma}_{\mathbf{p}}$ with frequency $2E_{\mathbf{p}}^\infty$ as described by Eq. (2.62).

We can also determine the Bogoliubov amplitudes corresponding to the 0-spin solution from Eqs. (2.53) and (2.54),

$$U_{\mathbf{p}} = \sqrt{\frac{1}{2} + \frac{\xi_{\mathbf{p}}}{2E_{\mathbf{p}}^\infty}}e^{-iE_{\mathbf{p}}^\infty t - i\mu_\infty t - i\varphi},$$
$$(2.63)$$
$$V_{\mathbf{p}} = \sqrt{\frac{1}{2} - \frac{\xi_{\mathbf{p}}}{2E_{\mathbf{p}}^\infty}}e^{-iE_{\mathbf{p}}^\infty t + i\mu_\infty t + i\varphi}.$$
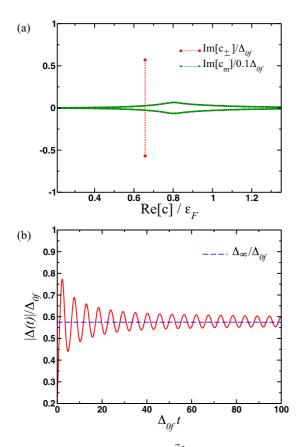
(a)

(b)

FIG. 13. (Color online) Roots of $\vec{L}^2(u)$ (top) and $|\Delta(t)|$ for a detuning quench in a 3D two-channel model for $N = 1024$ spins, $\gamma = 1.0$. There is one pair of isolated roots $c_{\pm} = \mu_{\infty} \pm i\Delta_{\infty}$ whose imaginary part remains finite in the large N limit and $N - 1$ continual roots c_m close to the real axis ($\mathrm{Im}[c_m]$ is magnified by 10). Observe $|\Delta(t)| \to \Delta_{\infty}$ in agreement with the few-spin conjecture. Here $\Delta_{0i} = 0.18\Delta_{\max}$, $\Delta_{0f} = 0.78\Delta_{\max}$, and $\delta\omega = -2.26\gamma$.

These in turn determine the "real" asymptotic amplitudes according to Eq. (2.51) and therefore the many-body wave function (1.29), which allows one to calculate various few-particle Green's functions.

As before, to verify the few-spin conjecture in the present case it is enough to check that the large-time asymptote of $\Delta(t)$ after the quench is given by Eq. (2.60) as long as $\vec{L}^2(u)$ has one pair of isolated complex conjugate roots (regions II and II′ in quench phase diagrams above). We do so numerically; see, e.g., Figs. 7 and 13 and Refs. [16,18]. The large-time asymptote of $|\Delta(t)|$ is in excellent agreement with Δ_{∞} derived as the imaginary part of the isolated root; see, e.g., Fig. 2 in Ref. [18]. This is, however, guaranteed by conservation laws without reliance on the few-spin conjecture. Indeed, suppose we find $\Delta(t) \to \tilde{\Delta}_{\infty} e^{-2i\tilde{\mu}_{\infty}t - 2i\tilde{\varphi}}$. Starting with this, one can retrace the steps that lead to Eq. (2.62) backwards and show that $\vec{L}^2(u)$ has a single pair of isolated complex conjugate roots at $\tilde{\mu}_{\infty} \pm i\tilde{\Delta}_{\infty}$. In other words, $\tilde{\mu}_{\infty} = \mu_{\infty}$, $\tilde{\Delta}_{\infty} = \Delta_{\infty}$, and the constant φ is arbitrary in the 0-spin solution, so we can always set $\tilde{\varphi} = \varphi$. Let us prove this somewhat differently using Bloch rather than BdG equations.

Going to a reference frame rotating around the z axis with frequency $2\tilde{\mu}_{\infty}$ eliminates time dependence in the asymptotic

$\Delta(t)$. In this frame, the effective magnetic field acting on each spin $\vec{s}_{\mathbf{p}}$ in Eq. (1.8) is $\vec{B}_{\mathbf{p}} = -2\tilde{\Delta}_{\infty}\hat{\mathbf{x}} + 2(\epsilon_{\mathbf{p}} - \tilde{\mu}_{\infty})\hat{\mathbf{z}}$ and is time independent. The spin therefore rotates around the field, making a constant angle (call it $\pi - \theta_{\mathbf{p}}$) with it. It is straightforward to determine spin components in this situation. They are given by Eq. (2.62) with $\mu_{\infty} \to \tilde{\mu}_{\infty}$, $\Delta_{\infty} \to \tilde{\Delta}_{\infty}$, and absent $e^{2i\mu_{\infty}t + 2i\varphi}$ on the left-hand side in the rotating frame.

Next we evaluate Lax vector (2.1) for this spin configuration. For u away from the real axis, summations over $\mathbf{p}$ can be safely replaced with integrations in the continuum limit and contributions from oscillating terms on the right-hand side of Eqs. (2.62) vanish at $t \to \infty$. The same cancellation occurs in the gap equation of motion (1.33), so that it becomes Eq. (5.4) that we will later also need in a different context. Using this gap equation to simplify the expression for $\vec{L}(u)$, we obtain

$$\vec{L}(u) = [\tilde{\Delta}_{\infty}\hat{\mathbf{x}} - (u - \tilde{\mu}_{\infty})\hat{\mathbf{z}}]L_{\infty}(u), \qquad (2.64)$$

where

$$L_{\infty}(u) = \frac{2}{g^2} - \sum_{\mathbf{p}} \frac{1}{2(u - \varepsilon_{\mathbf{p}})E_{\mathbf{p}}^{\infty}}. \qquad (2.65)$$

We see that $\vec{L}^2(u) = [\tilde{\Delta}_{\infty}^2 - (u - \tilde{\mu}_{\infty})^2]L_{\infty}^2(u)$ has a pair of isolated roots at $u = \tilde{\mu}_{\infty} \pm i\tilde{\Delta}_{\infty}$; i.e., the parameters of the asymptotic $\Delta(t)$ must coincide with those of an isolated root.

Finally, there is a general argument explaining why the actual quench dynamics at $t \to \infty$ should be described by the above asymptotic solutions derived from -1 and 0 spin solutions at least when $\vec{L}^2(u)$ has none or only one isolated root pair ($m = -1$ and 0). The general motion of a classical Hamiltonian integrable model with N degrees of freedom is quasiperiodic with N independent frequencies, $\vec{\omega} = (\omega_1, \ldots, \omega_N)$, which are determined solely by the values of its integrals of motion [63,64]. There are two types of (quasi)periodic motion: libration and rotation [65]. Let us explain this terminology with a 1D example. In libration, the coordinate returns to its initial value after each period, such as, e.g., the coordinate of a harmonic oscillator. In rotation, it increases each time by a fixed amount, such as, e.g., the angle of a rotating pendulum. Dynamical variables of libration type can be decomposed in a multidimensional Fourier series as

$$Q(t) = \sum_{\vec{m}} c_{\vec{m}} e^{i\vec{\omega}\cdot\vec{m}t}, \qquad (2.66)$$

where $\vec{m} = (m_1, \ldots, m_N)$ is a vector with integer components. Dynamical variables of rotation type contain an additional linear term, i.e.,

$$Q(t) = c_0 t + \sum_{\vec{m}} c_{\vec{m}} e^{i\vec{\omega}\cdot\vec{m}t}; \qquad (2.67)$$

see, e.g., Ref. [65] for further details. In our case, the absolute value of the order parameter, $|\Delta(t)|$ is of libration type, while its phase is of rotation type.

The frequency spectra of asymptotic solutions constructed above are $\omega(\varepsilon_{\mathbf{p}}) = 2\varepsilon_{\mathbf{p}}$ for $m = -1$ and $\omega(\varepsilon_{\mathbf{p}}) = 2\sqrt{(\varepsilon_{\mathbf{p}} - \mu_{\infty})^2 + \Delta_{\infty}^2}$ for $m = 0$. Important for us is that the spectra are continuous with no isolated frequencies in the thermodynamic limit. Since setting $2\sigma_{\mathbf{p}} = \cos\theta_{\mathbf{p}}$ ensures that the quench dynamics has the same integrals as this

solution (lives on the same invariant torus), it also must have an identical frequency spectrum. Assuming $|\Delta(t)|$ is continuously distributed over the spectrum as a collective variable, i.e., the discrete summation in Eq. (2.66) turns into a continuous Fourier transform, it must dephase at large times, $|\Delta(t)| \to$ const. Under the same assumption, the phase of the order parameter according to Eq. (2.67) must tend to a linear-in-time function as $t \to \infty$. Therefore, $\Delta(t)$ at large times is of the form $\Delta_\infty e^{-2i\mu_\infty t - 2i\varphi}$. Since finite Δ_∞ also implies an isolated root at $\mu_\infty \pm i\Delta_\infty$, while for $m = -1$ there are no isolated roots by definition, we must have $\Delta_\infty = 0$, i.e., $\Delta(t) \to 0$ in this case.

We also prove the few-spin conjecture for infinitesimal quenches in Sec. V D independently of above arguments and numerics.

2. $m = 1$

Suppose we found that for some initial condition (quench parameters) $\vec{L}^2(u)$ has two pairs of isolated complex conjugate roots $c, \bar{c}, c', \bar{c}'$. Given c and c', the above method allows us to determine the long-time asymptote of $\Delta(t)$, asymptotic spin configuration, and time-dependent Bogoliubov amplitudes $u_\mathbf{p}(t), v_\mathbf{p}(t)$ for the dynamics of the two-channel model (1.9) starting from this initial condition at $t = 0$.

By construction, c, c' are also the roots of $\vec{L}_m^2(u)$ furnishing the spectral polynomial for the reduced problem $Q_4(u) = (u - c)(u - \bar{c})(u - c')(u - \bar{c}')$ and therefore the parameters μ, ρ, κ, χ through Eq. (2.35). We further obtain from Eq. (2.41)

$$\Delta(t) = \sqrt{\Lambda^2 + h_1} \exp\left(-2i\mu t - i\int \frac{\kappa \, dt}{\Lambda^2 + h_1}\right), \quad (2.68)$$

where Λ is the Jacobi elliptic function dn,

$$\Lambda = \sqrt{h_3 - h_1} \, \mathrm{dn}\left[\sqrt{h_3 - h_1}(t - t_0), \sqrt{\frac{h_3 - h_2}{h_3 - h_1}}\right], \quad (2.69)$$

t_0 is a constant, and $h_3 \geqslant h_2 \geqslant h_1$ are the roots of the third-order polynomial $P_3(w) = w^3 + 4\rho w^2 + 4\chi w + \kappa^2$. The amplitude $|\Delta(t)|$ oscillates between a minimum $\Delta_b = \sqrt{h_2}$ and a maximum $\Delta_a = \sqrt{h_1}$. Plots of Δ_a, Δ_b, and h_1 for various quenches are shown in Figs. 9 and 10. As we now see, the parameter h_1 also quantifies the deviation from the weak-coupling limit, where $h_1 = 0$.

Of interest is the particular case when the parameter $\kappa = 0$. As we see below, this is realized for quenches deep within the weak-coupling BCS regime in the broad resonance limit when the two-channel model is equivalent to the BCS Hamiltonian (1.11). $\kappa = 0$ implies $h_1 = 0$, $4\chi = h_2 h_3$, $4\rho = -h_2 - h_3$, and $Q_4(u) = [(u - \mu)^2 - \rho]^2 - \chi$. Let $h_3 = \Delta_+^2$, $h_2 = \Delta_-^2$ in accordance with the notation of Eq. (2.38). The roots of $Q_4(u)$ in this case take a simple form with shared real part. Namely, they are

$$\mu \pm i\frac{\Delta_+ \pm \Delta_-}{2}, \quad (2.70)$$

and the expression (2.68) simplifies as well,

$$\Delta(t) = \Delta_+ \mathrm{dn}[\Delta_+(t - t_0)]e^{-2i\mu t - 2i\varphi}. \quad (2.71)$$

This expression for $\Delta(t)$ and the corresponding $m = 1$ spin solution were constructed in Ref. [7].

The general expression for the reduced spins obtain from Eqs. (2.23), (2.27), and (2.34),

$$\frac{\sigma_\mathbf{p}^z}{\sigma_\mathbf{p}} = -\frac{|\Delta|^2 - 2\xi_\mathbf{p}^2 + 2\rho}{2\sqrt{Q_4(\varepsilon_\mathbf{p})}},$$

$$\frac{\sigma_\mathbf{p}^-}{\sigma_\mathbf{p}} = -\frac{2\xi_\mathbf{p}\Delta - 2\mu\Delta + i\dot{\Delta}}{2\sqrt{Q_4(\varepsilon_\mathbf{p})}}, \quad (2.72)$$

where $\xi_\mathbf{p} = \varepsilon_\mathbf{p} - \mu$ and Δ is given by Eq. (2.68). Bogoliubov amplitudes corresponding to the 1-spin solution can now be derived from Eq. (2.58). The imaginary and real parts of the right-hand sides determine the absolute values of the amplitudes and their phases, respectively,

$$U_\mathbf{p} = \frac{\sqrt{2c_\mathbf{p}^+ - |\Delta|^2}}{2Q_4^{1/4}(\varepsilon_\mathbf{p})} e^{-i\mu t + i\xi_\mathbf{p} t} \exp\left[i\int \frac{\kappa - 4\xi_\mathbf{p} c_\mathbf{p}^+}{2c_\mathbf{p}^+ - |\Delta|^2} dt\right],$$

$$V_\mathbf{p} = \frac{\sqrt{2c_\mathbf{p}^- + |\Delta|^2}}{2Q_4^{1/4}(\varepsilon_\mathbf{p})} e^{i\mu t - i\xi_\mathbf{p} t} \exp\left[i\int \frac{\kappa + 4\xi_\mathbf{p} c_\mathbf{p}^-}{2c_\mathbf{p}^- + |\Delta|^2} dt\right], \quad (2.73)$$

where $c_\mathbf{p}^\pm = \sqrt{Q_4(\varepsilon_p)} \pm (\xi_\mathbf{p}^2 - \rho)$.

The common phase of the amplitudes $\alpha_\mathbf{p}$ is the sum of their phases in the above equations; i.e.,

$$\alpha_\mathbf{p} = \int \left[\frac{\kappa - 4\xi_\mathbf{p} c_\mathbf{p}^+}{2c_\mathbf{p}^+ - |\Delta|^2} + \frac{\kappa + 4\xi_\mathbf{p} c_\mathbf{p}^-}{2c_\mathbf{p}^- + |\Delta|^2}\right] dt. \quad (2.74)$$

The integrand is a periodic function of time. Therefore, $\alpha_\mathbf{p}$ is of the form (2.57), which is seen, e.g., by expanding the expression under the integral in Fourier series. The linear part $e_\mathbf{p} t$ comes from the zeroth harmonics. We only need to show that $e_\mathbf{p}$ is a nonconstant (dispersing) function of $\varepsilon_\mathbf{p}$. For this, we expand the integrand for large $\varepsilon_\mathbf{p}$, $e_\mathbf{p} = \varepsilon_\mathbf{p} + O(1)$. Therefore, $e_\mathbf{p}$ is indeed dispersing and the contribution of second terms on the right-hand sides of Eq. (2.55) to $\vec{L}(u)$ and $J_-(t)$ dephases similarly to $m = -1, 0$ cases. By few-spin conjecture the asymptotic behavior of $\Delta(t)$ is then given by Eqs. (2.68). The asymptotic spin configuration obtain by substituting Eqs. (2.74) and (2.72) into Eq. (2.55), where $\cos\theta_\mathbf{p} \equiv \cos(\varepsilon_\mathbf{p})$ is given by Eq. (2.49) and $e^{-i\phi_\mathbf{p}} = \sigma_\mathbf{p}^-/|\sigma_\mathbf{p}^-|$ straightforwardly derives from the second equation in Eq. (2.72).

As before, to verify the few-spin conjecture, it is sufficient to check that $\Delta(t)$ at large times after the quench is described by Eq. (2.68) whenever $\vec{L}^2(u)$ has two pairs of isolated roots. We do this numerically; see Figs. 8 and 14–16. In these plots we compare $\Delta(t)$ from direct numerical evolution of 5024 spins to Eq. (2.68), where parameters h_1, h_2, h_3, and μ obtain from the isolated roots of $\vec{L}^2(u)$. Note that there are no fitting parameters apart from an overall shift t_0 along the time axis.

III. QUENCH PHASE DIAGRAM AND ASYMPTOTIC SPIN DISTRIBUTION FOR THE TWO-CHANNEL MODEL

We established in the previous section that the long-time dynamics of the system after a quench are determined by
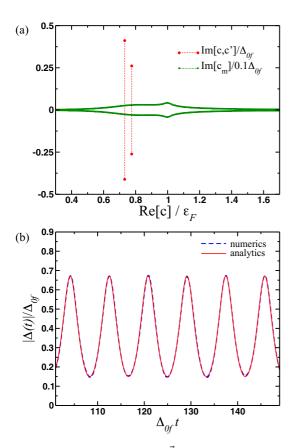
FIG. 14. (Color online) Roots of $\vec{L}^2(u)$ (top) and $|\Delta(t)|$ for a detuning quench in a 3D two-channel model with $N = 1024$ spins and $\gamma = 1.0$. There are two pairs of isolated roots $(c,\bar{c})$ and $(c',\bar{c}')$ and $N - 2$ continual roots close to the real axis. The large-time asymptote of $|\Delta(t)|$ is described by Eq. (2.68), where parameters h_i are extracted from the isolated roots, in agreement with the few-spin conjecture. The phase of $\Delta(t)$ is also in excellent agreement; see, e.g., Figs. 8 and 15. Quench parameters are $\Delta_{0i} = 2.68\Delta_{\max}$, $\Delta_{0f} = 0.76\Delta_{\max}$, and $\delta\omega = -4.13\gamma$.

the isolated complex roots of $\vec{L}^2(u)$. We now proceed to evaluate the roots and thus construct the quench phase diagram: identify all possible steady states for quenches throughout the BCS-BEC crossover. We find that, depending on the quench parameters, $\vec{L}^2(u)$ has zero, one, or two pairs of complex conjugate roots and the long-time behavior is therefore that described in Secs. II D, II D 1, or II D 2, respectively. Imaginary and real parts of the roots determine the parameters of the asymptotic behavior. For example, in the Volkov and Kogan regime (region II in our quench phase diagrams) where $\Delta(t \to \infty) \to \Delta_\infty e^{-2i\mu_\infty t - 2i\varphi}$, the roots are $\mu_\infty \pm i\Delta_\infty$. We first derive general equations for the roots, lines separating distinct regimes, and the asymptotic distribution function and then consider various cases, such as 2D and 3D, wide (one-channel) and narrow resonance limits, and deep BCS and BEC regimes.

After the quench the system evolves with the Hamiltonian (1.9), where $\omega = \omega_f$ starting from the spin configuration (1.28), which is the ground state for $\omega = \omega_i$. Since $\vec{L}^2(u)$ is conserved, we can evaluate it at any t. It is convenient to do so at $t = 0$. The Lax vector at $t = 0$ obtains by plugging the
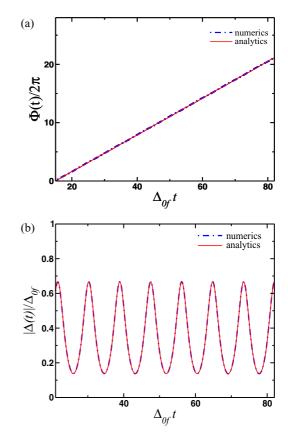

FIG. 15. (Color online) Magnitude and phase of $\Delta(t)$ in region III (two pairs of isolated roots) after detuning quench from deep BCS to BEC in a 3D two-channel model for $\gamma = 1$. Numerical evolution with 5024 spins against Eq. (2.68). Parameters h_1, h_2, etc., are obtained from isolated roots of $\vec{L}^2(u)$ as described in the text. $\Delta_{0i} = 2.65 \times 10^{-2}\Delta_{\max}$, $\Delta_{0f} = 0.80\Delta_{\max}$, $\mu_i = 1.00\varepsilon_F$, $\delta\omega = -4.59\gamma$.

initial condition into the definition (2.1)

$$\vec{L}(u)|_{t=0} = [\Delta_{0i}\hat{\mathbf{x}} - (u - \mu_i)\hat{\mathbf{z}}]L_0(u) - \frac{\delta\omega}{g^2}\hat{\mathbf{z}}, \quad (3.1)$$

where $\delta\omega = \omega_f - \omega_i$ and

$$L_0(u) = -\frac{2}{g^2} + \sum_{\mathbf{p}} \frac{1}{2(u - \varepsilon_{\mathbf{p}})E_i(\varepsilon_{\mathbf{p}})}, \quad (3.2)$$

$E_i(\varepsilon_{\mathbf{p}}) = E(\varepsilon_{\mathbf{p}}; \Delta_{0i}, \mu_i) = \sqrt{(\varepsilon_{\mathbf{p}} - \mu_i)^2 + \Delta_{0i}^2}$ and we also used the gap equation (1.18).

Taking the square of the above expression for $\vec{L}(u)$ and equating it to zero, we obtain an equation for the roots

$$(u - \mu_i \mp i\Delta_{0i})\left[\frac{2}{g^2} - \sum_{\mathbf{p}} \frac{1}{2(u - \varepsilon_{\mathbf{p}})E_i(\varepsilon_{\mathbf{p}})}\right] = \frac{\delta\omega}{g^2}. \quad (3.3)$$

Suppose first that the single-particle levels $\varepsilon_{\mathbf{p}}$ are discrete and there are $N \gg 1$ distinct $\varepsilon_{\mathbf{p}}$. Then this is a polynomial equation with $N + 1$ pairs of complex conjugate roots. Most of the pairs are close to the real axis, at distances of the order of the spacing between $\varepsilon_{\mathbf{p}}$, which is inversely proportional to N (system volume) and goes to zero in the thermodynamic limit. In the thermodynamic limit most of the roots of $\vec{L}^2(u)$ coalesce to the real axis merging with its poles to form a branch cut along

FIG. 17. (Color online) Roots of $\vec{L}^2(u)$ for the ground state of a 3D two-channel model for $N = 54$ spins and $\gamma = 1.0$. There are N doubly degenerate real roots c_m (shown as circles and squares), $N - 1$ of them located between discretized energy levels $\varepsilon_{\mathbf{p}} \to \varepsilon_m$, and two isolated complex roots $c_{\pm} = \mu_i \pm \Delta_{0i}$. Here $\Delta_{0i} = 0.1\varepsilon_F$.
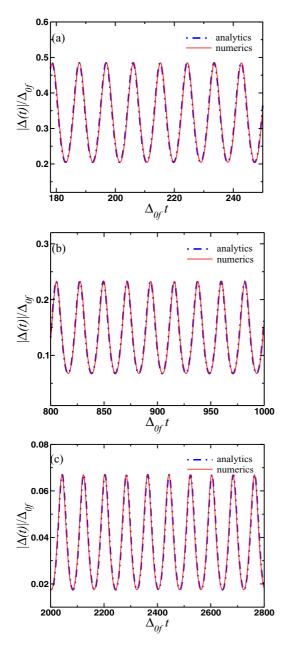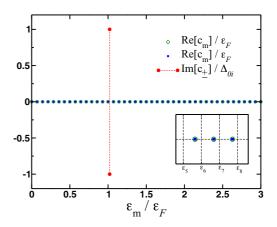

FIG. 16. (Color online) Postquench $|\Delta(t)|$ for a 3D two-channel model in region III, where $\vec{L}^2(u)$ has two pairs isolated roots. Numerical evolution with 5024 spins against Eq. (2.68). $\gamma = 0.1$, $\Delta_{0i} = 0.035\Delta_{\max}$ in all three panels. $\Delta_{0f}/\Delta_{\max} = 0.54, 0.67$, and 0.85 in (a)–(c), respectively.

the real axis. We fully verify this picture in this section and in Appendix B. Here we consider the roots whose imaginary part remains finite as $N \to \infty$ and in Appendix B we evaluate the roots with vanishing imaginary parts to order $1/N$.

Consider first the ground state. This corresponds to $\delta\omega = 0$ in Eq. (3.3) and $\vec{L}^2(u) = [(u - \mu)^2 + \Delta_0^2]L_0^2(u)$. There is a pair of complex roots at $c_{\pm} = \mu \pm i\Delta_0$. The remaining $2N$ roots solve $L_0(u) = 0$ and are double degenerate and real; see Fig. 17. This is because $L_0(u)$ goes from $+\infty$ to $-\infty$ as u goes from the left vicinity of one pole at $u = \varepsilon_{\mathbf{p}}$ to the right vicinity of the next one along the real axis, always crossing zero between consecutive $\varepsilon_{\mathbf{p}}$'s. In the thermodynamic

limit, spacings between $\varepsilon_{\mathbf{p}}$'s vanish and real zeros and poles merge into a continuous line. For $\delta\omega \neq 0$ the real roots acquire imaginary parts, each degenerate root splitting into a complex conjugate pair, as shown in Figs. 12–14. The imaginary parts, however, scale as $1/N$.

We first take the continuum limit in Eq. (3.3) for u away from the real axis. Then only isolated complex roots remain and we find that there are only zero, one, or two pairs of such roots depending on $\delta\omega$. At $\delta\omega = 0$ there are two isolated complex conjugate roots at $u = \mu_i \pm i\Delta_{0i}$. One pair of roots persists for sufficiently small $|\delta\omega|$, but beyond a certain threshold the number of isolated roots changes, as we now demonstrate. The continuum limit of Eq. (3.3) reads

$$\frac{2}{u - \mu_i \mp i\Delta_{0i}} \frac{\delta\omega}{\gamma} + \int_0^\infty \frac{f(\varepsilon)d\varepsilon}{(u - \varepsilon)E_i(\varepsilon)} = \frac{4}{\gamma}, \quad (3.4)$$

where, as always, we measure energies in units of ε_F and $f(\varepsilon)$ is the dimensionless density of states defined in Eq. (1.22).

As $\delta\omega$ is decreased or increased, the single pair of roots can collapse to the real axis or a new pair of isolated roots can emerge from it. The threshold (critical) value of $\delta\omega$ when this occurs is determined by looking for roots of Eq. (3.4) with an infinitesimal imaginary part. Replace $u \to u \pm i\delta$ in Eq. (3.4) and use $(u - \varepsilon \pm i\delta)^{-1} = P(u - \varepsilon)^{-1} \mp i\pi\delta(u - \varepsilon)$ to separate its real and imaginary parts. The latter yields critical values of $\delta\omega$ when the number of roots changes

$$\frac{|\delta\omega|}{\gamma} = \frac{\pi f(u)E_i(u)}{2\Delta_{0i}}, \quad (3.5)$$

where u is real positive and obtains from the real part of Eq. (3.4),

$$\fint_0^\infty \frac{f(\varepsilon)d\varepsilon}{(u - \varepsilon)E_i(\varepsilon)} + \text{sgn}(\delta\omega)\frac{\pi(u - \mu_i)f(u)}{E_i(u)\Delta_{0i}} = \frac{4}{\gamma}, \quad (3.6)$$

where the dashed integral indicates principal value.

The last two equations determine critical lines in quench phase diagrams shown in Figs. 2, 3, 20, and 21. We construct the diagrams in the $(\Delta_{0f}, \Delta_{0i})$ plane, ground-state gaps at final and initial detunings ω_i and ω_f. The resonance width

(dimensionless interaction strength) γ is fixed throughout the diagram. Δ_{0i}, Δ_{0f}, and γ uniquely determine μ_i, ω_i, and ω_f through ground-state Eqs. (1.25) and (1.26). Each point in this plane represents a particular quench of the detuning $\omega_i \rightarrow \omega_f$. We choose Δ_{0i} (or, equivalently, the ratio μ_i/Δ_{0i}) and the sign of $\delta\omega$ and solve Eq. (3.6) for real u. Equation (3.5) then yields the final detuning ω_f and therefore Δ_{0f}. We thus obtain a critical line, Δ_{0f} as a function of Δ_{0i}, in the $(\Delta_{0f}, \Delta_{0i})$ plane. The number of isolated root pairs changes by one as one crosses this line.

It turns out there is one critical line for either sign of $\delta\omega$. There are therefore three nonequilibrium phases or regimes, qualitatively different long-time behaviors, indicated as regions I, II (including subregion II'), and III in Figs. 2, 3, 20, and 21. Region II contains the $\Delta_{0f} = \Delta_{0i}$ or, equivalently, $\omega_f = \omega_i$ line, which corresponds to no quench, i.e., to the system remaining in the ground state at all times. Therefore, in region II Eq. (3.4) yields a single pair of isolated complex roots $u = \mu_\infty \pm i\Delta_\infty$. This, in turn, implies that $\Delta(t) \rightarrow \Delta_\infty e^{-2i\mu_\infty t - 2i\varphi}$ as $t \rightarrow \infty$. For all quenches in region II the system thus goes into the asymptotic state described in Sec. II D 1.

Negative $\delta\omega$ corresponds to $\Delta_{0f} > \Delta_{0i}$. As we cross the critical line going from region II into region III the number of isolated root pairs changes by one. It can be shown both analytically and numerically by analyzing Eq. (3.4) that this number increases; i.e., there are two pairs of complex conjugate isolated roots in region III. For quenches in this part of the diagram the large-time asymptote of $\Delta(t)$ is given by Eq. (2.68) and the large-time state of the system is that obtained in Sec. II D 2. Plots of Δ_∞ and μ_∞ as functions of Δ_{0f} at two fixed values of Δ_{0i} are shown in Figs. 18 and 19.

Similarly, as we enter region I from region II, $\Delta_\infty \rightarrow 0$ and the single pair of isolated roots collapses to the real axis at the critical line. There are hence no isolated roots in region I and therefore $\Delta(t) \rightarrow 0$ for quenches in this regime and the system goes into the gapless steady state detailed at the beginning of Sec. II D.

Of interest is the line along which the real part of the root pair $\mu_\infty \pm i\Delta_\infty$ in region II vanishes, i.e., $\mu_\infty = 0$ (the line separating subregions II and II' in quench phase diagrams). This can be thought of as a nonequilibrium extension of the BCS-BEC crossover going from a positive to a negative chemical potential. Out of equilibrium, as we see below, the change of sign of μ_∞ affects the approach of $\Delta(t)$ to its asymptote. For example, in 3D the approach changes from $1/t^{1/2}$ in II to $1/t^{3/2}$ in II'. Setting $u = \pm i\Delta_\infty$ in Eq. (3.4) and separating the real and imaginary parts, we obtain equations determining this line,

$$\frac{\mu_i}{\Delta_{0i} - \Delta_\infty} \text{Im}\,\mathcal{F} + \text{Re}\,\mathcal{F} = \frac{4}{\gamma},$$

$$\frac{\delta\omega}{\gamma} \frac{2(\Delta_\infty - \Delta_{0i})}{\mu_i^2 + (\Delta_\infty - \Delta_{0i})^2} = \text{Im}\,\mathcal{F}, \tag{3.7}$$

where

$$\mathcal{F} = \int_0^\infty \frac{f(\varepsilon)d\varepsilon}{(i\Delta_\infty - \varepsilon)E_i(\varepsilon)}. \tag{3.8}$$
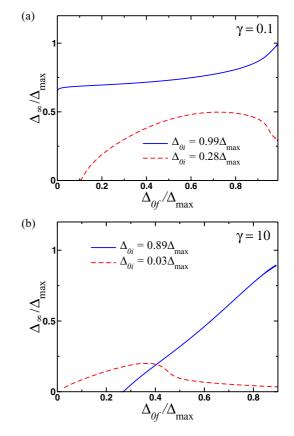

FIG. 18. (Color online) $\Delta(t) \rightarrow \Delta_\infty e^{-2i\mu_\infty t - 2i\varphi}$ as $t \rightarrow \infty$ after a detuning quench $\omega_i \rightarrow \omega_f$ in a 3D two-channel model in region II of the quench phase diagram in Fig. 3. Δ_∞ extracted from the single isolated root pair of the Lax vector norm is shown as a function of Δ_{0f} (ground-state gap for ω_f) at two fixed values of Δ_{0i} (ground-state gap for the initial detuning ω_i). Note that $\Delta_\infty > \Delta_{0f}$ for BEC to BCS quenches $\Delta_{0i} = 0.99\Delta_{\max}$ for $\gamma = 0.1$.

Equation (3.7) determines the $\mu_\infty = 0$ line via a procedure similar to that for critical lines separating region I from II and II from III. For a given Δ_{0i}, the first equation yields Δ_∞. We then find $\delta\omega$ and consequently ω_f and Δ_{0f} from the second equation.

Note the intersection of the $\mu_\infty = 0$ line with the $\Delta_{0i} = \Delta_{0f}$ (no-quench) line. Along the latter line we also have $\Delta_\infty = \Delta_{0i}$ and, therefore, at the intersection point $\mu_i = \mu_f = 0$ or the first term in the first equation in Eq. (3.7) would blow up. In equilibrium $\mu = 0$ corresponds to a certain ground-state gap $\Delta_0 = \Delta_{0\times}$, which obtains from Eq. (1.25) and provides a characteristic energy scale for the crossover from the BCS to BEC regime. Vanishing of μ_i and μ_f at the intersection point implies that straight lines $\Delta_{0i} = \Delta_{0\times}$, $\Delta_{0f} = \Delta_{0\times}$, and $\Delta_{0i} = \Delta_{0f}$ and the $\mu_\infty = 0$ line must cross at the same point, which is indeed seen in all quench phase diagrams in Figs. 2, 3, 20, and 21.

Let us also obtain an explicit expression for the asymptotic spin distribution function Eq. (2.49) in all three regimes. Equation (3.1) implies

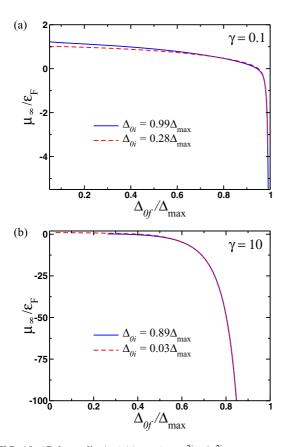$$\vec{L}^2(u) = \Delta_{0i}^2 L_0^2(u) + \left[(u - \mu_i)L_0(u) + \frac{\delta\omega}{g^2}\right]^2. \tag{3.9}$$

FIG. 19. (Color online) $\Delta(t) \to \Delta_\infty e^{-2i\mu_\infty t - 2i\varphi}$ as $t \to \infty$ after a detuning quench $\omega_i \to \omega_f$ in a 3D two-channel model in region II of the quench phase diagram in Fig. 3, where μ_∞ plays the role of the out-of-equilibrium analog of the chemical potential. Here μ_∞ is extracted from the single isolated root pair of the Lax vector norm and is shown as a function of Δ_{0f} (ground-state gap for ω_f) at two fixed values of Δ_{0i} (ground-state gap for the initial detuning ω_i). Note that μ_∞ behaves similarly to the ground-state chemical potential in Fig. 1.

In the thermodynamic limit,

$$L_0(u) = -\frac{2}{g^2} + \int_0^\infty \frac{f(\varepsilon)d\varepsilon}{2(u - \varepsilon)E_i(\varepsilon)}. \tag{3.10}$$

We evaluate $L_0(\varepsilon_\pm)$ using $(\varepsilon - \varepsilon' \pm i\delta)^{-1} = P(\varepsilon - \varepsilon')^{-1} \mp i\pi\delta(\varepsilon - \varepsilon')$. This results in

$$\cos\theta(\varepsilon) = \frac{z(\varepsilon)}{i\pi f(\varepsilon)}\sqrt{A_-^2 \Delta_{0i}^2 + \left[(\varepsilon - \mu_i)A_- + \frac{\delta\omega}{\gamma}\right]^2}$$
$$- \frac{z(\varepsilon)}{i\pi f(\varepsilon)}\sqrt{A_+^2 \Delta_{0i}^2 + \left[(\varepsilon - \mu_i)A_+ + \frac{\delta\omega}{\gamma}\right]^2}, \tag{3.11}$$

where

$$A_\mp = -\frac{2}{\gamma} \pm \frac{i\pi f(\varepsilon)}{2E_i(\varepsilon)} + \int_0^\infty \frac{f(\varepsilon')d\varepsilon'}{2(\varepsilon - \varepsilon')E_i(\varepsilon')}. \tag{3.12}$$

The integral here is the same as in Eq. (3.6). We evaluate it in elementary functions in 2D, in the weak-coupling BCS
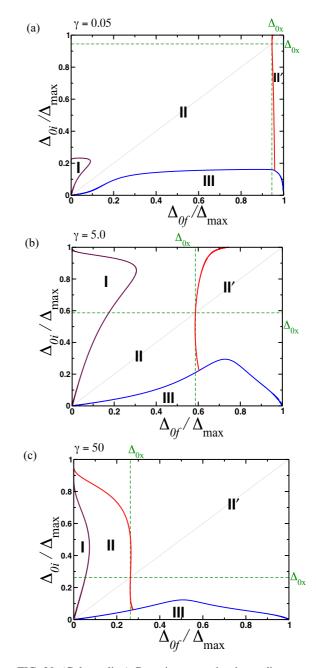

FIG. 20. (Color online) Detuning quench phase diagrams for two-channel model in 2D for various resonance widths γ obtained from Eqs. (3.16) and (3.17). Each point represents a single quench labeled by Δ_{0i} and Δ_{0f}, pairing gaps the system would have in the ground state for initial and final detunings. At large times the system ends up in one of three steady states shown as regions I, II (including II'), and III. For quenches in region I the order parameter vanishes. In II $\Delta(t) \to \Delta_\infty e^{-2i\mu_\infty t - 2i\varphi}$ and III $|\Delta(t)|$ oscillates persistently. Subregions II and II' differ in the sign of μ_∞ (out-of-equilibrium analog of the chemical potential): $\mu_\infty > 0$ in II and $\mu_\infty < 0$ in II'. The diagonal, $\Delta_{0i} = \Delta_{0f}$, is the no-quench line. $\Delta_{0\times}$ is the ground-state gap corresponding to zero chemical potential; i.e., $\Delta_{0\times}$ is given by Eq. (1.25) for $\mu = 0$.

regime, and in BEC regime in Secs. III A and III B below; see also Eqs. (B4) through (B7) for explicit expressions. Note $\cos\theta(\varepsilon) = 1$ for $\delta\omega = 0$ (no quench) as it should.
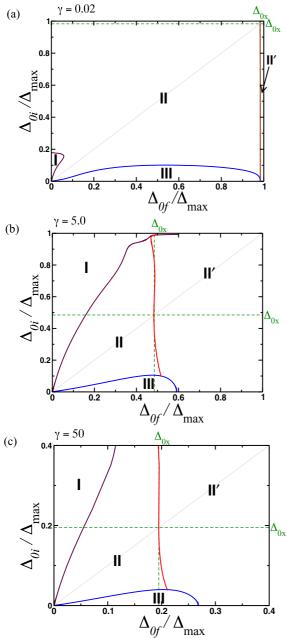
FIG. 21. (Color online) Detuning quench phase diagrams for a two-channel model in 3D for various resonance widths γ obtained from Eqs. (3.40) and (3.41) (otherwise, the same as Fig. 20).

Representative plots of the spin distribution function for two quenches appear in Fig. 11. For future use we also write the first two terms in large ε expansion of Eq. (3.11),

$$\cos\theta(\varepsilon) \approx 1 - \left(\frac{\delta\omega}{\gamma}\right)^2 \frac{2\Delta_{0i}^2}{E_i^2(\varepsilon)[H^2(\varepsilon) + \pi^2 f^2(\varepsilon)]}, \quad (3.13)$$

which are also independently the first two terms in its small $\delta\omega$ expansion. The function $H(\varepsilon)$ is defined in Eq. (B8).

Next, we consider 2D and 3D separately, as well as various special cases such as wide (single-channel limit) and narrow resonance and deep BCS and BEC regimes.

A. 2D

In 2D the dimensionless density of states $f(\varepsilon) = 1$ and all integrals above in this section can be evaluated in terms of elementary functions. It is convenient to introduce a notation:

$$x = \frac{\mu_i}{\Delta_{0i}}, \quad v = \frac{u - \mu_i}{\Delta_{0i}}. \quad (3.14)$$

Equation (3.4) reads

$$\ln\left[-\frac{(v+x)(v+\sqrt{1+v^2})}{\sqrt{1+x^2}\sqrt{1+v^2} - xv + 1}\right]$$
$$= -\frac{2\delta\omega(v \mp i)}{\gamma\sqrt{1+v^2}} + \frac{4\Delta_{0i}}{\gamma}\sqrt{1+v^2}. \quad (3.15)$$

The critical lines separating the three asymptotic regimes are determined by Eqs. (3.6) and (3.5), which become

$$\frac{|\delta\omega|}{\gamma} = \frac{\pi}{2}\sqrt{1+v^2}, \quad (3.16)$$

$$\ln\left[\frac{(v+x)(v+\sqrt{1+v^2})}{\sqrt{1+x^2}\sqrt{1+v^2} - xv + 1}\right]$$
$$= -\text{sgn}(\delta\omega)\pi v + \frac{4\Delta_{0i}}{\gamma}\sqrt{1+v^2}, \quad (3.17)$$

where v is real and $v > -x$. It is straightforward to analyze Eq. (3.17) graphically and to find v and thus the critical lines numerically.

Positive $\delta\omega$ mean $\Delta_{0f} > \Delta_{0i}$ and the corresponding v determine the critical line separating regions I and II. In this case, for γ above a certain threshold γ_c to be determined below, there is a single root for any Δ_{0i}. This means that a horizontal $\Delta_{0i} = \text{const}$ line intersects the I-II line once for any value of the const and region I therefore extends all the way up to $\Delta_{0i} = \sqrt{\gamma} = \Delta_{\max}$ as seen in Figs. 2(c), 20(b), and 20(c). When $\gamma < \gamma_c$, the number of roots for positive $\delta\omega$ changes from one to two and then to zero as Δ_{0i} increases. The I-II line then displays peculiar reentrant behavior; see the inset in Fig. 2(b).

Negative $\delta\omega$ means $\Delta_{0f} < \Delta_{0i}$. The roots v in this case yield the II-III critical line. There are two roots for Δ_{0i} below a certain threshold and no roots above it, implying that a horizontal $\Delta_{0i} = \text{const}$ line intersects the II-III critical line twice for a sufficiently small value of the const.

The shape of the critical lines as well as the complex roots of Eq. (3.15) can be determined analytically when the initial and/or final value of the detuning ω is deep in the BCS or BEC regime. The BCS limit corresponds to detuning $\omega \to +\infty$. For the ground state this implies $\mu \to \varepsilon_F = 1$, $\Delta_0 \to 0$. The gap equation (1.26) then yields

$$\ln\frac{4\varepsilon_\Lambda}{\Delta_0^2} = \frac{2\omega - 4}{\gamma}. \quad (3.18)$$

The deep BEC regime obtains when $\omega \to -\infty$. In this case $\mu \to -\infty$ in the ground state. The gap and chemical potential equations switch roles in the sense that the former determines the chemical potential and the latter the ground-state gap. Equation (1.26) becomes

$$\ln\frac{\varepsilon_\Lambda}{|\mu|} = \frac{2\omega + 4|\mu|}{\gamma} \quad (3.19)$$

and Eq. (1.25) reads in this limit

$$\Delta_0 = \left(\frac{1}{\gamma} + \frac{1}{4|\mu|} \right)^{-1/2}. \tag{3.20}$$

First, we consider quenches originating deep in the BCS regime; i.e., $\omega_i \to +\infty$ and, therefore, $\Delta_{0i} \to 0$, $\mu_i \to 1$. Such initial states correspond to $x \to +\infty$. Equation (3.17) becomes

$$\ln \left[\frac{(v+x)(\sqrt{1+v^2}+v)}{x(\sqrt{1+v^2}-v)} \right] = -\text{sgn}(\delta\omega)\pi v. \tag{3.21}$$

The roots are $v \to 0$ for either sign of $\delta\omega$ and $v \to -x + 0$ for $\delta\omega < 0$. This translates into

$$u \approx \begin{cases} \mu_i, & \delta\omega > 0, \\ \mu_i \text{ or } +0, & \delta\omega < 0. \end{cases} \tag{3.22}$$

For $v \to 0$ Eq. (3.16) yields $\delta\omega/\gamma = \pm\pi/2$. Therefore, both Δ_{0f} and Δ_{0i} are deep in the BCS regime. The gap equation Eq. (3.18) implies $\Delta_0 \propto \exp(-\omega/\gamma)$ and, hence,

$$\frac{\Delta_{0i}}{\Delta_{0f}} = e^{\pm\pi/2}. \tag{3.23}$$

This result has been already obtained in Refs. [17,18], which studied quenches within the single-channel model in the weak-coupling (BCS) limit. Weak coupling means small Δ_{0i} and Δ_{0f}, which corresponds to a vicinity of the origin, $\Delta_{0i} = \Delta_{0f} = 0$, in our phase diagrams. Equation (3.23) is the slope of the I-II and II-III critical lines at the origin in Figs. 2, 3, 20, and 21.

As we see below, Eq. (3.23) also holds in 3D. This is expected on general grounds because, in the BCS limit, superconducting correlations come from a narrow energy window around the Fermi energy. The main contribution to integrals determining the roots comes from these energies. The density of states is then well approximated by a constant rendering the 2D and 3D cases equivalent.

The second root at $\delta\omega < 0$, $v \to -x + 0$, yields $\delta\omega/\gamma \approx -\pi x/2$. This means that the initial state is deep in the BCS regime, while $\omega_f \to -\infty$ and the ground state at ω_f is in the BEC limit. Further, $\mu_i \to \varepsilon_F = 1$, so $x \approx 1/\Delta_{0i}$. Subtracting Eq. (3.18) from Eq. (3.19), we obtain

$$\ln \frac{\Delta_{0i}^2}{4|\mu_f|} = -\frac{\pi}{\Delta_{0i}} + \frac{4|\mu_f|}{\gamma} + \frac{4}{\gamma}. \tag{3.24}$$

Here we assume that γ is finite and treat the single-channel limit $\gamma \to \infty$ separately below. Since the $1/\Delta_{0i}$ term diverges much faster than the logarithm in the above equation, we get $4|\mu_f| \approx \pi\gamma/\Delta_{0i}$. Equation (3.20) now obtains

$$\frac{\Delta_{0f}}{\Delta_{max}} = 1 - \frac{\Delta_{0i}}{2\pi}. \tag{3.25}$$

This equation shows that the II-III critical line terminates at $(\Delta_{0f}, \Delta_{0i}) = (\Delta_{max}, 0)$ linearly with a slope $\Delta_{0i}/(\Delta_{0f} - \Delta_{max}) = -2\pi/\sqrt{\gamma}$.

Simpler expressions can also be derived for complex roots for quenches within the BCS regime, i.e., in the vicinity of the of the origin in the phase diagrams. By Eq. (3.22) the real parts of the roots in this regime $\text{Re}[u] \approx \mu_i \approx \varepsilon_F$. Then v is purely imaginary and also $|v| \ll x$ because $\text{Im}[u]$ is related to

the asymptotic value of order-parameter amplitude, which is much smaller than ε_F. Equation (3.15) becomes

$$\ln \left[\frac{v + \sqrt{1+v^2}}{v - \sqrt{1+v^2}} \right] = -\frac{v \mp i}{\sqrt{1+v^2}} \frac{2\delta\omega}{\gamma}. \tag{3.26}$$

This equation is symmetric with respect to complex conjugation and with respect to $v \to -v$. The latter symmetry reflects emergence of the particle-hole symmetry in the BCS limit. Note that when there is only one root, these two symmetries together require that it be purely imaginary.

Let $v = -i \cosh\phi$ in Eq. (3.26), where ϕ is either purely real or purely imaginary, so that v is purely imaginary. Equation (3.26) yields, depending on the sign choice on the right-hand side,

$$\phi = -\frac{\delta\omega}{\gamma} \coth(\phi/2), \tag{3.27}$$

$$\phi = -\frac{\delta\omega}{\gamma} \tanh(\phi/2). \tag{3.28}$$

Note that in this regime $\delta\omega/\gamma = \ln(\Delta_{0i}/\Delta_{0f})$. It is straightforward to analyze these equations graphically and to determine when they have solutions. We summarize the results.

Region I: $\Delta_{0i}/\Delta_{0f} > e^{\pi/2}$. There are no isolated roots and, hence, $\Delta(t) \to 0$ at large times.

Region II: $e^{-\pi/2} < \Delta_{0i}/\Delta_{0f} < e^{\pi/2}$. There is a single pair of isolated roots at $\mu_\infty \pm i\Delta_\infty$,

$$\mu_\infty = \varepsilon_F, \quad \Delta_\infty = \Delta_{0i} \cosh\phi, \tag{3.29}$$

where ϕ is real for $\delta\omega < 0$ and imaginary for $\delta\omega > 0$ and is the solution of Eq. (3.27). One can show $\Delta_\infty \leqslant \Delta_{0f}$ for any $\delta\omega$, where the equality is achieved only at $\delta\omega = 0$. The long-time dynamics is that described in Sec. II D 1.

It is instructive to evaluate Δ_∞, the asymptotic value of the magnitude of the gap, for infinitesimal quenches, when $|\Delta_{0f} - \Delta_{0i}| \ll \Delta_{0i}$. Expanding Eqs. (3.27) and (3.29) in small ϕ, we obtain, after some calculation,

$$\Delta_\infty = \Delta_{0f} - \frac{(\Delta_{0f} - \Delta_{0i})^2}{6\Delta_{0f}}. \tag{3.30}$$

Note that within linear analysis $\Delta_\infty = \Delta_{0f}$. As we show in Sec. V, this is a general feature of linearized dynamics around the ground state regardless of coupling strength or initial conditions: $|\Delta(t)|$ tends to its ground-state value corresponding to the Hamiltonian with which the system evolves at $t > 0$.

Region III: $\Delta_{0i}/\Delta_{0f} < e^{-\pi/2}$. There are two pairs of complex conjugate roots,

$$\varepsilon_F \pm i\Delta_{0i} \cosh\phi_1, \quad \varepsilon_F \pm i\Delta_{0i} \cosh\phi_2, \tag{3.31}$$

where ϕ_1 is the solution of Eq. (3.27) and ϕ_2 is the solution of Eq. (3.28); ϕ_2 is real when $\delta\omega/\gamma = \ln(\Delta_{0i}/\Delta_{0f}) \leqslant -2$ and imaginary otherwise. We see that the roots are indeed of the form Eq. (2.70). The asymptotic state is that of Sec. II D 2, while $\Delta(t)$ takes the simplified form Eq. (2.71).

Just as in Eq. (3.23), the above results starting with Eq. (3.26) are universal in that they hold for quenches within the BCS regime independent of the dimensionality and also hold for the single-channel model.

Next, consider quenches originating deep in the BEC, which corresponds to $\mu_i \to -\infty$, $\Delta_{0i} \to \sqrt{\gamma}$, and $x \to -\infty$. Since $v > -x$ in Eq. (3.17), we also have $v \to \infty$ provided a real root exists. Equation (3.17) for $\delta\omega > 0$ simplifies to

$$\ln\left[\frac{v+x}{|x|}\right] = v\left(\frac{4\Delta_{0i}}{\gamma} - \pi\right). \qquad (3.32)$$

For $4\Delta_{0i}/\gamma < \pi$, there is a single root at $v \to -x$, which corresponds to $u \approx 0$. Since $\Delta_{0i} \leqslant \sqrt{\gamma} = \Delta_{\max}$, the condition $\Delta_{0i} < \pi\gamma/4$ can be fulfilled only if $\gamma > \gamma_c$, where

$$\gamma_c = \frac{16}{\pi^2}. \qquad (3.33)$$

For $\gamma \geqslant \gamma_c$ Eq. (3.17) at $\delta\omega > 0$ has a single root for any Δ_{0i} and, in particular, for $\Delta_{0i} \to \Delta_{\max}$. This means that the I-II critical line extends all the way up to $\Delta_{0i} = \Delta_{\max}$, terminating at $(\Delta_{0i}, \Delta_{0f}) = (\Delta_{\max}, 0)$.

It is interesting to work out the shape of the I-II critical line near its termination point. First, let $\gamma > \gamma_c$. Since $v \approx -x$, Eq. (3.16) implies $\delta\omega/\gamma \approx \pi|x|/2$. Using Eqs. (3.19) and (3.20) to determine Δ_{0i} and μ_i and Eq. (3.18) for Δ_{0f}, we get

$$\frac{\Delta_{0f}}{\Delta_{\max}} = \frac{1}{\sqrt{2\varepsilon}} \exp\left(-\frac{\alpha}{2\varepsilon}\right),$$
$$\varepsilon = \frac{\Delta_{\max} - \Delta_{0i}}{\Delta_{\max}}, \quad \alpha = \sqrt{\frac{\gamma}{\gamma_c}} - 1. \qquad (3.34)$$

This behavior is seen in Figs. 2(c), 20(b), and 20(c). Note the difference between $\gamma = 5$ and $\gamma = 50$ in Figs. 20(b) and 20(c) that correspond to $\alpha \approx 0.8$ and $\alpha \approx 4.6$, respectively.

Next, let $\gamma < \gamma_c$. In this case, the I-II critical line goes up, then bends backward, reaching a maximum, goes down, and terminates on the Δ_{0i} axis below $\Delta_{\max}$; see, e.g., the inset in Fig. 2(b). Near the termination point μ_i and ω_i are finite since $\Delta_{0i} < \Delta_{\max}$, while $\omega_f \to \infty$ since $\Delta_{0f} \to 0$. Equation (3.16) implies $v \to \infty$ and $\delta\omega/\gamma \approx \pi v/2$. In this limit, Eq. (3.17) becomes

$$\ln\left[\frac{2v}{\sqrt{1+x^2} - x}\right] = v\left(\frac{4\Delta_{0i}}{\gamma} - \pi\right). \qquad (3.35)$$

We see that v diverges as $\Delta_{0i} \to \pi\gamma/4 = \pi\sqrt{\gamma}\Delta_{\max}/4 \equiv \Delta_{\text{th}}$. Therefore, the I-II critical line terminates at $(\Delta_{0i}, \Delta_{0f}) = (\Delta_{\text{th}}, 0)$. For Δ_{0i} above Δ_{th} and below a certain upper value, which we do not determine explicitly, Eq. (3.17) has two roots. For Δ_{0i} below Δ_{th} there is one root.

The shape of the I-II critical line as it approaches the termination point for $\gamma < \gamma_c$ obtains from Eq. (3.35). Let $\varepsilon = (\Delta_{0i} - \Delta_{\text{th}})/\Delta_{\text{th}} \ll 1$. Equation (3.35) implies

$$v \approx \frac{1}{\pi\varepsilon} \ln\left[\frac{2(\sqrt{1+x^2} + x)}{\pi\varepsilon}\right]. \qquad (3.36)$$

The gap equation (1.26) yields in 2D

$$\sqrt{1+x^2} + x = \frac{2(\gamma - \Delta_{0i}^2)}{\gamma\Delta_{0i}}. \qquad (3.37)$$

Since $\omega_f \to \infty$ corresponds to the BCS limit, we have $\Delta_{0f} \propto e^{-\omega_f/\gamma} \propto e^{-\pi v/2}$. Combining this with the last two equations

and using $\Delta_{0i} \approx \Delta_{\text{th}} = \pi\gamma/4$, we get

$$\Delta_{0f} = C\exp\left(-\frac{1}{2\varepsilon}\ln\left[\frac{\gamma_c - \gamma}{\gamma\varepsilon}\right]\right), \qquad (3.38)$$

where C is independent of ε.

The I-II critical line for $\gamma < \gamma_c$ is shown in Figs. 2(a), 2(b), and 20(a), which correspond to $\Delta_{\text{th}}/\Delta_{\max} \approx 0.25, 0.78$, and 0.18, respectively. Δ_{th} appears somewhat larger in these plots since exponentially small, but finite, Δ_{0f} in Eq. (3.38) is not noticeable; the critical line effectively goes down along the Δ_{0i} axis. In the same way, the I-II critical line appears to terminate below $\Delta_{\max}$ in Fig. 20 for $\gamma = 50$ due to exponential smallness of Δ_{0f} in Eq. (3.34).

B. 3D

Three-dimensional diagrams for various values of resonance width γ are shown in Figs. 3 and 21. Overall, they are qualitatively similar to 2D diagrams. A notable difference is that, in 3D, region III of the oscillating order parameter $\Delta(t)$ for sufficiently large γ terminates at $\Delta_{0f} < \Delta_{\max} = \sqrt{2\gamma/3}$. This means that quenches from infinitesimally weak to sufficiently strong coupling produce no oscillations. Also, in contrast to the 2D case, the critical line separating the gapless region I, in principle, always extends all the way up to $\Delta_{0i} = \Delta_{\max}$ and terminates at $\Delta_{0f} = \Delta_{0f}^{\text{I-II}} > 0$. This is, however, not noticeable at small γ because in this case the value of $\Delta_{0f}^{\text{I-II}}$ is exponentially small.

In 3D the dimensionless density of states $f(\varepsilon) = \sqrt{\varepsilon}$ and Eq. (3.4) becomes

$$\int_{-x}^{\infty} \frac{dy\sqrt{\Delta_{0i}(x+y)}}{(v-y)\sqrt{y^2+1}} = -\frac{2\delta\omega}{\gamma(v \pm i)} + \frac{4\Delta_{0i}}{\gamma}, \qquad (3.39)$$

where $y = \varepsilon/\Delta_{0i} - x$, and x and v are defined in Eq. (3.14). Similarly, Eqs. (3.6) and (3.5) determining critical lines read

$$\frac{|\delta\omega|}{\gamma} = \frac{\pi}{2}\sqrt{\Delta_{0i}(x+v)(v^2+1)}, \qquad (3.40)$$

$$\int_{-x}^{\infty}\frac{dy\sqrt{\Delta_{0i}(x+y)}}{(v-y)\sqrt{y^2+1}} + \text{sgn}(\delta\omega)\frac{\pi v\sqrt{\Delta_{0i}(x+v)}}{\sqrt{v^2+1}} = \frac{4\Delta_{0i}}{\gamma}, \qquad (3.41)$$

The integral here is a complete elliptic integral. Substitution $y = 1/t - x$ reduces it to one of the Carlson elliptic integrals with known asymptotic behaviors in various regimes [66,67]. We, however, find it more convenient to evaluate the limiting behaviors by a direct analysis of the integral.

First, we consider initial states deep in the BCS regime, i.e., $\omega_i \to +\infty$, which implies $\Delta_{0i} \to 0$, $\mu_i \to 1$, and $x \to 1/\Delta_{0i} \to +\infty$. To evaluate the integral in Eqs. (3.39) and (3.41) in this regime, we split the integration range into three intervals—$(-x, -y_\Lambda), (-y_\Lambda, y_\Lambda)$, and (y_Λ, ∞)—where y_Λ is such that $1 \ll y_\Lambda \ll x$. Let the corresponding integrals be I_1, I_2, and I_3. To the leading order in $1/y_\Lambda$ and y_Λ/x we can replace $\sqrt{y^2+1} \to |y|$ in I_1 and I_3 and replace $\sqrt{x+y} \to \sqrt{x}$ in I_2. The resulting integrals evaluate in terms

of elementary functions

$$I_1 + I_3 = \frac{2\sqrt{x}}{v} \ln \frac{4x}{y_\Lambda}$$
$$- \frac{\sqrt{x+v}}{v} \ln \frac{4x(\sqrt{x+v} + \sqrt{x})^2}{y_\Lambda^2 - 4x(\sqrt{x+v} - \sqrt{x})^2},$$

$$I_2 = \frac{\sqrt{x}}{\sqrt{1+v^2}} \ln \frac{(\sqrt{1+v^2}\sqrt{1+y_\Lambda^2} + vy_\Lambda)(v + y_\Lambda)}{(\sqrt{1+v^2}\sqrt{1+y_\Lambda^2} - vy_\Lambda)(v - y_\Lambda)},$$

where we used $1 \ll y_\Lambda \ll x$ to simplify expressions. The dependence on y_Λ should, of course, cancel from $I_1 + I_2 + I_3$ to the leading order in $1/y_\Lambda$ and y_Λ/x.

The gap equation (1.26) in the BCS regime is handled similarly by splitting the integral into three, resulting in

$$\frac{\omega}{\gamma} - \frac{2}{\gamma} = \sqrt{\varepsilon_\Lambda} - 2 + \ln \frac{8}{\Delta_0}. \quad (3.42)$$

Suppose the final detuning is also in the BCS regime. The above equation then implies

$$\frac{\delta\omega}{\gamma} = \ln \frac{\Delta_{0i}}{\Delta_{0f}}, \quad (3.43)$$

the same as in 2D. Because $\delta\omega/\gamma$ must remain of order one as $x \to +\infty$, it follows from Eq. (3.40) that v is also of order one for quenches within the BCS regime. Therefore, $|v| \ll y_\Lambda$ in the above expressions for $I_1 + I_2$ and I_3. We obtain $|I_1 + I_2| \ll 1$ and

$$I_1 + I_2 + I_3 \approx I_3 \approx \frac{1}{1+v^2} \ln \left[\frac{v + \sqrt{1+v^2}}{v - \sqrt{1+v^2}} \right]. \quad (3.44)$$

Equation (3.39) now turns into the 2D Eq. (3.26), and Eq. (3.40) yields $|\delta\omega|/\gamma = \pi/2$ and therefore Eq. (3.23). Thus, quenches within the BCS regime in 3D are identical to those in 2D and all results from Eq. (3.26) to Eq. (3.31) also hold in 3D. As we already commented above, this is expected since in the BCS regime superconductivity comes from the vicinity of the Fermi energy, making the dependence of the density of states on the energy and thus the dimensionality inessential.

The horizontal $\Delta_{0i} = $ const line for infinitesimal values of the const intersects the II-III critical line twice, once near the origin and the second time near the termination point of the II-III critical line. The former intersection corresponds to small v, as we saw above, and the latter to v of order x. To determine the termination point, we therefore take $|v| \gg y_\Lambda$ in the above expressions for $I_1 + I_3$ and I_2. Equation (3.39) becomes

$$\frac{\sqrt{x+v}}{\sqrt{x}} \ln \frac{(\sqrt{x+v} + \sqrt{x})^2}{-(\sqrt{x+v} - \sqrt{x})^2}$$
$$= -2 \left[\frac{\delta\omega}{\gamma} + \ln \frac{8}{\Delta_{0i}} - \frac{2v\Delta_{0i}}{\gamma} \right] \pm \frac{2i\delta\omega}{v\gamma}. \quad (3.45)$$

The real root of this equation is $v \approx -x \approx -1/\Delta_{0i}$, yielding

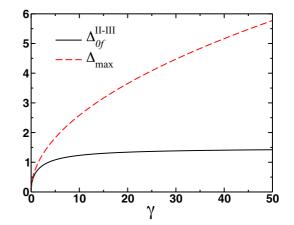$$\frac{\delta\omega}{\gamma} = -\ln \frac{8}{\Delta_{0i}} - \frac{2}{\gamma}. \quad (3.46)$$

FIG. 22. (Color online) Termination point of the II-III critical line as a function of resonance width γ in units of Fermi energy for a 3D two-channel model. This line encloses region III of persistent oscillations in Figs. 3 and 21. It starts at the origin and ends at $\Delta_{0f}^{\text{II-III}}$ along the Δ_{0f} axis. This reflects an interesting phenomenon: There are no persistent oscillations for quenches to couplings stronger than a certain threshold (i.e., quenches to detunings ω_f such that the corresponding ground-state gaps $\Delta_{0f} \geqslant \Delta_{0f}^{\text{II-III}}$) no matter how weak the initial coupling is (i.e., for any initial detuning). At $\gamma \to \infty$ (one-channel limit) $\Delta_{0f}^{\text{II-III}}$ saturates at $1.49\varepsilon_F$, in agreement with Eq. (4.19).

Combining this with Eq. (3.42), taking the limit $\Delta_{0i} \to 0$, and plugging into the gap equation (1.26), we obtain

$$4 + \frac{4\mu_f}{\gamma} = \int_0^\infty \left[\frac{1}{\varepsilon} - \frac{1}{\sqrt{(\varepsilon - \mu_f)^2 + \Delta_{0f}^2}} \right] \sqrt{\varepsilon} \, d\varepsilon, \quad (3.47)$$

where we sent the cutoff ε_Λ to infinity. Equation (3.47), together with the chemical potential equation (1.25), determine the value of $\Delta_{0f}^{\text{II-III}}$, where the II-III critical line terminates on the Δ_{0f} axis. $\Delta_{0f}^{\text{II-III}}$ is a function of γ only; see Fig. 22.

We also note that it follows from the above analysis that, just as in 2D, for initial states deep in the BCS regime, there are three roots: $v \to 0$ for either sign of $\delta\omega$ and $v \to -x + 0$ for $\delta\omega < 0$. Therefore, Eq. (3.22) holds in 3D as well.

Second, consider quenches from deep BEC to larger detuning $\omega_f > \omega_i$, i.e., $\omega_i \to -\infty, \delta\omega > 0, \mu_i \to -\infty, x \to -\infty, \Delta_{0i} \to \Delta_{\text{max}}$. Since $y \geqslant |x| \gg 1$ in Eq. (3.41), we can replace $\sqrt{y^2 + 1} \to y$. The principal value integral evaluates to $-\pi\sqrt{|x|}/v$ and Eq. (3.41) becomes

$$-\frac{\pi\sqrt{|x|}}{v} + \pi\sqrt{v - |x|} = \frac{4\sqrt{\Delta_{0i}}}{\gamma}, \quad (3.48)$$

where we also took into account that we need $v \geqslant |x|$ so that Eq. (3.40) yields real $\delta\omega$. The solution for large $|x|$ is

$$\sqrt{v - |x|} \approx \frac{4\sqrt{\Delta_{0i}}}{\pi\gamma} + \frac{1}{\sqrt{|x|}}. \quad (3.49)$$

Equation (3.40) now yields

$$\frac{\delta\omega}{\gamma} \approx \frac{2|\mu_i|}{\gamma} + \frac{\pi}{2}\sqrt{|\mu_i|} + \frac{32\Delta_{\text{max}}^2}{\pi^2\gamma^3}, \quad (3.50)$$
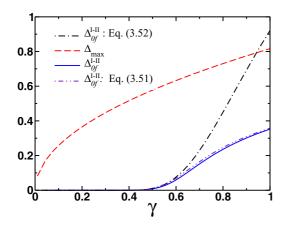
FIG. 23. (Color online) Unlike 2D, in 3D Δ_{0f} tends to a finite value $\Delta_{0f}^{\text{I-II}}$ along the I-II critical line as the initial detuning $\omega_i \to -\infty$ ($\Delta_{0i} \to \Delta_{\max}$) for quenched two-channel model; see, e.g., Fig. 21. The gapless regime thus persists even for quenches from arbitrarily large negative ω_i to finite ω_f. Here we compare $\Delta_{0f}^{\text{I-II}}$ (in units of the Fermi energy) as a function of the resonance width γ extrapolated from actual phase diagrams with that obtained from Eqs. (3.51) and (3.52). Note that $\Delta_{0f}^{\text{I-II}}$ is exponentially small at small γ, so that the I-II critical line *appears* to close earlier at zero Δ_{0f} in Fig. 21(a).

where we replaced $\Delta_{0i}^2 \to \Delta_{\max}^2 = 2\gamma/3$ up to terms of order $|\mu_i|^{-1/2}$. The overall correction to this expression is also proportional to $|\mu_i|^{-1/2}$ at large $|\mu_i|$.

Similar simplifications occur in the gap equation (1.26). We replace the square root with $\varepsilon - \mu_i$ to obtain

$$\frac{\omega_i}{\gamma} \approx \sqrt{\varepsilon_\Lambda} - \frac{2|\mu_i|}{\gamma} - \frac{\pi}{2}\sqrt{|\mu_i|}.$$

The last two equations determine ω_f and from the gap equation (1.26) for $\omega = \omega_f$ we obtain

$$\frac{128}{3\pi^2\gamma^2} - \frac{4\mu_f}{\gamma} = \int_0^\infty \left[\frac{\sqrt{\varepsilon}}{\sqrt{(\varepsilon - \mu_f)^2 + \Delta_{0f}^2}} - \frac{1}{\sqrt{\varepsilon}} \right] d\varepsilon,$$
(3.51)

where we eliminated the cutoff similar to Eq. (3.47). This equation combined with Eq. (1.25) determines the termination point $(\Delta_{0i}, \Delta_{0f}) = (\Delta_{\max}, \Delta_{0f}^{\text{I-II}})$ of the I-II critical line. The plot of $\Delta_{0f}^{\text{I-II}}$ as a function of γ is shown in Fig. 23.

Note that, in contrast to the 2D case, this critical line formally always extends up to $\Delta_{0i} = \Delta_{\max}$ and $\Delta_{0f}^{\text{I-II}}$ does not vanish as $\Delta_{0i} \to \Delta_{\max}$. This means that the gapless regime persists even for quenches to finite final detunings from initial states lying arbitrarily deep in the BEC regime. But for small γ the value of $\Delta_{0f}^{\text{I-II}}$ is exponentially small and the critical line *appears* to have closed at smaller Δ_{0i}; see Figs. 3(a) and 21(a). Small γ implies a large left-hand side in Eq. (3.51) and therefore the final state deep in the BCS regime. In this regime $\mu_f \to 1$ and the integral in Eq. (3.51) is twice the right-hand side of Eq. (3.42) without $\sqrt{\varepsilon_\Lambda}$ resulting in

$$\Delta_{0f}^{\text{I-II}} = 8 \exp\left[-\frac{64}{3\pi^2\gamma^2} + \frac{2}{\gamma} - 2 \right].$$
(3.52)

We see from Fig. 23 that $\Delta_{0f}^{\text{I-II}}$ becomes noticeable for $\gamma \gtrsim 0.45$. For smaller γ the gapless region I appears to close at smaller Δ_{0i} and zero Δ_{0f}. Figure 23 also shows that Eq. (3.52) provides a reasonable estimate of $\Delta_{0f}^{\text{I-II}}$ even for large γ, which is useful in our analysis of the one-channel model below.

IV. ONE-CHANNEL MODEL

In this section we collect for reference purposes analogous results for the asymptotic steady state after a quench $\lambda_i \to \lambda_f$ in the one-channel model given by Eqs. (1.3) and (1.5).

As explained in Sec. I A, the one-channel model obtains in the broad resonance limit via replacements,

$$\frac{\omega}{\gamma} = \frac{\omega}{g^2\nu_F} \to \frac{1}{\lambda}, \quad \gamma = g^2\nu_F \to \infty \tag{4.1}$$

(in units of ε_F). Our task is to go over equations of previous sections performing these replacements. All essential reasoning and methods are the same.

Chemical potential and gap Eqs. (1.25) and (1.26) now read

$$\frac{4}{d} = \int_0^\infty \left[1 - \frac{\varepsilon - \mu}{\sqrt{(\varepsilon - \mu)^2 + \Delta_0^2}} \right] f(\varepsilon) d\varepsilon, \tag{4.2}$$

and

$$\frac{2}{\lambda} = \int_0^{\varepsilon_\Lambda} \frac{f(\varepsilon) d\varepsilon}{\sqrt{(\varepsilon - \mu)^2 + \Delta_0^2}}, \tag{4.3}$$

respectively.

The Lax vector becomes

$$\vec{L}(u) = \sum_{\mathbf{p}} \frac{\vec{s}_{\mathbf{p}}}{u - \varepsilon_{\mathbf{p}}} - \frac{\hat{\mathbf{z}}}{\lambda\nu_F}. \tag{4.4}$$

Gaudin algebra, i.e., Eqs. (2.2) and (2.3), as well as the Lax equation of motion (2.8) are the same. The numerator of the conserved $\vec{L}^2(u)$ is now a polynomial of degree $2N$,

$$\vec{L}^2(u) = \frac{Q_{2N}(u)}{(\lambda\nu_F)^2 \prod_{\mathbf{p}}(u - \varepsilon_{\mathbf{p}})^2}, \tag{4.5}$$

where N is the number of nondegenerate $\varepsilon_{\mathbf{p}}$.

Reduced solutions are constructed in the same way with minor modifications. Specifically, the expressions for $\vec{L}^{\text{red}}(u)$ in terms of $\vec{\sigma}_{\mathbf{p}}$ and $\vec{L}_m(u)$ in terms of $\vec{t}_j$ are replaced in Eqs. (2.10) and (2.11) with the corresponding one-channel Lax vectors according to Eq. (4.4). The Hamiltonian governing the collective spin variables $\vec{t}_j$ is

$$H_{\text{1ch}}^{\text{red}} = \sum_{j=0}^{m-1} 2\eta_j t_j^z - \lambda\nu_F \sum_{j,k=0}^{m-1} t_j^- t_k^+. \tag{4.6}$$

Equations (2.13) and (2.14) as well as constraints (2.15) are the same, except that the last equation relating ω and ω' is absent. In terms of the m-spin spectral polynomial $Q_{2m}(u)$ the constraints become

$$\sum_{\mathbf{p}} \frac{\sigma_{\mathbf{p}} \varepsilon_{\mathbf{p}}^{r-1}}{\sqrt{Q_{2m}(\varepsilon_{\mathbf{p}})}} = -\frac{\delta_{rm}}{(\lambda\nu_F)^2}, \quad r = 1, \ldots, m. \tag{4.7}$$

Further, since the degree of the m-spin spectral polynomial is $2m$ rather than $2(m + 1)$, an m-spin solution of the two-channel model becomes an $(m + 1)$-spin solution of the one-channel model. This name change reflects the fact that the oscillator mode b in the two-channel model is effectively an additional spin, which was not counted as such.

All remaining equations in Sec. II, i.e., Eqs. (2.18) through (2.74), are identical for the one-channel model, except Eq. (2.21) is replaced with Eq. (4.6) for $m = 2$ and the self-consistency condition (2.50) is now given by Eq. (1.13).

Equations determining isolated roots, critical lines, and $\mu_\infty = 0$ line for the one-channel model are Eq. (3.4), Eqs. (3.6) and (3.5), and Eq. (3.7), respectively, with replacements

$$\frac{\delta\omega}{\gamma} \to \frac{1}{\lambda_f} - \frac{1}{\lambda_i} \equiv \beta, \quad \frac{1}{\gamma} \to 0. \quad (4.8)$$

Asymptotic spin distribution—the constant angle the spin $\vec{s}(\varepsilon)$ makes with the spin $\vec{\sigma}(\varepsilon)$ in the corresponding m-spin solution—is

$$\cos\theta(\varepsilon) = \frac{z(\varepsilon)}{i\pi f(\varepsilon)}\sqrt{A_-^2 \Delta_{0i}^2 + [(\varepsilon - \mu_i)A_- + \delta\beta]^2}$$
$$- \frac{z(\varepsilon)}{i\pi f(\varepsilon)}\sqrt{A_+^2 \Delta_{0i}^2 + [(\varepsilon - \mu_i)A_+ + \delta\beta]^2}, \quad (4.9)$$

where

$$A_\pm = \pm\frac{i\pi f(\varepsilon)}{2E_i(\varepsilon)} + \int_0^\infty \frac{f(\varepsilon')d\varepsilon'}{2(\varepsilon - \varepsilon')E_i(\varepsilon')}. \quad (4.10)$$

Equation (4.9) is in excellent agreement with the actual spin distribution obtained from direct simulation of spin dynamics [18]; see Fig. 3 therein.

A. Quench phase diagram

Quench phase diagrams for one-channel model in 2D and 3D are shown in Figs. 4 and 5. There is only one diagram in each case extending to positive infinity in both Δ_{0i} and Δ_{0f} directions because $\gamma \to \infty$ and therefore $\Delta_{max} \to \infty$.

As we commented below Eqs. (3.23) and (3.31), the weak-coupling part of the diagrams (the region of small Δ_{0i} and Δ_{0f} near the origin) is independent of the dimensionality and is exactly the same for the one-channel model. In other words, all results contained in Eqs. (3.26) through (3.31) and the surrounding text apply to the one-channel model in both 2D and 3D; one only needs to replace $\delta\omega/\gamma \to \delta\beta$.

When either the initial or final coupling is outside the deep BCS regime, we need to treat 2D and 3D cases separately.

1. 2D

It is straightforward to take the broad resonance limit in Eqs. (3.15) to (3.21). In particular, the critical lines are determined by taking this limit in Eqs. (3.16) and (3.17),

$$|\delta\beta| = \frac{\pi}{2}\sqrt{1 + v^2}, \quad (4.11)$$

$$\ln\left[\frac{(v + x)(v + \sqrt{1 + v^2})}{\sqrt{1 + x^2}\sqrt{1 + v^2} - xv + 1}\right] = -\text{sgn}(\delta\beta)\pi v. \quad (4.12)$$

Equation (3.22), describing quenches originating in deep BCS, remains as is, except the sign of $\delta\omega$ translates into the sign of

$\delta\beta$. The two roots $u \approx \mu_i$ for either sign of $\delta\beta$ correspond to quenches also terminating in deep BCS, so they are in the universal regime given by Eqs. (3.26) through (3.31), which is shared by both models regardless of the dimensionality.

The analysis for the root $u \approx +0$ at $\delta\beta < 0$ leading to Eq. (3.25) requires some modifications. The $\gamma \to \infty$ limit in Eqs. (3.24) and (3.20) yields $4|\mu_f| = \Delta_{0i}^2 e^{\pi/\Delta_{0i}}$, $\Delta_{0f} = \sqrt{4|\mu_f|}$, and finally

$$\Delta_{0f} = \Delta_{0i}e^{\pi/2\Delta_{0i}}, \quad \Delta_{0i} \to 0. \quad (4.13)$$

This equation gives the asymptotic form of the II-III critical line in the $(\Delta_{0i}, \Delta_{0f})$ plane in Fig. 4. We see that this line never terminates in the 2D one-channel model.

Finally, let us work out the shape of the I-II critical line for large Δ_{0i}, i.e., for quenches originating deep in the BEC regime. Equation (3.32) becomes

$$\ln\left[\frac{v + x}{|x|}\right] = -\pi v. \quad (4.14)$$

Now there is always a single root $v \to -x$ ($u \approx 0$). Equation (4.11) implies

$$\delta\beta = \frac{1}{\lambda_f} - \frac{1}{\lambda_i} = \frac{\pi|x|}{2} = \frac{\pi|\mu_i|}{2\Delta_{0i}}. \quad (4.15)$$

We also need the gap equation in BCS and BEC limits and the chemical potential equation in the BEC limit. Sending γ to infinity in Eqs. (3.18)–(3.20), we obtain

$$\ln\frac{4\varepsilon_\Lambda}{\Delta_{0i}^2} = \frac{2}{\lambda_i}, \quad \ln\frac{\varepsilon_\Lambda}{|\mu_f|} = \frac{2}{\lambda_f}, \quad \Delta_{0i} = \sqrt{4|\mu_i|}. \quad (4.16)$$

Combining these equations with Eq. (4.15), we get

$$\Delta_{0f} = \Delta_{0i}e^{-\pi\Delta_{0i}/8}, \quad \Delta_{0i} \to \infty. \quad (4.17)$$

We see that Δ_{0f} exponentially vanishes along the I-II critical line (gapless regime closes) as Δ_{0i} increases. The vertical range of Fig. 4 is not enough to fully display this behavior, though we see that I-II line does incline towards the Δ_{0i} axis at large Δ_{0i}.

2. 3D

In addition to quenches that fall within the universal weak-coupling regime described in Eqs. (3.26) to (3.31) and the corresponding text, let us derive the termination point of the II-III critical line and analyze the I-II line at large Δ_{0i}.

First, we consider the II-III line. The termination point is given by Eq. (3.47). In the $\gamma \to \infty$ limit we have

$$4 = \int_0^\infty \left[\frac{1}{\varepsilon} - \frac{1}{\sqrt{(\varepsilon - \mu_f)^2 + \Delta_{0f}^2}}\right]\sqrt{\varepsilon}d\varepsilon. \quad (4.18)$$

Chemical potential equation (4.2) provides another relation between μ_f and Δ_{0f}. Numerical solution of these two equations is

$$\mu_f^{\text{II-III}} \approx -1.4602\varepsilon_F, \quad \Delta_{0f}^{\text{II-III}} \approx 1.4875\varepsilon_F. \quad (4.19)$$

This value of $\Delta_{0f}^{\text{II-III}}$ agrees with Fig. 22. Unlike 2D, in 3D region III encloses a finite area, resembling a dome between the origin and the point $(\Delta_{0i}, \Delta_{0f}) = (0, \Delta_{0f}^{\text{II-III}})$.

Next we turn to the critical line separating the gapless region I from region II. For finite γ we analyzed the termination point $(\Delta_{0i}, \Delta_{0f}) = (\Delta_{\max}, \Delta_{0f}^{\text{I-II}})$ of this line at the end of Sec. III B. In the single-channel case, $\Delta_{\max} \to \infty$, so the I-II line does not close. As $\Delta_{0i} \to \infty$, the value of Δ_{0f} for a point on this line tends to $\Delta_{0f}^{\text{I-II}}$, which is determined by the $\gamma \to \infty$ limit of Eq. (3.51),

$$0 = \int_0^\infty \left[\frac{1}{\sqrt{(\varepsilon - \mu_f)^2 + \Delta_{0f}^2}} - \frac{1}{\varepsilon} \right] \sqrt{\varepsilon}\, d\varepsilon, \qquad (4.20)$$

together with Eq. (4.2). The solution of these equations is

$$\mu_f \approx 0.5906\varepsilon_F, \quad \Delta_{0f}^{\text{I-II}} \approx 0.6864\varepsilon_F. \qquad (4.21)$$

V. TRANSIENT DYNAMICS: LINEAR ANALYSIS

Here we solve the dynamics for small deviations from the ground state. Linear analysis for the one-channel model in the weak-coupling BCS regime was performed by Volkov and Kogan [3]; see also Ref. [18]. Gurarie [23] extended this study to strongly coupled superconductors. Both these studies of the linearized dynamics conclude that

$$\Delta(t) \to \Delta_\infty e^{-2i\mu_\infty t - 2i\varphi} \qquad (5.1)$$

as $t \to \infty$, but the approach to this asymptote is different. Our analysis adds several new results to this prior work. We demonstrate that within linear analysis the amplitude of the order parameter asymptotes to its ground-state value for the Hamiltonian with which the system evolves after nonequilibrium conditions are created, i.e., $\Delta_\infty = \Delta_{0f}$, a point that seems to have been missed by the earlier work. Also, $\mu_\infty = \mu_f$, the ground-state chemical potential. In other words, $\Delta_\infty - \Delta_0$ and $\mu_\infty - \mu_f$ are second order in the deviation. This is a general result that holds for both one- and two-channel models and is independent of the type of perturbation that drives the system out of equilibrium.

Further, we solve linearized equations of motion using the machinery of the exact solution [13,15], which provides much more detailed information. For example, we also determine the short-time behavior, normal modes, full explicit long-time form $\Delta(t)$, and individual spins with all prefactors and phases, etc., unavailable to conventional linear analysis. Note that in quench phase diagrams constructed above small quenches correspond to the vicinity of the diagonal $\Delta_{0i} = \Delta_{0f}$; see, e.g., Figs. 20 and 21.

A. Asymptotic $\Delta(t)$ and spins

Consider an infinitesimal quench of the detuning $\delta\omega = \omega_f - \omega_i$. More generally, $\delta\omega$ can be any small parameter that measures the deviation from the ground state in the two- or one-channel model. We work to linear order in $\delta\omega$. Suppose $\Delta(t) \to \Delta_\infty e^{-2i\mu_\infty t - 2i\varphi}$. For the detuning or interaction quenches, this follows from the few-spin conjecture and quench phase diagrams derived above and we also verify it independently below. Let us go to a reference frame that rotates with frequency $2\mu_\infty$ around the z axis. In this frame $\Delta(t) = \Delta_\infty$ and the magnetic field $\vec{B}_{\mathbf{p}} = (-2\Delta_\infty, 0, 2\varepsilon_{\mathbf{p}} - 2\mu_\infty)$ acting on spin $\vec{s}_{\mathbf{p}}$ in Eq. (1.8) is time-independent. Note

that transformation to the rotating frame results in shifts to $\varepsilon_{\mathbf{p}}$ and ω_f. Then the spin rotates around $\vec{B}_{\mathbf{p}}$, making a constant angle $\pi - \theta_{\mathbf{p}}$ with it. This is, in fact, the asymptotic solution described in Sec. II D 1,

$$\vec{s}_{\mathbf{p}}(t) = \frac{\vec{n}_{\mathbf{p}}}{2} \cos\theta_{\mathbf{p}} + \vec{s}_{\mathbf{p}}^\perp(t), \qquad (5.2)$$

where $\vec{n}_{\mathbf{p}}$ is a unit vector along $-\vec{B}_{\mathbf{p}}$,

$$n_p^x = \frac{\Delta_\infty}{E_{\mathbf{p}}^\infty}, \quad n_{\mathbf{p}}^y = 0, \quad n_{\mathbf{p}}^z = -\frac{\varepsilon_{\mathbf{p}} - \mu_\infty}{E_{\mathbf{p}}^\infty}. \qquad (5.3)$$

Equation (1.8) with $\dot{b} = 0$ further implies $\Delta_\infty = -gb = g^2 J_- / (\omega_f - 2\mu_\infty)$. The contribution of $\vec{s}_{\mathbf{p}}^\perp$ to J_- dephases as $t \to \infty$. The latter is therefore $\sum_{\mathbf{p}} n_p^x / 2$, the sum of components of $\vec{s}_{\mathbf{p}}$ along $\vec{B}_{\mathbf{p}}$ projected onto the xy plane,

$$\Delta_\infty = \frac{g^2}{\omega_f - 2\mu_\infty} \sum_{\mathbf{p}} \frac{\Delta_\infty \cos\theta_{\mathbf{p}}}{2\sqrt{(\varepsilon_{\mathbf{p}} - \mu_\infty)^2 + \Delta_\infty^2}}. \qquad (5.4)$$

In the ground state $\vec{s}_{\mathbf{p}}$ is aligned with $-\vec{B}_{\mathbf{p}}$; i.e., $\theta_{\mathbf{p}} = 0$. This implies that $\theta_{\mathbf{p}}$ must be proportional to $\delta\omega$ and therefore corrections to $\cos\theta_{\mathbf{p}} = 1$ are second order in $\delta\omega$. However, for $\cos\theta_{\mathbf{p}} = 1$, Eq. (5.4) is the ground-state gap equation (1.18) for $\omega = \omega_f$. Moreover, applying the same argument to J_z and Eq. (1.19), we find that Δ_∞ and μ_∞ also satisfy the ground-state chemical potential equation (1.20). It follows that for small oscillations around the ground state one always has

$$\Delta_\infty = \Delta_{0f}, \quad \mu_\infty = \mu_f. \qquad (5.5)$$

For the same reason the nonoscillatory part of $\vec{s}_{\mathbf{p}}$ (zeroth harmonic) in the steady state is the same as in the ground state at $\omega = \omega_f$, i.e., is given by Eq. (1.15) with $\Delta_0 \to \Delta_{0f}$ and $\mu \to \mu_f$.

The same is true for the one-channel model. Note also that infinitesimal quenches in the BCS regime conform to this conclusion; see Eq. (3.30). Moreover, this result generalizes to finite spin dynamics, where, as we show below, zeroth harmonics of $\Delta(t)$ and $\vec{s}_{\mathbf{p}}$ to linear order in $\delta\omega$ coincide with the $\omega = \omega_f$ ground-state values.

B. Normal modes and finite-size dynamics

Now we turn to the linear analysis per se. At this point it is convenient to rewrite summations over $\mathbf{p}$ as summations over single-particle energies. We adopt the following model of discrete spectrum. Let us discretize the magnitude of the momentum, $p \to p_k$. The corresponding energies are $\varepsilon_k = p_k^2 / 2m$ with degeneracy $N_k = N(\varepsilon_k)$, the number of states in a momentum shell between p_k and p_{k+1}, which is a smooth function of ε_k. The level spacing $\delta_k = \varepsilon_{k+1} - \varepsilon_k$ is also assumed to depend on ε_k smoothly. We include this dependence in N_k, so without loss of generality we take it to be constant, $\delta_k = \delta$. Our final results depend only on the density of states $\nu(\varepsilon_k) = N_k / \delta$, the number of states per unit energy. Equivalently, ε_i can represent levels of some other single-particle potential, e.g., a 3D harmonic oscillator potential; see the discussion at the end of Sec. I A. All quantities and equations, including spins $\vec{s}_{\mathbf{p}}$, Hamiltonians, equations of motion, and initial conditions, considered in this

paper depend on **p** only through $\varepsilon_{\mathbf{p}}$. For any such quantity $A_{\mathbf{p}} = A(\varepsilon_{\mathbf{p}})$,

$$\sum_{\mathbf{p}} A_{\mathbf{p}} = \sum_{k=1}^{N} N_k A_k \rightarrow \int \nu(\varepsilon) d\varepsilon, \tag{5.6}$$

where $A_k = A(\varepsilon_k)$. In particular, the Lax vector (2.1) reads

$$\vec{L}(u) = \sum_{k=1}^{N} \frac{N_k \vec{s}_k}{u - \varepsilon_k} - \frac{(\omega - 2\mu)}{g^2} \hat{\mathbf{z}} + \frac{2}{g^2} [(u - \mu)\hat{\mathbf{z}} - \vec{\Delta}]. \tag{5.7}$$

A convenient tool for linear analysis of the dynamics are the separation variables introduced in Refs. [13,15] for the one- and two-channel models, respectively. As we will see, in linearized dynamics these variables are simply the normal modes. Separation variables u_j are defined as the solutions of $L_-(u_j) \equiv L_x(u_j) - i L_y(u_j) = 0$; i.e.,

$$L_-(u) = \frac{2b}{g} + \sum_{k=1}^{N} \frac{N_k s_k^-}{u - \varepsilon_k} = 0. \tag{5.8}$$

Because $u = u_j$ are the zeros of the rational function $L_-(u)$ and $u = \varepsilon_k$ are its poles, we can also write it as

$$L_-(u) = \frac{2b}{g} \frac{\prod_j (u - u_j)}{\prod_k (u - \varepsilon_k)}. \tag{5.9}$$

Matching the residues at $u = \varepsilon_k$ and $u = \infty$ in Eqs. (5.8) and (5.9), we express the spins in terms of u_j,

$$N_k s_k^- = \frac{2b}{g} \frac{\prod_j (\varepsilon_k - u_j)}{\prod_{m \neq k} (\varepsilon_k - \varepsilon_m)}, \tag{5.10}$$

$$J_- = \sum_k N_k s_k^- = \frac{2b}{g} \sum_k (\varepsilon_k - u_k). \tag{5.11}$$

Equations of motion in terms of new variables are

$$\dot{u}_k = -\frac{2i \sqrt{Q_{2N+2}(u_k)}}{\prod_{m \neq k} (u_k - u_m)},$$
$$\dot{b} = -2ib \left[\frac{\omega}{2} + \sum_k (\varepsilon_k - u_k) \right]; \tag{5.12}$$

see Ref. [15] for a detailed derivation. Here $Q_{2N+2}(u)$ is the spectral polynomial defined in Eq. (2.9).

Roots of $Q_{2N+2}(u)$ are the same as roots of $\vec{L}^2(u)$ determined by Eq. (3.3). In our new notation,

$$\left(u - \mu \mp i\Delta_0 \right) \left[\frac{2}{g^2} - \sum_k \frac{N_k}{2(u - \varepsilon_k) E(\varepsilon_k)} \right] = \frac{\delta\omega}{g^2}, \tag{5.13}$$

where $E(\varepsilon_k) = \sqrt{(\varepsilon_k - \mu)^2 + \Delta_0^2}$. Here and everywhere below in this section μ and Δ_0 without a subscript indicate ground-state values μ_i and Δ_{0i} for the initial detuning $\omega = \omega_i$. In the ground state $\vec{L}^2(u) = [(u - \mu_i)^2 + \Delta_{0i}^2] L_0^2(u)$. There is a pair of complex roots $c_{\pm} = \mu_i \pm i\Delta_{0i}$ and $2N$ real double degenerate roots x_k that solve

$$L_0(x) = -\frac{2}{g^2} + \sum_k \frac{N_k}{2(x - \varepsilon_k) E(\varepsilon_k)} = 0, \tag{5.14}$$

A plot of $L_0(x)$ reveals that x_k are located between consecutive ε_k, i.e., $\varepsilon_k < x_k < \varepsilon_{k+1}$.

Since $\vec{L}^2(x_k) = L_x^2(x_k) + L_y^2(x_k) + L_z^2(x_k) = 0$ in the ground state and x_k is real, all components of $\vec{L}(x_k)$ must vanish, $L_x(x_k) = L_y(x_k) = L_z(x_k) = 0$. It follows that $L_-(x_k) = 0$, meaning that the separation variables are frozen in the real double roots, $u_k = x_k$. After a quench they start to move from these initial positions, $u_k(t) = x_k + \delta u_k$, where δu_k vanishes at $t = 0$ and is proportional to $\delta\omega$ for an infinitesimal quench. For $\delta\omega \neq 0$ real double roots of $Q_{2N+2}(u)$ split into pairs of complex conjugate roots $c_k = x_k + \delta c_k$ and $\bar{c}_k = x_k + \delta\bar{c}_k$. Therefore, the expression for $Q_{2N+2}(u_k)$,

$$Q_{2N+2}(u_k) = (u_k - c_k)(u_k - \bar{c}_k)(u_k - c_+)(u_k - c_-)$$
$$\times \prod_{m \neq k} (u_k - c_m)(u_k - \bar{c}_m), \tag{5.15}$$

to lowest nonzero order in $\delta\omega$ becomes

$$Q_{2N+2}(u_k) = (\delta u_k - \delta c_k)(\delta u_k - \delta\bar{c}_k)\Omega_k^2$$
$$\times \prod_{m \neq k} (x_k - x_m)^2, \tag{5.16}$$

with $\Omega_k = \sqrt{(x_k - \mu)^2 + \Delta_0^2}$, not to be confused with function $\Omega(t)$ in Sec. II B 3. Similarly, the denominator of the equation of motion (5.12) for u_k to the lowest order $\prod_{m \neq k}(u_k - u_m) = \prod_{m \neq k}(x_k - x_m)$, so this equation reads

$$\delta\dot{u}_k = \pm 2i\Omega_k \sqrt{(\delta u_k - \delta c_k)(\delta u_k - \delta\bar{c}_k)}. \tag{5.17}$$

Corrections to the roots due to the quench obtain by setting $u = x_k + \delta c_k$ in Eq. (5.13) and linearizing in δc_k. Separating real and imaginary parts, $\delta c_k = a_k + ib_k$, we have

$$a_k = \frac{\delta\omega(x_k - \mu)}{g^2 \Omega_k^2 F_k}, \quad b_k = \frac{\delta\omega\Delta_0}{g^2 \Omega_k^2 F_k}, \tag{5.18}$$

where

$$F_k = \sum_m \frac{N_k}{2(x_k - \varepsilon_m)^2 E(\varepsilon_m)}. \tag{5.19}$$

Let us also evaluate the correction to the complex root pair $c_{\pm} = \mu_i \pm i\Delta_{0i}$. Writing the perturbed roots as $\mu' \pm i\Delta'$, we obtain from Eq. (5.13) to linear order in $\delta\omega$

$$\mu' - \mu_i = \frac{\delta\omega}{g^2} \frac{\beta_k}{\alpha_k^2 + \beta_k^2},$$
$$\Delta' - \Delta_{0i} = -\frac{\delta\omega}{g^2} \frac{\alpha_k}{\alpha_k^2 + \beta_k^2}, \tag{5.20}$$

where α_k and β_k are defined in Eq. (C5). Comparing this with first-order shifts in the ground-state gap and chemical potentials that readily derive from Eqs. (C7), we conclude that

$$\mu' = \mu_f, \quad \Delta' = \Delta_{0f}, \tag{5.21}$$

as it should be according to Sec. II D 1; see the text following Eq. (2.65) and also below.

Equation (5.17) is a harmonic oscillator equation, which yields

$$\delta u_k(t) = a_k(1 - \cos 2\Omega_k t) + i l_k \sin 2\Omega_k t, \tag{5.22}$$
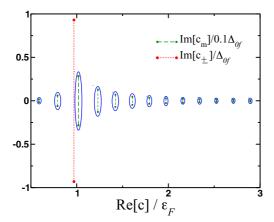
FIG. 24. (Color online) As a result of a quench, doubly degenerate roots of $\vec{L}^2(u)$ in Fig. 17 split into pairs of complex conjugate roots c_m (not all $N = 54$ pairs of roots are shown). In linear analysis, separation variables move periodically on ellipses around the brunch cuts of $[\vec{L}^2(u)]^{-1/2}$ connecting complex conjugate c_m without crossing any of the brunch cuts. Each separation variable has its own distinct frequency and corresponds to a normal mode of small oscillations around the ground state. Here $\Delta_{0f} = 0.12\varepsilon_F$, $\delta\omega/\gamma = -0.1$, and other parameters are the same as in Fig. 17.

where

$$l_k = \pm\sqrt{a_k^2 + b_k^2} = \frac{\delta\omega}{g^2\Omega_k F_k}. \tag{5.23}$$

In deriving Eq. (5.22) we took into account the initial condition $\delta u_k(0) = 0$ and used expressions (5.18). We set the sign in the last equation in Eq. (5.23) to be plus, which we justify later in this section.

Equation (5.22) shows that $u_k(t)$ are the normal modes of small oscillations around the ground state and that the normal frequencies are $2\Omega_k = 2\sqrt{(x_k - \mu)^2 + \Delta_0^2}$, where x_k are the roots of Eq. (5.14). Equation (5.22) also shows that in linear analysis separation variable $u_k(t)$ moves on an ellipse with semiaxes a_k and $\sqrt{a_k^2 + b_k^2}$ around the roots $c_k, \bar{c}_k$. The latter are the focal points of the ellipse. The function $\sqrt{Q_{2N+2}(u)}$ entering equations of motion for separation variables has branch cuts connecting pairs of conjugate roots c_k and $\bar{c}_k$, so one can also say that separation variables move on ellipses around brunch cuts without crossing any of them; see Fig. 24.

Next, we determine deviations of the spins $\delta\vec{s}_k(t)$ and the order parameter $\delta\Delta(t)$ from their initial ground-state configuration (1.14) and (1.15). We go to a rotating reference frame,

$$s_k^- \to s_k^- e^{-2i\mu t}, \quad b \to b e^{-2i\mu t}, \tag{5.24}$$

to get rid of the time dependence in the unperturbed dynamical variables. This shifts $\omega \to \omega - 2\mu$ in the equation of motion (5.12) and now $\dot{b} = 0$ in the ground state *before* the quench, i.e., for $\omega = \omega_i$. Linearizing Eq. (5.10), we obtain a decomposition of spin deviations in terms of the normal modes,

$$\frac{\delta s_k^-(t)}{s_k^-(0)} = \frac{\delta\Delta(t)}{\Delta_0} - \sum_j \frac{\delta u_j}{\varepsilon_k - x_j}. \tag{5.25}$$

Similarly, the second equation in Eq. (5.12) linearized and integrated in the rotating frame *after* the quench, i.e., with $\omega = \omega_f$, yields

$$\frac{\Delta(t)}{\Delta_0} = 1 - \sum_k l_k \frac{1 - \cos 2\Omega_k t}{\Omega_k} - i\delta\omega t + 2it\sum_k a_k$$
$$- i\sum_k \frac{a_k \sin 2\Omega_k t}{\Omega_k}, \tag{5.26}$$

where we took into account $\Delta(t) = -gb(t)$, $\Delta(0) = \Delta_0$ and expressions (5.22). The $i\delta\omega t$ appears because for unperturbed u_k the bracketed term in the second equation in Eq. (5.12) vanishes for $\omega = \omega_i$, while after the quench $\omega = \omega_f$.

Linearizing spin equations of motion (1.8) directly and plugging expressions (5.25) and (5.26), one can verify that the correct sign in the last equation in Eq. (5.23) is indeed plus, even though there is probably a simpler way to show this.

The imaginary part in Eq. (5.26) comes from the phase of the order parameter, so we write

$$\Delta(t) = \left(\Delta_0 - \Delta_0 \sum_k l_k \frac{1 - \cos 2\Omega_k t}{\Omega_k}\right)$$
$$\times \exp\left[-i\delta\omega t + 2it\sum_k a_k - i\sum_k \frac{a_k \sin 2\Omega_k t}{\Omega_k}\right]. \tag{5.27}$$

This coincides with Eq. (5.26) to first order in $\delta\omega$. Moreover, we know from Eq. (5.5) that the linear part of the phase (zeroth harmonic in the derivative of the phase) is $-2\mu_f t$ in the continuum limit, where μ_f is the ground-state chemical potential at detuning ω_f. Similarly, the zeroth harmonic in the amplitude of $\Delta(t)$ is equal to Δ_{0f}. It turns out that this is true even in the discrete case, i.e.,

$$\Delta_0 - \Delta_0 \sum_k \frac{l_k}{\Omega_k} = \Delta_{0f},$$
$$2\mu + \delta\omega - 2\sum_k a_k = 2\mu_f, \tag{5.28}$$

where we restored the phase of $\Delta(t)$ to the original reference frame according to Eq. (5.24). Recall that in this section μ and Δ_0 without a subscript indicate ground-state values μ_i and Δ_{0i} for the initial detuning $\omega = \omega_i$. With the help of Eqs. (5.18) and (5.23) these relations become

$$\sum_k \frac{x_k - \mu}{\Omega_k^2 F_k} = \frac{g^2}{2} - g^2\frac{\delta\mu}{\delta\omega},$$
$$\sum_k \frac{\Delta_0}{\Omega_k^2 F_k} = -g^2\frac{\delta\Delta_0}{\delta\omega}, \tag{5.29}$$

where $\delta\mu = \mu_f - \mu$ and $\delta\Delta_0 = \Delta_{0f} - \Delta_0$. These are in fact identities, as we prove in Appendix C. Thus,

$$\Delta(t) = \left(\Delta_{0f} + \Delta_0 \sum_k l_k \frac{\cos 2\Omega_k t}{\Omega_k}\right)$$
$$\times \exp\left[-2i\mu_f t - i\sum_k \frac{a_k \sin 2\Omega_k t}{\Omega_k}\right], \tag{5.30}$$

in the original reference frame.

An expression for $s_k^-(t)$ obtains similarly from Eqs. (5.25) and (5.26) with the help of identity (C8),

$$
s_k^-(t) = s_{kf}^- \left(1 + \sum_j \frac{l_j \cos 2\Omega_j t}{\Omega_j} \right.
$$

$$
+ \sum_j \frac{a_j \cos 2\Omega_j t}{\varepsilon_k - x_j} - i \sum_j \frac{l_j \sin 2\Omega_j t}{\varepsilon_k - x_j} \bigg)
$$

$$
\times \exp \left[-2i\mu_f t - i \sum_j \frac{a_j \sin 2\Omega_j t}{\Omega_j} \right], \quad (5.31)
$$

where

$$
s_{kf}^- \equiv s_f^-(\varepsilon_k) = \frac{\Delta_{0f}}{2\sqrt{(\varepsilon_k - \mu_f)^2 + \Delta_{0f}^2}}. \quad (5.32)
$$

The last term in round brackets in Eq. (5.31) can be as well included into the phase; to linear order the two versions are equivalent. The present form is more convenient for the long-time analysis below. We see that again nonoscillatory parts of the magnitude and phase of $s_k^-(t)$ and magnitude of s_k^z are the same as in the ground state for final detuning $\omega = \omega_f$.

Finally, the expression for $s_k^z(t)$ follows the conservation of $|\vec{s}_k| = 1/2$, $s_k^z = \pm\sqrt{1/4 - |s_k^-|^2}$ expanded to the linear order in $\delta\omega$,

$$
s_k^z(t) = s_{kf}^z \left[1 - \frac{\Delta_{0f}^2}{(\varepsilon_k - \mu_f)^2} \sum_j \frac{l_j \cos 2\Omega_j t}{\Omega_j} \right.
$$

$$
\left. - \frac{\Delta_{0f}^2}{(\varepsilon_k - \mu_f)^2} \sum_j \frac{a_j \cos 2\Omega_j t}{\varepsilon_k - x_j} \right], \quad (5.33)
$$

where

$$
s_{kf}^z \equiv s_f^z(\varepsilon_k) = -\frac{\varepsilon_k - \mu_f}{2\sqrt{(\varepsilon_k - \mu_f)^2 + \Delta_{0f}^2}}. \quad (5.34)
$$

C. Continuum limit

In $N \to \infty$ limit, $x_k \to \varepsilon_k$ and summations in the above expressions for $s_k^z(t)$, $s_k^-(t)$, and $\Delta(t)$ turn into integrations. With the help of Eqs. (5.18), (5.23), (5.6), and (B9), Eq. (5.30) obtains (as always in units of the Fermi energy ε_F)

$$
\frac{\Delta(t)}{\Delta_{0f}} = [1 + X_1(t)] \exp[-2i\mu_f t - i X_2(t)], \quad (5.35)
$$

where

$$
X_1(t) = \frac{\delta\omega}{\gamma} \int_0^\infty \frac{2\cos[2E(\varepsilon)t] f(\varepsilon) d\varepsilon}{E(\varepsilon)[\pi^2 f^2(\varepsilon) + H^2(\varepsilon)]}, \quad (5.36)
$$

$$
X_2(t) = \frac{\delta\omega}{\gamma} \int_0^\infty \frac{2(\varepsilon - \mu)\sin[2E(\varepsilon)t] f(\varepsilon) d\varepsilon}{E^2(\varepsilon)[\pi^2 f^2(\varepsilon) + H^2(\varepsilon)]}, \quad (5.37)
$$

where $E(\varepsilon) = \sqrt{(\varepsilon - \mu)^2 + \Delta_0^2}$ and $H(\varepsilon)$ is defined in Eq. (B8). In deriving this expression, we also used, $\Omega_k \to E(\varepsilon_k)$, $\nu(\varepsilon) = \nu_F f(\varepsilon)$, $g^2 \nu_F = \gamma$, and $\delta = N_k/\nu(\varepsilon_k)$. Equa-
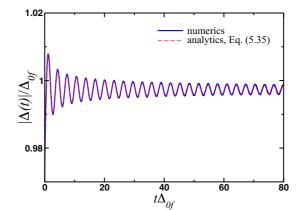

FIG. 25. (Color online) Comparison of Eq. (5.35) with $|\Delta(t)|$ computed by numerically evolving $N = 5024$ spins in a 3D two-channel model after a detuning quench. Here $\gamma = 1.0$, $\Delta_{0i} = 0.122\Delta_{\max}$, $\Delta_{0f} = 0.126\Delta_{\max}$, and both Eq. (5.35) and the spin chain in the numerics are cut off at $\varepsilon_\Lambda = 10\varepsilon_F$.

tion (5.35) is in excellent agreement with numerical results; see, e.g., Fig. 25.

Expressions (5.33) and (5.31) for $s_k^-(t)$ and $s_k^z(t)$ contain two extra summations as compared to $\Delta(t)$. These are handled as in Appendix C by splitting each sum into two parts, over x_j inside and outside a small interval around ε_k. The same method works for summations over x_j because according to Eq. (B8) $\varrho(\varepsilon)$ is a smooth function and therefore x_j are locally equally spaced with spacing δ just as ε_k. The second and the third sums in round brackets in Eq. (5.31) are

$$
Y_1(\varepsilon,t) = \frac{\delta\omega}{\gamma} \int_0^\infty \frac{2(\varepsilon' - \mu)\cos[2E(\varepsilon')t] f(\varepsilon') d\varepsilon'}{(\varepsilon - \varepsilon')E(\varepsilon')[\pi^2 f^2(\varepsilon') + H^2(\varepsilon')]}
$$

$$
- \frac{\delta\omega}{\gamma} \frac{2(\varepsilon - \mu)H(\varepsilon)\cos[2E(\varepsilon)t]}{E(\varepsilon)[\pi^2 f^2(\varepsilon) + H^2(\varepsilon)]}, \quad (5.38)
$$

$$
Y_2(\varepsilon,t) = \frac{\delta\omega}{\gamma} \int_0^\infty \frac{2\sin[2E(\varepsilon')t] f(\varepsilon') d\varepsilon'}{(\varepsilon - \varepsilon')[\pi^2 f^2(\varepsilon') + H^2(\varepsilon')]}
$$

$$
- \frac{\delta\omega}{\gamma} \frac{2H(\varepsilon)\sin[2E(\varepsilon)t]}{\pi^2 f^2(\varepsilon) + H^2(\varepsilon)}, \quad (5.39)
$$

respectively. Thus,

$$
\frac{s^-(\varepsilon,t)}{s_f^-(\varepsilon)} = [1 + X_1(t) + Y_1(\varepsilon,t) - i Y_2(\varepsilon,t)]
$$

$$
\times \exp[-2i\mu_f t - i X_2(t)], \quad (5.40)
$$

$$
\frac{s^z(\varepsilon,t)}{s_f^z(\varepsilon)} = 1 - \frac{\Delta_{0f}^2}{(\varepsilon - \mu_f)^2}[X_1(t) + Y_1(\varepsilon,t)]. \quad (5.41)
$$

Functions X_1 and X_2 are related via differentiation. Define

$$
\widetilde{X}_1(t) = \int_0^\infty K(\varepsilon) e^{2i\widetilde{E}(\varepsilon)t} d\varepsilon, \quad (5.42)
$$

where $\widetilde{E}(\varepsilon) = \sqrt{(\varepsilon - \widetilde{\mu})^2 + \Delta_0^2}$ and

$$
K(\varepsilon) = \frac{\delta\omega}{\gamma} \frac{2f(\varepsilon)}{E(\varepsilon)[\pi^2 f^2(\varepsilon) + H^2(\varepsilon)]}. \quad (5.43)
$$

Then

$$X_1(t) = \mathrm{Re}\,\widetilde{X}_1(t)|_{\widetilde{\mu}=\mu}, \qquad (5.44)$$

$$X_2(t) = \frac{1}{2t}\mathrm{Re}\,\frac{\partial \widetilde{X}_1(t)}{\partial \widetilde{\mu}}\bigg|_{\widetilde{\mu}=\mu}. \qquad (5.45)$$

A similar relationship holds for Y_1 and Y_2.

D. Validity of the few-spin conjecture

We are now in the position to prove the few-spin conjecture for infinitesimal quenches independently of either numerics or arguments of Sec. II. At $t \to \infty$ integrals in Eqs. (5.36) and (5.37) vanish by the Riemann-Lebesgue lemma. Therefore,

$$\Delta(t) \to \Delta_{0f}e^{-2i\mu_f t}. \qquad (5.46)$$

According to the few-spin conjecture this asymptotic behavior of $\Delta(t)$ occurs when there is a single isolated root pair at $\mu_f \pm i\Delta_{0f}$. Equation (5.21) shows that our $\vec{L}^2(u)$ does have this pair of roots. Moreover, the remaining $2N$ roots are given by Eq. (5.18) and we explicitly see from Appendix B that their imaginary parts scale as $1/N$ at large N and that they merge into a continuum of roots on the real axis in the $N \to \infty$ limit. Thus, there is indeed a single isolated root pair at $\mu_f \pm i\Delta_{0f}$ in the thermodynamic limit.

E. Weak-coupling limit

Simpler expressions obtain in the weak-coupling (BCS) limit when Δ_0 is much smaller than other energy scales (Fermi energy in gases and Debye energy in metals). This limit describes superconductivity in metals and applies to recent experiments on nonadiabatic BCS dynamics [25,31]. In our quench phase diagrams (Figs. 2–4, etc.) the weak-coupling regime corresponds to a small neighborhood of the origin.

At weak coupling $\mu \approx \varepsilon_F = 1$. Integrals (5.36) and (5.37) are dominated by energies close to the Fermi energy, $|\varepsilon - \mu| \sim \Delta_0$, where $f(\varepsilon) \approx 1$ independent of dimensionality. It is convenient to change the integration variable to $\xi = \varepsilon - \mu$ and extend the integration to the entire real axis. $X_2(t)$ vanishes by particle-hole symmetry (integrand is odd in ξ). The error due to these approximations is proportional to Δ_0/ε_F, which vanishes in the weak-coupling limit. Equation (5.35) implies

$$|\Delta(t)| = \Delta_{0f} - 4\delta\Delta_0 \int_0^\infty \frac{\cos[2E(\xi)t]d\xi}{E(\xi)[\pi^2 + H^2(\xi)]}, \qquad (5.47)$$

where $E(\xi) = \sqrt{\xi^2 + \Delta_0^2}$, $\delta\Delta_0 = \Delta_{0f} - \Delta_{0i}$, and

$$H(\varepsilon) = \ln\left[\frac{E(\xi) - \xi}{E(\xi) + \xi}\right]. \qquad (5.48)$$

In deriving Eq. (5.47) we used the weak-coupling gap formula $\Delta_0 \propto \exp(-\omega/\gamma)$ and Eqs. (B6) and (B8). [Note that at relevant energies $4E(\varepsilon)/\gamma \propto \Delta_0/\varepsilon_F \to 0$.] We also used the fact that the integrand is even in ξ to convert the integration range from $(-\infty,\infty)$ to $(0,\infty)$.

The phase of the order parameter defined through

$$\Delta(t) = |\Delta(t)|e^{-i\Phi(t)} \qquad (5.49)$$

is simply $\Phi(t) = 2\varepsilon_F t$. Let us also note that in terms of $\xi = \Delta_0 \sinh(\pi x/2)$ Eq. (5.47) reads

$$|\Delta(t)| = \Delta_{0f} - 2\delta\Delta_0 \int_0^\infty \frac{dx}{\pi} \frac{\cos[2\tau\cosh(\pi x/2)]}{1+x^2}, \quad (5.50)$$

where $\tau = \Delta_0 t$.

F. Long-time behavior of $\Delta(t)$: BCS side

Integrands in Eqs. (5.36) and (5.37) are highly oscillatory. The argument of the cosine is stationary at $\varepsilon = \mu$, $E'(\mu) = 0$. For $\mu > 0$ the stationary point is inside the integration range. For $\mu < 0$ there are no stationary points on the integration path. This leads to qualitatively different behavior of $\Delta(t)$ on the BCS ($\mu > 0$) and BEC ($\mu < 0$) sides.

Consider first the BCS regime. We evaluate $\widetilde{X}_1(t)$ in Eq. (5.42) in stationary-phase approximation

$$\widetilde{X}_1(t) = K(\widetilde{\mu})\sqrt{\frac{\pi\Delta_0}{t}}e^{2i\Delta_0 t + i\pi/4} + O(1/t), \qquad (5.51)$$

where we used $\widetilde{E}(\widetilde{\mu}) = \Delta_0$, $\widetilde{E}''(\widetilde{\mu}) = 1/\Delta_0$. With the help of Eq. (5.44) we obtain from Eq. (5.35) for the order parameter amplitude

$$|\Delta(t)| = \Delta_{0f} + \sqrt{\pi}K(\mu)\Delta_0^2\frac{\cos(2\Delta_0 t + \pi/4)}{\sqrt{\Delta_0 t}}. \qquad (5.52)$$

The phase of the order parameter obtains with the help of Eq. (5.45),

$$\Phi(t) = 2\mu_f t + \sqrt{\pi}K'(\mu)\Delta_0^2\frac{\cos(2\Delta_0 t + \pi/4)}{2(\Delta_0 t)^{3/2}}. \qquad (5.53)$$

Coefficients $K(\mu), K'(\mu)$ are given by Eqs. (5.43), (B8), and (B4). Simpler expressions for $G(\varepsilon)$ are available in 2D and in the weak-coupling (BCS) limit; see Eqs. (B5) and (B6). For example, in the BCS limit ($\Delta_0/\varepsilon_F \to 0$),

$$\Delta(t) = \left[\Delta_{0f} - \frac{2\delta\Delta_0}{\pi^{3/2}}\frac{\cos(2\Delta_0 t + \pi/4)}{\sqrt{\Delta_0 t}}\right]e^{-2i\mu_f t}, \quad (5.54)$$

where $\delta\Delta_0 = \Delta_{0f} - \Delta_{0i}$ and we additionally used $\Delta_0 \propto \exp(-\omega/\gamma)$. Note that the second term in Eq. (5.53) is proportional to Δ_0/ε_F. This expression for $\Delta(t)$ holds in the BCS limit for both one- and two-channel models in 2D and 3D. Equation (5.54) for $\mu_f = 0$ appeared in Ref. [18] without derivation.

Let us also mention that long times for which asymptotes of the order parameter derived in this section apply in practice (e.g., in numerical simulations) mean t such that $1/\Delta_0 \ll t \ll 1/\delta$. At times of order of the inverse level spacing $1/\delta$ partial recurrences occur; see Fig. 26. Oscillations with frequency $2\Delta_0$ and $1/\sqrt{t}$ decay in the weak-coupling limit of the one-channel model were identified by Volkov and Kogan [3].

G. Long-time behavior of $\Delta(t)$: BEC side

In the absence of stationary points, integrals of the type of Eq. (5.42) are dominated by the end point, $\varepsilon = 0$ here. Normally, they vanish as $1/t$ at large t, but in the present case
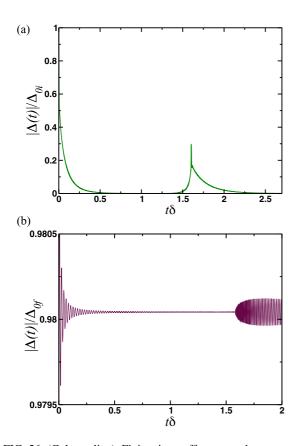
FIG. 26. (Color online) Finite-size effects, such as partial recurrences in $|\Delta(t)|$, develop at times of order of the inverse level spacing $\delta \propto 1/N$ between discretized single-particle energy levels ε_k. Long-time behaviors derived in our paper apply at times $t\delta \ll 1$. In other words, we take the thermodynamic limit first and large-time limit second. Two detuning quenches in a 3D two-channel model are shown for $N = 5024$ and (a) $\gamma = 0.5$, $\Delta_{0i} = 3.0 \times 10^{-2}\Delta_{max}$, $\Delta_{0f} = 2.9 \times 10^{-4}\Delta_{max}$, $\delta = 3.4 \times 10^{-3}\Delta_{max}$, and (b) $\gamma = 0.1$, $\Delta_{0i} = 0.97\Delta_{max}$, $\Delta_{0f} = 0.99\Delta_{max}$, $\delta = 8.0 \times 10^{-3}\Delta_{max}$.

$K(0) = 0$ in both 2D and 3D, so they vanish faster. Unlike the BCS side, the long-time behavior on the BEC side is not universal in that it depends on the form of $K(\varepsilon)$ at small ε, i.e., on the density of states and on the asymptotic spin distribution. As a result, for example, it is different in 2D and 3D.

We first integrate by parts to obtain

$$\widetilde{X}_1(t) = -\frac{1}{2it}\int_0^\infty \left[\frac{K(\varepsilon)}{\widetilde{E}'(\varepsilon)}\right]' e^{2i\widetilde{E}(\varepsilon)t}d\varepsilon. \qquad (5.55)$$

In 2D the dimensionless density of states $f(\varepsilon) = 1$ and it follows from Eqs. (5.43), (B8), and (B5) that $K(\varepsilon) \propto 1/\ln^2 \varepsilon$. We evaluate the large t asymptote of this integral by splitting the integration range into three, $(0, 1/\Lambda t), (1/\Lambda t, \Lambda/t)$, and $(\Lambda/t, \infty)$, where Λ is such that $1 \ll \ln \Lambda \ll \ln t$. In the first integral we expand the integrand in small ε, which leads to an integral $\int_0^{1/\Lambda t} d(\ln \varepsilon)/\ln^3 \varepsilon$ and

$$\widetilde{X}_1(t) = \frac{\delta\omega}{\gamma}\frac{ie^{2i\widetilde{E}(0)t}}{\widetilde{E}'(0)E(0)}\frac{1}{t\ln^2 t}. \qquad (5.56)$$

The other two integrals vanish as $1/t\ln^3 t$ and are therefore negligible. Equations (5.35), (5.44), and (5.45) yield the amplitude and the phase of the order parameter,

$$|\Delta(t)| = \Delta_{0f}\left[1 - \frac{\delta\omega}{\gamma}\frac{\sin(2E_{min}t)}{|\mu|t\ln^2 t}\right], \qquad (5.57)$$

$$\Phi(t) = 2\mu_f t - \frac{\delta\omega}{\gamma}\frac{\cos(2E_{min}t)}{E_{min}t\ln^2 t}, \qquad (5.58)$$

where $E_{min} = \sqrt{\mu^2 + \Delta_0^2}$.

In 3D $f(\varepsilon) = \sqrt{\varepsilon}$ and $K(\varepsilon) \propto \sqrt{\varepsilon}$ at small ε. This follows from Eqs. (5.43), (B8), and (B4) and is, for example, readily verified in the strong-coupling limit with the help of the last expression in Eq. (B7). We split the integration range in Eq. (5.55) into two, $(0, 1/\Lambda)$ and $(1/\Lambda, \infty)$, where $t \gg \Lambda \gg 1$. In the first integral we can expand in small t, which results in a Gaussian integral that behaves as $1/\sqrt{t}$ at large t. The second integral vanishes faster as $t \to \infty$. We thus determine the following (exact) large-time asymptote:

$$\widetilde{X}_1(t) = -\frac{\pi^{1/2}}{(2t)^{3/2}}\frac{\delta\omega}{\gamma}\frac{e^{2i\widetilde{E}(0)t+i\pi/4}}{[-\widetilde{E}'(0)]^{3/2}E(0)H^2(0)}. \qquad (5.59)$$

With the help of Eqs. (5.44) and (5.45) we finally derive

$$|\Delta(t)| = \Delta_{0f}\left[1 - c\frac{\delta\omega}{\gamma}\frac{\cos(2E_{min}t + \pi/4)}{(2|\mu|t)^{3/2}}\right], \qquad (5.60)$$

$$\Phi(t) = 2\mu_f t - c\frac{|\mu|}{E_{min}}\frac{\delta\omega}{\gamma}\frac{\sin(2E_{min}t + \pi/4)}{(2|\mu|t)^{3/2}}. \qquad (5.61)$$

The coefficient c depends on μ, Δ_0, and γ. It is known exactly from Eq. (5.59), but involves $G(0)$, which in 3D is an elliptic integral according to Eq. (B4). In the strong-coupling BEC limit, $\mu \to -\infty$, $G(\varepsilon)$ is independent of ε and takes a simple form (B7). In this case,

$$c = \sqrt{\frac{\pi|\mu|}{\varepsilon_F}}\left(\frac{4|\mu|}{\gamma\varepsilon_F} + \pi\sqrt{\frac{|\mu|}{\Delta_0}}\right)^{-2}, \qquad (5.62)$$

where we restored the original energy units.

H. Long-time behavior of spins

Let us also work out the long-time behavior of individual spins given by Eqs. (5.40) and (5.41) and compare it to the asymptotic spin distribution, Eqs. (2.62) and (3.11), obtained earlier. The latter result is based on the few-spin conjecture, so the agreement with linear analysis provides yet another (though redundant because we already proved the few-spin conjecture for infinitesimal quenches in Sec. V D) check.

Functions $X_{1,2}$ vanish as $t \to \infty$, while the large-time limit of $Y_{1,2}$ derives from the identity

$$\lim_{t\to\infty}\int_0^\infty \frac{d\varepsilon' F(\varepsilon')e^{\pm 2iE(\varepsilon')t}}{\varepsilon' - \varepsilon} = \pm i\pi\alpha F(\varepsilon)e^{\pm 2iE(\varepsilon)t}, \qquad (5.63)$$

where α is the sign of $t\,dE(\varepsilon')/d\varepsilon'$ at $\varepsilon' = \varepsilon$ and $F(\varepsilon')$ is an arbitrary bounded continuous function.

Applying this identity to Eqs. (5.38) and (5.39) and substituting resulting expressions into Eqs. (5.40) and (5.41),

we obtain

$$\frac{s_\infty^-(\varepsilon,t)e^{2i\mu_f t}}{s_f^-(\varepsilon)} = 1 - \frac{2\delta\omega}{\gamma}\frac{\exp[-2iE(\varepsilon)t - i\phi]}{\sqrt{\pi^2 f^2(\varepsilon) + H^2(\varepsilon)}}$$
$$- \frac{2\delta\omega}{\gamma}\left[\frac{\xi}{E(\varepsilon)} - 1\right]\frac{\cos[2E(\varepsilon)t + \phi]}{\sqrt{\pi^2 f^2(\varepsilon) + H^2(\varepsilon)}},$$

(5.64)

$$\frac{s_\infty^z(\varepsilon,t)}{s_f^z(\varepsilon)} = 1 + \frac{2\delta\omega}{\gamma}\frac{\Delta_{0f}^2}{\xi E(\varepsilon)}\frac{\cos[2E(\varepsilon)t + \phi]}{\sqrt{\pi^2 f^2(\varepsilon) + H^2(\varepsilon)}}, \quad (5.65)$$

where $\xi = \varepsilon - \mu$ and ϕ is defined through

$$\cos\phi = \frac{H(\varepsilon)}{\sqrt{\pi^2 f^2(\varepsilon) + H^2(\varepsilon)}},$$
$$\sin\phi = \frac{\pi f(\varepsilon)\,\mathrm{sgn}(t\xi)}{\sqrt{\pi^2 f^2(\varepsilon) + H^2(\varepsilon)}}.$$

(5.66)

In our case $t > 0$, but we still kept it under the sign function to ensure proper behavior under time reversal; see Eq. (6.2). Equations (5.64) and (5.65) match Eq. (2.62) with

$$\theta(\varepsilon) \approx \sin\theta(\varepsilon) = \frac{2\delta\omega}{\gamma}\frac{\Delta_0}{E(\varepsilon)\sqrt{\pi^2 f^2(\varepsilon) + H^2(\varepsilon)}}. \quad (5.67)$$

(Not that in the present case $\Delta_\infty = \Delta_{0f}$ and $\mu_\infty = \mu_f$.) This indeed agrees with Eq. (3.13) obtained from the few-spin conjecture.

I. Short-time behavior

Here we analyze the short-time behavior of $|\Delta(t)|$ for quenches within the universal weak-coupling regime. For large quenches from weaker to stronger coupling, when $\Delta_{0f}/\Delta_{0i} \gg 1$, or from the normal state (zero initial coupling) in this regime $|\Delta(t)|$ grows as $e^{\Delta_0 t}$. This exponential growth reflects the instability of the normal state in the presence of superconducting interactions [7,16]. At the same time, even for small quenches $|\Delta(t)|$ rises or falls sharply at short times; see Figs. 7 and 25. Sharp growth is seen in experiment, too, though most of it is probably due to a different mechanism [31].

A direct small t expansion of the cosine in Eq. (5.36) diverges at high energies. Cutting off the integral at ε_Λ (Debye energy in the case of metals), one obtains [12] $\delta|\Delta(t)| \propto \delta\Delta_0(\varepsilon_\Lambda t)^2$. This is cutoff dependent and applies only to ultrashort times $t \ll 1/\varepsilon_\Lambda$ that vanish as the cutoff is sent to infinity. We are interested in times $1/\varepsilon_\Lambda \ll t \ll 1/\Delta_0$.

Consider Eq. (5.50). The argument of the cosine is small for $x \ll x_0$, where x_0 is determined by $e^{\frac{\pi x_0}{2}} = 1/\tau$, i.e., $x_0 = \frac{2}{\pi}\ln(1/\tau)$. Let us divide the domain of the integration into three intervals: $[0, x_0 - a]$, $[x_0 - a, x_0 + a]$, and $[x_0 + a, \infty)$ and let the corresponding integrals be I_1, I_2, and I_3, respectively. The auxiliary parameter a, $1 \ll a \ll x_0$, is such that $1/a \to 0, a/x_0 \to 0$ as $x_0 \to \infty$. For example, one can take $a = \sqrt{x_0}$. Expanding the cosine in small τ in I_1 and integrating, we obtain

$$I_1 = \frac{1}{2} - \frac{1}{\pi x_0} - \frac{a}{\pi x_0^2} + o(a/x_0^2). \quad (5.68)$$

In I_2 we replace $x^2 + 1 \to x_0^2$ up to terms of order a/x_0. After this, a substitution $y = \exp \pi x/2$ transforms it into the cosine integral $\int dy \cos y/y$ with known behavior, leading to

$$I_2 = \frac{a}{\pi x_0^2} + o(a/x_0^2). \quad (5.69)$$

Integrating by parts in I_3, we see that it is proportional to $e^{-\pi a/2}/x_0^2$, which is negligibly small. Thus,

$$I_1 + I_2 + I_3 = \frac{1}{2} - \frac{1}{2|\ln(\tau)|} + o\left[\frac{1}{|\ln(\tau)|}\right]. \quad (5.70)$$

Note the cancellation of the auxiliary parameter a. Finally, plugging this into Eq. (5.50), we derive the short-time behavior of the gap function amplitude

$$|\Delta(t)| = \Delta_{0i} + \frac{\Delta_{0f} - \Delta_{0i}}{|\ln(\Delta_0 t)|}. \quad (5.71)$$

VI. APPROACH TO THE ASYMPTOTE IN THE NONLINEAR CASE

Here we discuss the approach of $\Delta(t)$ to its large-time asymptote in the nonlinear case. We consider regimes I and II, the gapless phase and the phase where $\Delta(t) \to \Delta_\infty e^{-2i\mu_\infty t - 2i\varphi}$. Rather than rigorously deriving the $t \to \infty$ asymptote in its entirety as we did for the linearized dynamics, we present an argument based only on our knowledge of the frequency spectrum that works under certain general assumptions about relevant Fourier amplitudes.

As $t \to \infty$ spins tend to their steady-state form, $\vec{s}(\varepsilon,t) \to \vec{s}_\infty(\varepsilon,t)$, where $\vec{s}_\infty(\varepsilon,t)$ is given by Eqs. (2.45) and (2.62) in regimes I and II, respectively. In phase II, in a reference frame rotating with frequency $2\mu_\infty$ around the z axis, $\vec{s}_\infty(\varepsilon)$ rotates with a constant frequency $2E_\infty(\varepsilon) = 2\sqrt{(\varepsilon - \mu_\infty)^2 + \Delta_\infty^2}$. As mentioned above, an integrable model with N degrees of freedom is characterized by N incommensurate frequencies [63] that are determined by the integrals of motion and are fixed throughout its time evolution. The Fourier decomposition of any dynamical quantity can have only these basic frequencies in its spectrum. In particular,

$$|\Delta(t)| = \Delta_\infty + \int_0^\infty F(\varepsilon)\cos[2E_\infty(\varepsilon)t]f(\varepsilon)d\varepsilon, \quad (6.1)$$

with some unknown function $F(\varepsilon)$.

Terms containing $\sin[2E_\infty(\varepsilon)t]$ are absent by time-reversal symmetry [cf. Eq. (5.35)] of the equations of motion (1.8) and (1.33) [see also Eq. (2.24)]

$$s^z(-t) = s^z(t), \quad s^+(-t) = s^-(t), \quad \bar{\Delta}(-t) = \Delta(t), \quad (6.2)$$

where we suppressed ε dependence of spins for compactness. These relations hold at all times as long as the initial condition at $t = 0$ satisfies them, which our initial state (1.28) does.

A common practice in previous work is to attempt to determine the approach of $|\Delta(t)|$ to its asymptotic value Δ_∞ from the steady-state spins $\vec{s}_\infty(\varepsilon,t)$. Consider the one-channel case for simplicity. Continuum version of Eq. (1.13) at $t = \infty$ is

$$\Delta_\infty(t) = \lambda \int_0^\infty s_\infty^-(\varepsilon,t)f(\varepsilon)d\varepsilon. \quad (6.3)$$

The constant part of $s_\infty^-(\varepsilon,t)$ yields Δ_∞, while the contribution of the oscillating part integrated over ε vanishes (dephases) as $t \to \infty$. One can further determine the large-time asymptote of Eq. (6.3) similarly to how we evaluated the large-time behavior of Eq. (5.35). This is, however, *not* the correct asymptote of the actual $\Delta(t)$. Not only does it not yield the correct coefficient of the time-dependent part of $\Delta(t)$ [such as the coefficient c in Eq. (5.60)], but also the actual time dependence can be different.

At finite t there is a correction to the steady-state value of the spin, $\vec{s}(\varepsilon,t) = \vec{s}_\infty(\varepsilon,t) + \delta\vec{s}(\varepsilon,t)$, so that the actual order parameter is

$$\Delta(t) = \lambda \int_0^\infty s_\infty^-(\varepsilon,t) f(\varepsilon) d\varepsilon + \lambda \int_0^\infty \delta s^-(\varepsilon,t) f(\varepsilon) d\varepsilon.$$

(6.4)

Even though $\delta s^-(\varepsilon,t)$ is small as compared to the oscillating part of $s_\infty^-(\varepsilon,t)$ at large times, this is no longer true after integrating these quantities over ε. Consider, for example, Eq. (5.40). We showed in Sec. V H that $s_\infty^-(\varepsilon,t)$ comes from functions $Y_{1,2}(\varepsilon,t)$. However, we see from Eq. (5.35) that the integral of these functions over ε vanishes and, as a result, they do not contribute to $\Delta(t)$. The correction $\delta s^-(\varepsilon,t)$, on the other hand, comes from both $X_{1,2}(t)$ and $Y_{1,2}(\varepsilon,t)$. It is this contribution from $X_{1,2}(t)$ to $\delta s^-(\varepsilon,t)$ that actually determines $\Delta(t)$. Thus, there is a partial cancellation between the two integrals in Eq. (6.4) and the true large-time behavior of $\Delta(t)$ can only be determined by keeping both.

Nevertheless, $\Delta_\infty(t)$ being a legitimate dynamical quantity has the right frequency spectrum and also contains the dimensionless density of states $f(\varepsilon)$. So, it still produces a correct large-time dependence when, for example, the latter is set by a stationary point as in Eq. (5.52) or by the behavior of $f(\varepsilon)$ at small ε as in Eq. (5.60). The situation on the BEC side in 2D is different. The $\ln^2 t$ dependence in the denominator of Eq. (5.57) comes from $K(\varepsilon) \propto 1/\ln^2 \varepsilon$ behavior of the Fourier amplitude at small ε; see Eq. (5.42) and the text below Eq. (5.55). This is, in turn, a consequence of $K(\varepsilon) \propto H^{-2}(\varepsilon)$ and $H(\varepsilon) \propto \ln \varepsilon$, which follow from Eqs. (5.43), (B8), and (B5). Were we to evaluate the large-time asymptote of $|\Delta(t)|$ using Eq. (6.3), we would obtain $1/(t \ln t)$ instead of $1/(t \ln^2 t)$. To see this, note that Eq. (5.64) implies that the oscillating part of $s_\infty^-(\varepsilon,t)$ is proportional to $H^{-1}(\varepsilon)$, i.e., to $1/\ln \varepsilon$, at small ε and apply the same steps as in the text below Eq. (5.55). The $1/\ln \varepsilon$ dependence cancels in Eq. (6.4) due to the second term on the right-hand side. We note also that Eqs. (2.62) and (3.11) imply $s_\infty^-(\varepsilon,t) \propto 1/\ln \varepsilon$ in all of region II in 2D, not just in the linear approximation.

Similar considerations apply in analyzing Eq. (6.1). Let us work out the large-time behavior of $|\Delta(t)|$ in steady states I, II, and II′ separately.

A. Regime II

In steady states II and II′ $\Delta(t) \to \Delta_\infty e^{-2i\mu_\infty t - 2i\varphi}$. For quenches in region II $\mu_\infty > 0$, so it can be viewed as a nonequilibrium extension of the BCS regime. The frequency spectrum $2E_\infty(\varepsilon)$ has a stationary point at $\varepsilon = \mu_\infty$, $E'_\infty(\mu_\infty) = 0$, which in regime II lies within the integration range. The large-time behavior of Eq. (6.1) obtains with the help of stationary point

method [cf. Eq. (5.52)]

$$|\Delta(t)| = \Delta_\infty + \sqrt{\pi} F(\mu_\infty) \Delta_\infty^2 \frac{\cos(2\Delta_\infty t + \pi/4)}{\sqrt{\Delta_\infty t}}. \quad (6.5)$$

The only assumption about $F(\varepsilon)$ here is that it is smooth. This is an extension of Eq. (5.52) to the nonlinear regime. In the weak-coupling BCS limit this result was published in Ref. [16]. In this limit Δ_∞ is given by Eq. (3.29) and generally it obtains from Eqs. (3.15) and (3.39) in 2D and 3D, respectively, and Eq. (3.14) as the imaginary part of u. Here we see that expression (6.5) holds throughout the entire region II for both one- and two-channel models.

B. Regime II′

Regime II′ has the same asymptotic $\Delta(t)$ as II by definition only with $\mu_\infty < 0$. There are now no stationary points on the integration path. The approach to the asymptote is therefore determined by the behavior of $F(\varepsilon)f(\varepsilon)$ near the end points, $\varepsilon = 0$ in this case. We *assume* this behavior is the same as in linear analysis, since we expect the time dependence to have the same functional form throughout a given regime. According to Sec. V G, this means finite nonzero $F(0)$ in 3D and $F(\varepsilon) \propto 1/\ln^2 \varepsilon$ for $\varepsilon \ll 1$ in 2D.

Expanding Eq. (3.11) in small ε and using Eq. (2.62), we see that the spin components at $t \to \infty$ do behave the same as in linear analysis, though this in itself does not prove our assumption. Moreover, the asymptotic spin distribution (3.11) is continuous across critical lines separating various regimes, so the same small ε form holds in gapless region I as well.

As long as our assumptions about $F(\varepsilon)$ are correct, the analysis of the integral in Eq. (6.3) is the same as that in Sec. V G, resulting in

$$|\Delta(t)| = \Delta_\infty \left[1 - c_1 \frac{\sin\left(2E_\infty^{\min} t\right)}{t \ln^2 t} \right] \quad \text{in 2D} \quad (6.6)$$

and

$$|\Delta(t)| = \Delta_\infty \left[1 - c_2 \frac{\cos\left(2E_\infty^{\min} t + \pi/4\right)}{t^{3/2}} \right] \quad \text{in 3D}, \quad (6.7)$$

at large times, where $E_\infty^{\min} = \sqrt{\mu_\infty^2 + \Delta_\infty^2}$ and c_1 and c_2 are real coefficients that depend on Δ_{0i}, Δ_{0f}, and γ.

C. Gapless regime

Finally, we turn to regime I. Now $\Delta(t) \to 0$ at $t \to \infty$. Spins $\vec{s}_\infty(\varepsilon)$ rotate with frequencies 2ε around the z axis, so that the Fourier transform of the order parameter magnitude is of the form

$$|\Delta(t)| = \int_0^\infty F(\varepsilon) \cos(2\varepsilon t) f(\varepsilon) d\varepsilon, \quad (6.8)$$

and the $\sin(2\varepsilon t)$ term vanishes by time-reversal symmetry (6.2).

In 3D we similarly assume finite and nonzero $F(0)$. Steps outlined below Eq. (5.58) in Sec. V G now lead to the following large-time behavior:

$$|\Delta(t)| = \frac{c_3}{t^{3/2}}. \quad (6.9)$$

In 2D we speculate that $F(\varepsilon) \propto 1/\ln^r \varepsilon$ at small ε, where r is either 1 or 2. As discussed before in this section, $s_\infty^-(\varepsilon,t) \propto 1/\ln \varepsilon$ in 2D, so that $\Delta_\infty(t) \propto 1/(t \ln t)$. The $1/\ln \varepsilon$ term, however, cancels from $F(\varepsilon)$ at least in linear analysis and it ends up being proportional to $1/\ln^2 \varepsilon$ instead. In the gapless case we allow for a possibility that such a cancellation does not occur. The analysis of the integral in Eq. (6.8), analogous to that leading to Eq. (5.60), then yields

$$|\Delta(t)| = \frac{c_4}{t \ln^r t}. \qquad (6.10)$$

The gapless regime contains the $\Delta_{0i} = \Delta_{0f} = 0$ point, the origin of quench phase diagrams. It therefore includes the weak-coupling limit $\Delta_{0i}/\varepsilon_F \to 0$ and $\Delta_{0f}/\varepsilon_F \to 0$. Equation (6.8) becomes in this limit [see Sec. V E]

$$|\Delta(t)| = \int_{-\infty}^{\infty} F(\xi) \cos(2\xi t) d\xi, \qquad (6.11)$$

where $F(\xi)$ is even in ξ. Now there can be no power law in t contribution at large t coming from integration limits. Instead, $|\Delta(t)|$ vanishes exponentially [17,18] as $A(t)e^{-2\alpha \Delta_{0i} t}$ independent of dimensionality, where $\alpha \sim 1$ and $A(t)$ is a decreasing power law, $A(t) \sim \Delta_{0i}$ at $t \sim 1/\Delta_{0i}$. Recall that throughout this paper we have been using units where $\varepsilon_F = 1$. To convert to arbitrary units in Eqs. (6.9) and (6.10), one needs to replace $t \to \varepsilon_F t$. Guided by linear analysis, we further assume that coefficients c_4 and c_5 are of order Δ_{0f}, which we take to be comparable to Δ_{0i}. It is clear that at any finite $\Delta_{0i}/\varepsilon_F \ll 1$ power laws in Eqs. (6.9) and (6.10) coming from the lower integration limit will eventually win over the exponential decay. The comparison of $e^{-2\alpha \Delta_{0i} t}$ with $(\varepsilon_F t)^{-1}$ shows that the weak-coupling result is valid at times such that $\ln(\varepsilon_F/\Delta_{0i}) \gg \Delta_{0i} t \gg 1$, while for $\Delta_{0i} t \gg \ln(\varepsilon_F/\Delta_{0i})$ it has to be replaced with Eqs. (6.9) and (6.10).

VII. EXPERIMENTAL SIGNATURES

Far-from-equilibrium states of fermionic superfluids described in this paper can be observed in different systems with various experimental techniques.

Matsunaga *et al.* [25,26] directly measured the time-dependent amplitude $|\Delta(t)|$ induced by an ultrafast electromagnetic perturbation in $Nb_{1-x}Ti_xN$ films using terahertz-pump–terahertz-probe spectroscopy. The underlying system is a BCS superconductor [weak-coupling regime of the one-channel model (1.3)] and for perturbation strength below certain threshold its nonadiabatic dynamics falls within region II of our quench phase diagrams. Even though we considered BCS interaction quenches in the one-channel model in this paper, it is clear from our arguments that our results apply more generally to any kind of nonadiabatic global perturbation. Therefore, we expect $|\Delta(t)|$ to be described by Eq. (6.5) derived originally in nonlinear regime by Yuzbashyan *et al.* [16]. These experiments indeed measure damped oscillations with frequency $2\Delta_\infty$, where Δ_∞ is the asymptotic value of $|\Delta(t)|$ even when the system is deep in the nonlinear regime and Δ_∞ is much different from the ground-state gap. The power-law approach, however, appears to be faster than $1/t^{1/2}$.

In this paper we primarily focused on detuning or interaction quenches in cold fermions. Experiments address-ing superfluidity in these systems include measurements of the molecular condensate fraction [47,48], radio-frequency absorption spectra [68], and observation of vortices [69]. Signatures of "far-from-equilibrium phases" I, II, and III—gapless, gapped (Volkov-Kogan), and oscillatory—in these experiments can be derived from the many-body wave function $\Psi(t)$ determined above.

The pseudospin (fermionic) part of $\Psi(t)$ is a direct product of spin-$\frac{1}{2}$ wave functions $\prod_{\mathbf{p}} (\bar{u}_{\mathbf{p}}|\downarrow\rangle + \bar{v}_{\mathbf{p}}|\uparrow\rangle)$ found in Sec. II D. In the gapless steady state

$$\begin{pmatrix} u_{\mathbf{p}} \\ v_{\mathbf{p}} \end{pmatrix} = \cos\frac{\theta_{\mathbf{p}}}{2} \begin{pmatrix} 1 \\ 0 \end{pmatrix} e^{-i\varepsilon_{\mathbf{p}} t} + \sin\frac{\theta_{\mathbf{p}}}{2} \begin{pmatrix} 0 \\ 1 \end{pmatrix} e^{i\varepsilon_{\mathbf{p}} t - i\delta_{\mathbf{p}}}, \qquad (7.1)$$

where $\cos\theta_{\mathbf{p}} \equiv \cos\theta(\varepsilon_{\mathbf{p}})$ is given by Eq. (3.11) in all three phases. The second term represents an occupied pair of states $\pm\mathbf{p}$ (pseudospin up); the first represents an empty pair of states (pseudospin down). $\Psi(t)$ in the gapless phase is a coherent superposition of eigenstates of a free Fermi gas with different energies reflecting the fact that $\Delta(t) \to 0$ implies vanishing of interactions between fermions on the mean-field level. Effectively, the system is governed by a noninteracting Hamiltonian at $t \to \infty$. It nevertheless retains superconducting correlations. For example, in the weak-coupling regime its superfluid density is half that in the ground state and in phase II [18]. Phase I is therefore a nonequilibrium gapless superfluid.

In the gapped steady state Eqs. (2.51) and (2.63) imply

$$\begin{pmatrix} u_{\mathbf{p}} e^{i\mu_\infty t} \\ v_{\mathbf{p}} e^{-i\mu_\infty t} \end{pmatrix} = \cos\frac{\theta_{\mathbf{p}}}{2} \overbrace{\begin{pmatrix} |U_{\mathbf{p}}| \\ |V_{\mathbf{p}}| \end{pmatrix}}^{\text{ground-state pair}} e^{-iE_{\mathbf{p}}^\infty t}$$

$$+ \sin\frac{\theta_{\mathbf{p}}}{2} \overbrace{\begin{pmatrix} |V_{\mathbf{p}}| \\ -|U_{\mathbf{p}}| \end{pmatrix}}^{\text{excited pair}} e^{iE_{\mathbf{p}}^\infty t}, \qquad (7.2)$$

where

$$|U_{\mathbf{p}}| = \sqrt{\frac{1}{2} + \frac{\xi_{\mathbf{p}}}{2E_{\mathbf{p}}^\infty}}, \quad |V_{\mathbf{p}}| = \sqrt{\frac{1}{2} - \frac{\xi_{\mathbf{p}}}{2E_{\mathbf{p}}^\infty}}, \qquad (7.3)$$

$\xi_{\mathbf{p}} = \varepsilon_{\mathbf{p}} - \mu_\infty$, and we dropped the nonessential constant phase φ. Bogoliubov amplitudes $|U_{\mathbf{p}}|$ and $|V_{\mathbf{p}}|$ are the same as in the BCS ground state [70] with gap Δ_∞ and chemical potential μ_∞. The two wave functions on the right-hand side of Eq. (7.2) are the two orthonormal eigenstates of the BdG Hamiltonian,

$$H_{\text{BdG}} = \begin{pmatrix} \xi_{\mathbf{p}} & \Delta_\infty \\ \Delta_\infty & -\xi_{\mathbf{p}} \end{pmatrix}. \qquad (7.4)$$

The first one is a Cooper pair wave function in the BCS ground state and corresponds to an alignment of the pseudospin $\vec{s}_{\mathbf{p}}$ antiparallel to the effective magnetic field. The second one is an excited state of the Cooper pair ($\vec{s}_{\mathbf{p}}$ parallel to the effective magnetic field) termed an *excited pair* in the original BCS work [71]. It is interesting to note that these excitations of the condensate in superconducting metals carry no charge and spin, so nonadiabatic dynamics considered here provides a unique venue for creating and measuring them [19]. The steady state in phase II therefore is a coherent mixture of ground-state

and excited pairs, a superposition of eigenstates of the BCS Hamiltonian with gap Δ_∞ and chemical potential μ_∞.

A similar interpretation of the oscillatory state obtains by Fourier transforming the amplitudes (2.73),

$$\begin{pmatrix} u_{\mathbf{p}} e^{i\tilde{\mu}t} \\ v_{\mathbf{p}} e^{-i\tilde{\mu}t} \end{pmatrix} = \sum_{n=-\infty}^{\infty} \left\{ \cos \frac{\theta_{\mathbf{p}}}{2} \begin{pmatrix} a_{\mathbf{p}n} \\ b_{\mathbf{p}n} \end{pmatrix} e^{-i(e_{\mathbf{p}} - n\omega_\Delta)t} \right.$$
$$\left. + \sin \frac{\theta_{\mathbf{p}}}{2} \begin{pmatrix} \bar{b}_{\mathbf{p}n} \\ -\bar{a}_{\mathbf{p}n} \end{pmatrix} e^{i(e_{\mathbf{p}} - n\omega_\Delta)t} \right\}, \qquad (7.5)$$

where ω_Δ is the oscillation frequency of $|\Delta(t)|$, $\tilde{\mu}$ and $-2e_{\mathbf{p}}$ are the zeroth harmonics of the phase of $\Delta(t)$ and the common phase of the amplitudes [see Eqs. (2.53) and (2.57)], and we again dropped the constant phase φ. This expression derives by first going to a frame rotating with frequency $2\tilde{\mu}$ to get rid of the linear term in the phase of $\Delta(t)$. This makes $e^{-i\phi_{\mathbf{p}}}$, the term involving the relative phase, periodic according to Eq. (2.54) and it does not contribute to the momentum-dependent phases on the right-hand side. Phase III, therefore, can be understood as a superposition of generalized excited- and ground-state pairs with dispersions $\pm e_{\mathbf{p}}$ and quanta of the amplitude (Higgs) mode $|\Delta(t)|$. As noted in Sec. II D 2, $e_{\mathbf{p}} \to \varepsilon_{\mathbf{p}}$ at large $\varepsilon_{\mathbf{p}}$.

The knowledge of the steady state allows us to compute far-from-equilibrium correlation and Green's functions in all three phases. For example [72],

$$i\mathcal{G}_{\mathbf{p},>}(t,t') = \langle \hat{a}_{\mathbf{p}\uparrow}(t) \hat{a}^\dagger_{\mathbf{p}\uparrow}(t') \rangle = \bar{u}_{\mathbf{p}}(t) u_{\mathbf{p}}(t'),$$

$$-i\mathcal{G}_{\mathbf{p},<}(t,t') = \langle \hat{a}^\dagger_{\mathbf{p}\uparrow}(t') \hat{a}_{\mathbf{p}\uparrow}(t) \rangle = \bar{v}_{\mathbf{p}}(t') v_{\mathbf{p}}(t), \qquad (7.6)$$

$$\mathcal{G}^+_{\mathbf{p}}(t,t') = \langle \hat{a}^\dagger_{-\mathbf{p}\downarrow}(t) \hat{a}^\dagger_{\mathbf{p}\uparrow}(t') \rangle = v_{\mathbf{p}}(t) \bar{u}_{\mathbf{p}}(t').$$

With these we can evaluate various observables such as the superfluid density mentioned earlier in this section. Note also that the steady-state momentum distribution $n_p^\infty(t) dp$ is simply related to the z component of the pseudospin according to Eq. (1.6). Taking into account that $\mathbf{p}$ and $-\mathbf{p}$ are both included in $s_{\mathbf{p}}^z$ and integrating over the angles, we have

$$n_p^\infty(t) = 2p^2 (2s_{\mathbf{p}}^z + 1). \qquad (7.7)$$

Expressions for $s_{\mathbf{p}}^z$ in phases I, II, and III appear in Eq. (2.48), Eq. (2.62), and Eqs. (2.55) and (2.72), respectively.

Finally, let us discuss the signatures of nonequilibrium phases in radio-frequency (RF) spectroscopy [73–79]. Recall that in an atomic Fermi gas the pairing occurs between atoms in two different hyperfine states, $|\uparrow\rangle \equiv |1\rangle$ and $|\downarrow\rangle \equiv |2\rangle$. The RF photon transfers atoms from one of these states, say $|2\rangle$, to the third hyperfine state $|3\rangle$ that does not interact with $|1\rangle$ and $|2\rangle$. In an unpaired Fermi gas where atoms $|2\rangle$ are free, the RF absorption spectrum has a peak at the atomic transition energy $\omega = \mathcal{E}_{23}$. In the paired ground state, the peak shifts to $\omega > \mathcal{E}_{23}$ by an amount equal to the minimum binding energy of Cooper pairs [73].

The RF response of steady states I, II, and III was calculated in Ref. [19] for quenches within the BCS regime and in Ref. [36] for quenched p-wave superfluids. The calculation in the present case is identical [80], so we do not reproduce it here. The RF spectrum of phase I is similar to that of the normal state, a peak at $\omega = \mathcal{E}_{23}$. In phase II there are two peaks—at $\omega > \mathcal{E}_{23}$ and $\omega < \mathcal{E}_{23}$—which come from the ground-state and excited pairs, respectively; see Eq. (7.2). The first peak corresponds to

a process in which an RF photon breaks a ground-state pair; the second peak corresponds to a process in which an RF photon breaks an excited pair. The RF response of phase III similarly reflects the structure of the corresponding steady-state wave function (7.5). There are two series of peaks spaced by ω_Δ, the frequency of oscillations of $|\Delta(t)|$, coming from processes where an RF photon breaks a ground-state (excited) pair and absorbs or emits several quanta of the amplitude (Higgs) mode $|\Delta(t)|$.

VIII. CONCLUSION

In this paper we studied the coherent dynamics of an isolated BCS-BEC condensate in two- and one-channel (BCS) models in two and three spatial dimensions. Our main focus was on detuning quenches $\omega_i \to \omega_f$ (interaction quenches $\lambda_i \to \lambda_f$ in the one-channel model). We constructed exact quench phase diagrams and predicted the order parameter dynamics $\Delta(t)$ and the full time-dependent wave function $\Psi(t)$ of the system at large times for any pair of values (ω_i, ω_f). In contrast to most previous work, we considered quenches beyond the weak-coupling limit of BCS-to-BCS quenches. We add to this BCS-to-BEC and BEC-to-BCS quenches across the Feshbach resonance, as well as quenches on the BEC side. We showed that the weak-coupling limit is universal in that it is model and dimension independent. Outside of this limit, there are several qualitatively different features, the two-channel model having richer quench phase diagram as it contains an extra parameter: dimensionless resonance width γ. All results for the one-channel model obtain from the two-channel ones by taking the broad resonance, $\gamma \to \infty$, limit.

We find the same three main nonequilibrium phases (asymptotic states) as in the weak-coupling regime. Interestingly, this seems to be a universal, model-independent feature of quench dynamics of fermionic condensates, at least when there is a global complex order parameter, so that the Cooper pairs interact only through this collective mode. The same three phases occur, for example, in p-wave superconductors [36,37], spin-orbit coupled superfluids [81], and s-wave superconductors with energy-dependent interaction [20]. One can speculate that similar universality according to the order parameter type exists among quench phase diagrams of multicomponent superfluids, such as three fermion species with pairing interactions or multiband superconductors.

The above three main phases are phase I, where $\Delta(t)$ vanishes; phase II, where $\Delta(t) \to \Delta_\infty e^{-2i\mu_\infty t}$ up to a constant phase factor; and phase III, where $|\Delta(t)|$ oscillates persistently. It turns out that μ_∞ plays the role of a nonequilibrium analog of the chemical potential. For quenches within the weak-coupling regime $\mu_\infty \approx \varepsilon_F$, while for quenches to deep BEC $\mu_\infty \to -\infty$. Some of the new effects as one moves beyond the weak-coupling regime are as follows. The oscillatory approach of $|\Delta(t)|$ to a constant (Volkov-Kogan behavior) changes from $1/\sqrt{t}$ for $\mu_\infty > 0$ to $1/t^{3/2}$ in 3D and $1/(t \ln^2 t)$ in 2D for $\mu_\infty < 0$, and the oscillation frequency changes from $2\Delta_\infty$ to $2\sqrt{\mu_\infty^2 + \Delta_\infty^2}$. For resonance width below a certain threshold, the asymptotic gap amplitude Δ_∞ can be much larger than Δ_{0f}, the ground-state gap at final detuning ω_f. Similarly, exponential vanishing of $|\Delta(t)|$ in phase I gives way to a power-law behavior. Persistent oscillations

in phase III are first suppressed for stronger quenches and then disappear altogether. For example, in 3D one-channel model there is a critical coupling λ_c, such that even quenches from an infinitesimally small λ_i to $\lambda_f > \lambda_c$ produce no such oscillations. As λ_f approaches λ_c from below, the oscillation amplitude first increases, then decreases, and finally vanishes at $\lambda_f = \lambda_c$.

The postquench asymptotic state of the condensate is a coherent superposition of ground-state and excited pairs at each momentum [multiple bands of such pairs shifted by the oscillation frequency of $|\Delta(t)|$ in phase III]. These are two orthogonal eigenstates of a Cooper pair in the self-consistent field, and, for instance, the BCS ground state is a direct product of ground-state pair wave functions. Our steady state in phases I and II is a direct product of such time-dependent superpositions. In the Anderson pseudospin language, ground-state (excited) pairs correspond to the alignment of pseudospin antiparallel (parallel) to the magnetic field. Even though we refer to these states as ground-state or excited pairs, we should stress that they are not the same as similar states of Cooper pairs in the ground or excited states of the BCS Hamiltonian since the self-consistent field is different. Excited pairs are elusive excitations in superconductors; it is difficult to couple to them as they carry no charge or spin. Nonadiabatic dynamics of the BCS-BEC condensate provides an opportunity to access them, e.g., in the RF absorption spectrum.

Our treatment of the dynamics of the BCS-BEC condensate neglects the coupling to the noncondensed modes (mean-field approximation), molecules with nonzero momenta **q** in the two-channel model. We check the validity of this approximation for the two-channel model by estimating the rates of the decoherence processes due to these terms for postquench steady states in phase II and comparing them to the typical time scale on which the quench dynamics occurs. Our preliminary results indicate that the mean-field approach is justified for quenches sufficiently far from the $\mu_\infty = 0$ line in the quench phase diagrams, e.g., quenches within deep BEC, deep BCS, or across the resonance from deep BCS to deep BEC and vice versa. A more thorough study of these effects is necessary to fully clarify the situation.

In mean-field various pairing Hamiltonians, e.g., one- and two-channel models considered here, chiral p-wave BCS, a certain class of d-wave BCS models [39], is equivalent to integrable classical spin (or spin-oscillator) chains with long-range interactions. The most remarkable general feature of their dynamics is a reduction in the number of effective degrees of freedom as $t \to \infty$. Consider, e.g., the one-channel model. As explained above, its dynamics in the thermodynamic limit at long times after the quench can be described in terms of just a few—zero (phase I), one (phase II), or two (phase III)—collective classical spin variables. In other words, the number of spins at long times reduces from infinity to zero, one, or two. Moreover, the spin times evolve with the same Hamiltonian only with "renormalized" parameters. For example, in phase I the effective Hamiltonian at large times is simply $H = 0$, and in phase II it is $H = 2\mu_\infty S_z - g S_- S_+$, where $\vec{S}$ is the collective spin of length $|\vec{S}| = \Delta_\infty/g$ and g is the original BCS coupling constant. The order parameter $\Delta(t)$ coincides with that of the few-spin problem, while the original spins relate to the collective ones in a more involved fashion.

It is this feature of the dynamics together with the integrability of the underlying model that allowed us to explicitly determine the exact postquench asymptotic state of the system. In this paper we presented for the first time a comprehensive, consistent overview of a general method to explicitly evaluate the large-time asymptotic solution in classical integrable systems that support this kind of reduction. We are not aware of any similar method for other integrable nonlinear models, the rather different soliton resolution conjecture [82] being the closest analog we were able to identify.

An interesting open question is whether a similar reduction in the number of degrees of freedom in the course of time evolution occurs also in nonintegrable pairing models. This can explain the aforementioned universality of the quench phase diagrams among systems characterized by a global complex order parameter. It seems nonaccidental indeed that the nonintegrable spin-orbit coupled superfluid [81] has the same three main postquench phases and that, moreover, $\Delta(t)$ in phase III is given by an elliptic function dn. Presumably, a generalization of this method to nonintegrable models would rely on more general considerations without recourse to integrability-specific techniques and thus would clarify the underlying physical mechanism. It would also make a number of interesting problems, such as, e.g., the competition between chiral and antichiral components in p-wave superconductors upon switching on superconducting interactions and, more generally, the dynamical interplay among various components in a multicomponent superfluid, potentially amenable to in-depth analysis.

APPENDIX A: PAIR-BREAKING RATES

In this Appendix, we perform a preliminary analysis of the validity of neglecting **q** $\neq 0$ terms far from equilibrium in the Hamiltonian (1.1). So far, we have studied the quench dynamics of the condensate decoupled from these noncon-densed modes. There are two kinds of relevant processes due to the **q** $\neq 0$ terms: (i) excitation of molecules out of the condensate and (ii) excitation of fermionic quasiparticles through two-particle collisions. We estimate characteristic time scales of both processes in the postquench steady state. We find that sufficiently far from the $\mu_\infty = 0$ line in our quench phase diagrams (see Figs. 3 and 21) these time scales are much larger than the characteristic time of the quench dynamics. This means that dropping **q** $\neq 0$ terms is indeed justified at times it takes for the quench dynamics to develop and reach the steady state. At much later times, after the quench dynamics plays out, these terms set in, presumably leading to decoherence and eventual thermalization of our (isolated) system. We note also that the $\mu_\infty = 0$ line can be very roughly interpreted as a far-from-equilibrium generalization of the unitarity point. Quenches away from this line are from BCS or BEC initial

detuning to the far BCS and BEC side, including quenches across the resonance.

In what follows we consider a 3D condensate and, for simplicity, we content ourselves with steady states in phase II (including II′), where pairing amplitude asymptotes to a constant, $|\Delta(t \to \infty)| = \Delta_\infty$.

1. Steady-state molecular production

Here we compute the rate at which molecules with nonzero momentum are produced in steady state II, where initially all molecules have zero momentum. To the lowest order in the interaction, the corresponding scattering amplitudes are [83]

$$\mathcal{A}_b(\mathbf{p}_1,\mathbf{p}_2)\delta(E_{\text{fin}} - E_{\text{in}}) = \int_{-\infty}^{\infty} \langle \Psi_{\text{fin}}|\hat{V}(t)|\Psi_{\text{in}}\rangle dt, \quad \text{(A1)}$$

where $|\Psi_{\text{in}}\rangle$ and E_{in} are the steady-state wave function and energy. $|\Psi_{\text{fin}}\rangle$ obtains from $|\Psi_{\text{in}}\rangle$ by destroying two pairs and creating a molecule with momentum $\mathbf{q} = \mathbf{p}_1 + \mathbf{p}_2$ and two unpaired atoms with momenta $\mathbf{p}_1$ and $\mathbf{p}_2$. The energy of the final state is

$$E_{\text{fin}} = E_{\text{in}} + \zeta_\mathbf{q} \pm E_{\mathbf{p}_1}^\infty \pm E_{\mathbf{p}_2}^\infty, \quad \text{(A2)}$$

where plus (minus) corresponds to a ground (excited) pair and

$$\zeta_\mathbf{q} = \frac{q^2}{4m} + \omega_f - 2\mu_\infty \quad \text{(A3)}$$

is the energy of the molecule. The interaction $\hat{V}(t)$ is described by the last term in Eq. (1.1),

$$\hat{V}(t) = g \sum_{\mathbf{p}_1,\mathbf{p}_2} \left[\hat{b}_{\mathbf{p}_1+\mathbf{p}_2}^\dagger(t)\hat{a}_{\mathbf{p}_1\uparrow}(t)\hat{a}_{\mathbf{p}_2\downarrow}(t) \right.$$
$$\left. + \hat{b}_{\mathbf{p}_1+\mathbf{p}_2}(t)\hat{a}_{\mathbf{p}_2\downarrow}^\dagger(t)\hat{a}_{\mathbf{p}_1\uparrow}^\dagger(t) \right]. \quad \text{(A4)}$$

Since our initial state does not contain molecules with nonzero momentum, only the first term in Eq. (A4) contributes to the matrix element (A1). One also needs to keep in mind that our steady state contains superpositions of a ground-state pair with energy $-E_\mathbf{p}^\infty$ and an excited pair with energy $+E_\mathbf{p}^\infty$ for each $\mathbf{p}$. Equations (7.2) and (A1) then yield four scattering amplitudes [72],

$$\mathcal{A}_b^{(--)}(\mathbf{p}_1,\mathbf{p}_2) = g \cos\frac{\theta_{\mathbf{p}_2}}{2} \cos\frac{\theta_{\mathbf{p}_1}}{2} |V_{\mathbf{p}_2}||V_{\mathbf{p}_1}|,$$

$$\mathcal{A}_b^{(+-)}(\mathbf{p}_1,\mathbf{p}_2) = g \sin\frac{\theta_{\mathbf{p}_2}}{2} \cos\frac{\theta_{\mathbf{p}_1}}{2} |U_{\mathbf{p}_2}||V_{\mathbf{p}_1}|, \quad \text{(A5)}$$

$$\mathcal{A}_b^{(++)}(\mathbf{p}_1,\mathbf{p}_2) = g \sin\frac{\theta_{\mathbf{p}_2}}{2} \sin\frac{\theta_{\mathbf{p}_1}}{2} |U_{\mathbf{p}_2}||U_{\mathbf{p}_1}|,$$

where $-(+)$ describes breaking a ground-state (excited) pair and $\mathcal{A}_b^{(-+)}(\mathbf{p}_1,\mathbf{p}_2) = \mathcal{A}_b^{(+-)}(\mathbf{p}_2,\mathbf{p}_1)$.

Molecular production rate per atom at zero temperature obtains from these amplitudes and Fermi's golden rule [83],

$$\tau_{\text{mol}}^{-1} = \frac{2\pi}{N_f} \sum_{\mathbf{p}_1\mathbf{p}_2\alpha\beta} \left|\mathcal{A}_b^{(\alpha\beta)}(\mathbf{p}_1,\mathbf{p}_2)\right|^2$$
$$\times \delta\left(\zeta_{\mathbf{p}_1+\mathbf{p}_2} - \alpha E_{\mathbf{p}_2}^\infty - \beta E_{\mathbf{p}_1}^\infty\right). \quad \text{(A6)}$$

In this expression N_f is the total number of fermions in the absence of molecules and we took into account that there are no molecules with nonzero momentum in our steady state.

Let us specialize to quenches into either deep BCS ($\omega_f \to +\infty$) or deep BEC ($\omega_f \to -\infty$). We expect a much higher rate in the latter case, because in the BCS regime $\zeta_\mathbf{q} \to +\infty$, requiring excited pairs of extremely high energy to create a molecule. For quenches to the far BEC side $\mu_\infty \to -\infty$, while Δ_∞ remains finite regardless of the initial detuning; see, e.g., Figs. 18 and 19. It follows that $E_\mathbf{p}^\infty \approx \xi_\mathbf{p} = |\mu_\infty| + p^2/2m$ and Eq. (5.4) implies $\omega_f \approx 2\mu_\infty$. For $\alpha = \beta = -1$ the argument of the δ function in Eq. (A6) is always positive; i.e., energy conservation cannot be satisfied, meaning that the ground-state pairs do not contribute to the rate. Similarly, if $\alpha = \beta = 1$ (two excited pairs),

$$\zeta_{\mathbf{p}_1+\mathbf{p}_2} - E_{\mathbf{p}_1}^\infty - E_{\mathbf{p}_2}^\infty \approx \frac{(\mathbf{p}_1+\mathbf{p}_2)^2}{4m} + \omega_f - \frac{p_1^2 + p_2^2}{2m}$$

$$= \omega_f - \frac{(\mathbf{p}_1-\mathbf{p}_2)^2}{4m} < 0. \quad \text{(A7)}$$

Therefore, only scattering processes involving one fermion from an excited pair and another from a ground-state pair contribute. Expression (A6) for the rate in this case is

$$\tau_{\text{mol}}^{-1} \approx \frac{4\pi g^2}{N_f} \sum_{\mathbf{p}_1,\mathbf{p}_2} \sin^2\frac{\theta_{\mathbf{p}_2}}{2} \cos^2\frac{\theta_{\mathbf{p}_1}}{2} |U_{\mathbf{p}_2}|^2 |V_{\mathbf{p}_1}|^2$$

$$\times \delta\left(\frac{3p_1^2 + 2\mathbf{p}_1\cdot\mathbf{p}_2 - p_2^2}{4m}\right). \quad \text{(A8)}$$

Next we go from summations to integrations, integrate over the angle between $\mathbf{p}_1$ and $\mathbf{p}_2$, and change integration variables from momenta to energies, which results in

$$\tau_{\text{mol}}^{-1} \approx \frac{3\gamma}{2\varepsilon_F} \int_0^\infty d\varepsilon_2 \sin^2\frac{\theta(\varepsilon_2)}{2} |U(\varepsilon_2)|^2$$

$$\times \int_{\varepsilon_2/9}^{\varepsilon_2} d\varepsilon_1 \cos^2\frac{\theta(\varepsilon_1)}{2} |V(\varepsilon_1)|^2. \quad \text{(A9)}$$

We replace the cosine with one, use $|V(\varepsilon_1)|^2 \approx \Delta_\infty^2/4(\varepsilon_1 + |\mu_\infty|)^2$, which follows from Eq. (7.3) together with $|U(\varepsilon_1)|^2 \approx 1$, and integrate over ε_1. According to Eq. (3.13), the probability of finding an excited pair is

$$\sin^2\frac{\theta(\varepsilon_2)}{2} \to \frac{\Delta_{0i}^2(\delta\omega)^2}{16E_i^4(\varepsilon_2)} \quad \text{as } \varepsilon_2 \to \infty. \quad \text{(A10)}$$

A larger rate obtains for finite ω_i than for ω_i close to ω_f. In this case, $\delta\omega \approx 2\mu_\infty$ and $\sin^2[\theta(\varepsilon_2)/2]$ appreciably differs from zero at energies about $\sqrt{\Delta_{0i}|\mu_\infty|}$. We obtain

$$\tau_{\text{mol}}^{-1} \sim \frac{\gamma\Delta_\infty^2\Delta_{0i}}{\varepsilon_F|\mu_\infty|} \to 0. \quad \text{(A11)}$$

In deriving Eq. (A10) we assumed finite resonance width γ. A separate estimate for the broad resonance limit for quenches to deep BEC finds a rate that also vanishes, but as $\gamma^{-1/3}|\mu_\infty|^{-1/2}$.

This result for the molecular production rate should be compared with the typical time scale τ_{dyn} of the quench dynamics for quenches to the far BEC side. Equations (5.60) and (6.7) imply

$$\tau_{\text{dyn}}^{-1} \sim |\mu_\infty|. \quad \text{(A12)}$$

We see that indeed $\tau_{\text{dyn}} \ll \tau_{\text{mol}}$.

2. Two-particle collisions

Next we estimate the relaxation rate due to two-particle collisions. In contrast to the molecular production, we find that here the contribution coming from just the ground-state pairs is of the same order of magnitude or larger than that from collisions that involve excited pairs. We therefore consider ground-state pairs only and take the probability of finding such a pair at a given momentum $\mathbf{p}$ to be $\cos^2(\theta_{\mathbf{p}}/2) \approx 1$. Let us analyze quenches to the far BCS side of the Feshbach resonance from any initial detuning. In this case, $\omega_f \gg \mu_\infty \approx \epsilon_F$; see, e.g., Fig. 19. The total scattering amplitude for this case has been studied in Ref. [2] [see Eq. (71) therein], which also estimates the corresponding rate as

$$\tau_{\text{in}}^{-1} \sim \left(\frac{g^2 \nu_F}{\omega_f}\right)^2 \frac{\Delta_\infty^2}{\epsilon_F} = \gamma^2 \epsilon_F \left(\frac{\Delta_\infty}{\omega_f}\right)^2. \quad (A13)$$

In fact, this is the well-known Fermi liquid result for the quasiparticle lifetime. Indeed, $\lambda = g^2 \nu_F / \omega_f$ is the strength of the effective interaction between fermions [see Eq. (1.4)] and Δ_∞ is the typical excitation energy, the energy scale at which spins deviate appreciably from their ground-state positions.

Equation (A13) has to be compared with the characteristic time scale of the dynamics for quenches to the far BCS side. According to Eq. (6.5) this time scale is

$$\tau_{\text{dyn}} \sim \frac{1}{\Delta_\infty}. \quad (A14)$$

We see that $\tau_{\text{dyn}} \ll \tau_{\text{in}}$ for any finite resonance width γ since $\omega_f \to \infty$ in deep BCS. In the broad resonance limit, too, $\tau_{\text{dyn}}/\tau_{\text{in}} = \lambda^2 \Delta_\infty / \varepsilon_F \ll 1$. This is because at large γ quenches to the far BCS in phase II are only possible from initial detunings also on the far BCS side; see, e.g., Figs. 3(c) and 5. It then follows from Eq. (3.29) that $\Delta_\infty \leqslant \Delta_{0f} \ll \varepsilon_F$.

A preliminary analysis for quenches to the far BEC side shows that, at least for a finite resonance width γ and sufficiently large $|\omega_f|$, one still has $\tau_{\text{dyn}} \ll \tau_{\text{in}}$. Thus, neglecting two-particle collisions is justified at the times it takes the quench dynamics to fully develop and reach its asymptote.

APPENDIX B: FINITE-SIZE CORRECTIONS TO THE ROOTS

As mentioned in Sec. III, in the thermodynamic limit $\vec{L}^2(u)$ for quench initial conditions has a continuum of roots along the positive real axis. Here we verify this and determine finite-size corrections to these roots.

Roots of $\vec{L}^2(u)$ are determined by Eq. (3.3) or, equivalently, by Eq. (5.13) in notation explained in the beginning Sec. V B, which we employ here as well. The level spacing δ is of order $1/N$. Thermodynamic limit means $N \to \infty$, so ε_k become continuous with density $\nu(\varepsilon)$.

Let us look for a pair of complex conjugate roots close to ε_m, writing it as $c_m = \varepsilon_m + \varsigma_m \delta$. We take $\varsigma_m \equiv \varsigma(\varepsilon_m)$ to be of order 1, to be confirmed below. Note that ς_m is generally complex. Our goal is to evaluate c_m to first order in $1/N$. We split the summation in Eq. (5.13) into two parts: over ε_k in a small interval $(\varepsilon_m - \Delta\varepsilon, \varepsilon_m + \Delta\varepsilon)$ and over remaining ε_k. The interval is, however, sufficiently large so that it

contains many ε_k. Specifically, $\Delta\varepsilon \to 0$, but $\Delta\varepsilon/\delta \to \infty$ in the thermodynamic limit. For example, $\Delta\varepsilon = \delta\sqrt{N}$ fulfills these conditions. The latter summation becomes a principal value integral in the $N \to \infty$ limit, while the former one to leading order in $1/N$ reads

$$\frac{N(\varepsilon_m)}{2E(\varepsilon_m)\delta} \sum_{p=0}^{\infty} \left[\frac{1}{p + \varsigma_m} - \frac{1}{p + 1 - \varsigma_m}\right] = \frac{\pi \nu(\varepsilon_m)}{2E(\varepsilon_m)} \cot \pi \varsigma_m. \quad (B1)$$

The first sum is from $\varepsilon_k < \varepsilon_m$, the second sum is from $\varepsilon_k > \varepsilon_m$. Here it is important that the degeneracy $N_k \equiv N(\varepsilon_k)$ and the spacing between ε_k vary smoothly with ε_k. As long as this is the case, we can include any variation of the spacing into N_k.

Thus, Eq. (5.13) to leading order in $1/N$ becomes

$$\frac{2}{g^2} - \int_0^\infty \frac{\nu(\varepsilon')d\varepsilon'}{2(\varepsilon_m - \varepsilon')E(\varepsilon')} - \frac{\nu(\varepsilon_m)}{2E(\varepsilon_m)} \cot \pi \varsigma_m$$
$$= \frac{\delta\omega}{g^2} \frac{\varepsilon_m - \mu \pm i\Delta_0}{E^2(\varepsilon_m)}. \quad (B2)$$

Recalling that $\nu(\varepsilon) = \nu_F f(\varepsilon)$ and $g^2 \nu_F = \gamma$ in units of Fermi energy, we obtain

$$\pi \cot \pi \varsigma(\varepsilon) = \frac{4E(\varepsilon)}{\gamma f(\varepsilon)} - \frac{G(\varepsilon)}{f(\varepsilon)} - \frac{2\delta\omega}{\gamma} \frac{\varepsilon - \mu \pm i\Delta_0}{E(\varepsilon)f(\varepsilon)}, \quad (B3)$$

where

$$G(\varepsilon) = E(\varepsilon) \int_0^\infty \frac{f(\varepsilon')d\varepsilon'}{(\varepsilon - \varepsilon')E(\varepsilon')}. \quad (B4)$$

This principal value integral is the same as in Eq. (3.6). We evaluated it in elementary functions for various cases in Secs. III A and III B. Specifically, in 2D,

$$G_{\text{2d}}(\varepsilon) = \ln\left\{\frac{\varepsilon[\varepsilon - \mu + E(\varepsilon)]}{E(\varepsilon)\sqrt{\mu^2 + \Delta_0^2} + \mu^2 + \Delta_0^2 - \mu\varepsilon}\right\}; \quad (B5)$$

in the weak-coupling (BCS) limit, $\mu \approx \varepsilon_F \gg \Delta_0$, for energies not too far from the Fermi energy, in both 2D and 3D,

$$G_{\text{wc}}(\varepsilon) = \ln\left[\frac{E(\varepsilon) + \varepsilon - \mu}{E(\varepsilon) - \varepsilon + \mu}\right]; \quad (B6)$$

in the strong-coupling (BEC) limit in 2D and 3D,

$$G_{\text{sc}}^{\text{2d}}(\varepsilon) = \ln\frac{\varepsilon}{|\mu|}, \quad G_{\text{sc}}^{\text{3d}}(\varepsilon) = -\pi\sqrt{\frac{|\mu|}{\Delta_0}}. \quad (B7)$$

Ground-state continual roots $x_k = \varepsilon_k + \varrho_k \delta$ obtain by setting $\delta\omega = 0$ in Eq. (B3); i.e.,

$$\pi \cot \pi \varrho(\varepsilon) = \frac{4E(\varepsilon)}{\gamma f(\varepsilon)} - \frac{G(\varepsilon)}{f(\varepsilon)} \equiv \frac{H(\varepsilon)}{f(\varepsilon)}. \quad (B8)$$

The quantity $F_k \equiv F(\varepsilon_k)$ defined in Eq. (5.19) evaluates similarly to Eq. (B1),

$$F(\varepsilon) = -\frac{N(\varepsilon)}{2E(\varepsilon)\delta^2} \frac{\partial}{\partial\varrho} \sum_{p=0}^{\infty} \left[\frac{1}{p + 1 - \varrho} - \frac{1}{p + \varrho}\right]$$
$$= \frac{\nu(\varepsilon)}{2E(\varepsilon)\delta} \frac{\pi^2 f^2(\varepsilon) + H^2(\varepsilon)}{f^2(\varepsilon)}. \quad (B9)$$

APPENDIX C: IDENTITIES

In this Appendix we prove Eq. (5.29). To this end, consider a function

$$R(u) = L_0(u)\big[(u - \mu)^2 + \Delta_0^2\big], \tag{C1}$$

where $L_0(u)$ is given by Eq. (5.14). Since zeros of $L_0(u)$ are x_k and its poles are ε_k it alternatively can be written

$$R(u) = -\frac{2}{g^2} \frac{\prod_{k=1}^{N}(u - x_k)}{\prod_{k=1}^{N}(u - \varepsilon_k)}\big[(u - \mu)^2 + \Delta_0^2\big]. \tag{C2}$$

Equation (5.29) follows by matching two leading terms in $1/u$ expansions of function $1/R(u)$ obtained with the help of these two alternative forms.

Because $1/R(u)$ is a rational function with poles at $u = x_k$ and $\mu \pm i\Delta_0$, we have

$$\frac{1}{R(u)} = \sum_k \frac{1}{(u - x_k)L_0'(x_k)\Omega_k^2} + \frac{1}{2i\Delta_0(u - c_+)L_0(c_+)}$$
$$- \frac{1}{2i\Delta_0(u - c_-)L_0(c_-)}, \tag{C3}$$

where $c_\pm = \mu \pm i\Delta_0$ and we took into account that the square bracket in Eq. (C1) evaluated at $u = x_k$ is equal to Ω_k^2. Note also that $L_0'(x_k) = -F_k$; see Eq. (5.19). Equation (5.14) implies

$$L_0(c_\pm) = -\beta_k \mp i\alpha_k, \tag{C4}$$

where

$$\alpha_k = \sum_k \frac{N_k \Delta_0}{2[E(\varepsilon_k)]^{3/2}}, \quad \beta_k = \frac{2}{g^2} + \sum_k \frac{N_k(\varepsilon_k - \mu)}{2[E(\varepsilon_k)]^{3/2}}. \tag{C5}$$

The leading term in $1/u$ expansion of $1/R(u)$ according to Eq. (C2) is $-2/(g^2 u^2)$. Therefore, the coefficient at $1/u$ in Eq. (C3) vanishes and that at $1/u^2$ is $-2/g^2$. This yields

$$\sum_k \frac{\Delta_0}{F_k \Omega_k^2} = \frac{\alpha_k}{\alpha_k^2 + \beta_k^2},$$
$$\sum_k \frac{x_k - \mu}{F_k \Omega_k^2} = \frac{g^2}{2} - \frac{\beta_k}{\alpha_k^2 + \beta_k^2}. \tag{C6}$$

Gap and chemical potential equations (1.18) and (1.20) in the notation of Sec. V B read

$$\frac{\omega - 2\mu}{g^2} = \sum_k \frac{N_k}{2E(\varepsilon_k)},$$
$$2n = \frac{2\Delta_0^2}{g^2} + \sum_k N_k\bigg[1 - \frac{\varepsilon_k - \mu}{E(\varepsilon_k)}\bigg]. \tag{C7}$$

Differentiation of these equations with respect to ω obtains $\delta\mu/\delta\omega$ and $\delta\Delta_0/\delta\omega$ and comparison of the resulting quantities with the right-hand side of Eq. (C6) proves Eq. (5.29).

Another identity used in Sec. V B derives by noting that, according to Eq. (C2), $1/R(\varepsilon_k) = 0$. Setting $u = \varepsilon_k$ in Eq. (C3), we obtain after some algebra

$$\sum_j \frac{1}{(\varepsilon_k - x_m)F_m \Omega_m^2} = \frac{\alpha_k(\varepsilon_k - \mu) - \Delta_0\beta_k}{2\Delta_0(\alpha_k^2 + \beta_k^2)[E(\varepsilon_k)]^2}. \tag{C8}$$

[1] P. W. Anderson, Phys. Rev. **112**, 1900 (1958).

[2] V. P. Galaiko, Sov. Phys. JETP **34**, 203 (1972).

[3] A. F. Volkov and S. M. Kogan, Zh. Eksp. Teor. Fiz **65**, 2038 (1974) [English translation: Sov. Phys. JETP, **38**, 1018 (1974)].

[4] Y. M. Galperin, V. I. Kozub, and B. Z. Spivak, Sov. Phys. JETP **54**, 1126 (1981).

[5] P. B. Littlewood and C. M. Varma, Phys. Rev. B **26**, 4883 (1982).

[6] V. S. Shumeiko, Ph.D. thesis, Institute for Low Temperature Physics and Engineering, Kharkov, Ukraine, 1990.

[7] R. A. Barankov, L. S. Levitov, and B. Z. Spivak, Phys. Rev. Lett. **93**, 160401 (2004).

[8] M. Amin, E. Bezuglyi, A. Kijko, and A. Omelyanchouk, Low Temp. Phys. **30**, 661 (2004).

[9] A. V. Andreev, V. Gurarie, and L. Radzihovsky, Phys. Rev. Lett. **93**, 130402 (2004).

[10] R. A. Barankov and L. S. Levitov, Phys. Rev. Lett. **93**, 130403 (2004).

[11] M. H. Szymanska, B. D. Simons, and K. Burnett, Phys. Rev. Lett. **94**, 170402 (2005).

[12] G. L. Warner and A. J. Leggett, Phys. Rev. B **71**, 134514 (2005).

[13] E. A. Yuzbashyan, B. L. Altshuler, V. B. Kuznetsov, and V. Z. Enolskii, J. Phys. A **38**, 7831 (2005).

[14] E. A. Yuzbashyan, B. L. Altshuler, V. B. Kuznetsov, and V. Z. Enolskii, Phys. Rev. B **72**, 220503(R) (2005).

[15] E. A. Yuzbashyan, V. B. Kuznetsov, and B. L. Altshuler, Phys. Rev. B **72**, 144524 (2005).

[16] E. A. Yuzbashyan, O. Tsyplyatyev, and B. L. Altshuler, Phys. Rev. Lett. **96**, 097005 (2006); **96**, 179905(E) (2006).

[17] R. A. Barankov and L. S. Levitov, Phys. Rev. Lett. **96**, 230403 (2006).

[18] E. A. Yuzbashyan and M. Dzero, Phys. Rev. Lett. **96**, 230404 (2006).

[19] M. Dzero, E. A. Yuzbashyan, B. L. Altshuler, and P. Coleman, Phys. Rev. Lett. **99**, 160402 (2007).

[20] R. A. Barankov and L. S. Levitov, arXiv:0704.1292.

[21] A. Tomadin, M. Polini, M. P. Tosi, and R. Fazio, Phys. Rev. A **77**, 033605 (2008).

[22] A. Nahum and E. Bettelheim, Phys. Rev. B **78**, 184510 (2008).

[23] V. Gurarie, Phys. Rev. Lett. **103**, 075301 (2009).

[24] A. Faribault, P. Calabrese, and J.-S. Caux, J. Math. Phys. **50**, 095212 (2009).

[25] R. Matsunaga, Y. I. Hamada, K. Makise, Y. Uzawa, H. Terai, Z. Wang, and R. Shimano, Phys. Rev. Lett. **111**, 057002 (2013).

[26] R. Matsunaga, N. Tsuji, H. Fujita, A. Sugioka, K. Makise, Y. Uzawa, H. Terai, Z. Wang, H. Aoki, and R. Shimano, Science **345**, 1145 (2014).

[27] T. Papenkort, V. M. Axt, and T. Kuhn, Phys. Rev. B **76**, 224522 (2007).

[28] T. Papenkort, T. Kuhn, and V. M. Axt, J. Phys. **193**, 012050 (2009).

[29] H. Krull, D. Manske, G. S. Uhrig, and A. P. Schnyder, Phys. Rev. B **90**, 014515 (2014).

[30] N. Tsuji and H.Aoki, arXiv:1404.2711.

[31] R. Matsunaga and R. Shimano, Phys. Rev. Lett. **109**, 187002 (2012).

[32] M. Beck, I. Rousseau, M. Klammer, P. Leiderer, M. Mittendorff, S. Winnerl, M. Helm, G. N. Gol'tsman, and J. Demsar, Phys. Rev. Lett. **110**, 267003 (2013).

[33] R. T. Brierley, P. B. Littlewood, and P. R. Eastham, Phys. Rev. Lett. **107**, 040401 (2011).

[34] Y. Pehlivan, T. Balantekin, A. B., Kajino, and T. Yoshida, Phys. Rev. D **84**, 065008 (2011).

[35] G. Raffelt, S. Sarikas, and D. d. S. Seixas, Phys. Rev. Lett. **111**, 091101 (2013).

[36] M. S. Foster, M. Dzero, V. Gurarie, and E. A. Yuzbashyan, Phys. Rev. B **88**, 104511 (2013).

[37] M. S. Foster, V. Gurarie, M. Dzero, and E. A. Yuzbashyan, Phys. Rev. Lett. **113**, 076403 (2014).

[38] M. Gaudin, *La fonction d'onde de Bethe* (Masson, Paris, 1983).

[39] R. W. Richardson, arXiv:cond-mat/0203512.

[40] M. Ibanez, J. Links, G. Sierra, and S.-Y. Zhao, Phys. Rev. B **79**, 180501(R) (2009).

[41] C. Dunning, M. Ibanez, J. Links, G. Sierra, and S.-Y. Zhao, J. Stat. Mech. (2010) P08025.

[42] S. M. A. Rombouts, J. Dukelsky, and G. Ortiz, Phys. Rev. B **82**, 224510 (2010).

[43] J. Dukelsky, S. Pittel, and G. Sierra, Rev. Mod. Phys. **76**, 643 (2004).

[44] G. Ortiz, R. Somma, J. Dukelsky, and S. Rombouts, Nucl. Phys. B **707**, 421 (2005).

[45] J. Dukelsky, C. Esebbag, and P. Schuck, Phys. Rev. Lett. **87**, 066403 (2001).

[46] L. Amico, A. Di Lorenzo, and A. Osterloh, Phys. Rev. Lett. **86**, 5759 (2001).

[47] C. A. Regal, M. Greiner, and D. S. Jin, Phys. Rev. Lett. **92**, 040403 (2004).

[48] M. W. Zwierlein, C. A. Stan, C. H. Schunck, S. M. F. Raupach, A. J. Kerman, and W. Ketterle, Phys. Rev. Lett. **92**, 120403 (2004).

[49] P. Calabrese and J. Cardy, Phys. Rev. Lett. **96**, 136801 (2006).

[50] C. Kollath, A. M. Läuchli, and E. Altman, Phys. Rev. Lett. **98**, 180601 (2007).

[51] A. Leggett, in *Modern Trends in the Theory of Condensed Matter* (Springer-Verlag, Berlin, 1980), pp. 13–27.

[52] P. Nozières and S. Schmitt-Rink, J. Low Temp. Phys. **59**, 195 (1985).

[53] V. Gurarie and L. Radzihovsky, Ann. Phys. **322**, 2 (2007).

[54] E. Burovski, N. Prokof'ev, B. Svistunov, and M. Troyer, New J. Phys. **8**, 153 (2006).

[55] A. Bulgac and S. Yoon, Phys. Rev. Lett. **102**, 085302 (2009).

[56] J. Levinsen and V. Gurarie, Phys. Rev. A **73**, 053607 (2006).

[57] R. Richardson, J. Math. Phys. **18**, 1802 (1977).

[58] C. Sträter, O. Tsyplyatyev, and A. Faribault, Phys. Rev. B **86**, 195101 (2012).

[59] D. Pekker and C. M. Varma, Rev. Condens. Matter Phys. **6**, 269 (2015).

[60] P. W. Anderson, J. Phys. Chem. Solids **11**, 26 (1959).

[61] I. L. Kurland, I. L. Aleiner, and B. L. Altshuler, Phys. Rev. B **62**, 14886 (2000).

[62] The integrand in Eq. (1.37) generally has a nonvanishing zeroth Fourier mode; i.e., it contributes to both linear and periodic parts.

[63] V. I. Arnold, *Mathematical Methods of Classical Mechanics* (Springer-Verlag, New York, 1978).

[64] M. Tabor, *Chaos and Integrability in Nonlinear Dynamics* (Wiley, New York, 1989).

[65] J. S. H. Goldstein, C. Poole, *Classical Mechanics*, 3rd ed. (Addison Wesley, Boston, 2002), Chap. 10.

[66] B. C. Carlson and J. L. Gustafson, SIAM J. Math. Anal. **25**(2), 288 (1994).

[67] DLMF, NIST Digital Library of Mathematical Functions, Chap. 19, Release date 2014-04-25, http://dlmf.nist.gov/.

[68] C. Chin, M. Bartenstein, A. Altmeyer, S. Riedl, S. Jochim, J. H. Denschlag, and R. Grimm, Science **305**, 1128 (2004).

[69] M. W. Zwierlein, A. S. J. R. Abo-Shaeer, C. H. Schunck, and W. Ketterle, Nature (London) **435**, 1047 (2005).

[70] R. Schrieffer, *Theory of Superconductivity* (Perseus, New York, 1989).

[71] J. Bardeen, L. N. Cooper, and J. R. Schrieffer, Phys. Rev. **108**, 1175 (1957).

[72] See Ref. [36] for a detailed calculation of analogous Green's functions and expectation values.

[73] P. Törmä and P. Zoller, Phys. Rev. Lett. **85**, 487 (2000).

[74] C. A. Regal and D. S. Jin, Phys. Rev. Lett. **90**, 230404 (2003).

[75] S. Gupta, Z. Hadzibabic, M. W. Zwierlein, C. A. Stan, K. Dieckmann, C. H. Schunck, E. G. M. van Kempen, B. J. Verhaar, and W. Ketterle, Science **300**, 1723 (2003).

[76] J. Kinnunen, M. Rodriguez, and P. Törmä, Science **305**, 1131 (2004).

[77] C. H. Schunk, Y. Shin, A. Schirotzek, and W. Ketterle, Nature (London) **454**, 739 (2008).

[78] S. Basu and E. J. Mueller, Phys. Rev. Lett. **101**, 060405 (2008).

[79] A. Schirotzek, Y. I. Shin, C. H. Schunck, and W. Ketterle, Phys. Rev. Lett. **101**, 140403 (2008).

[80] We note that the contribution of stimulated emission processes is missing in Ref. [19]. This mistake is fixed in Ref. [36]. Moreover, we computed the RF response for the two-channel model taking this term into account and we find that the absorbed intensity is not significantly affected by this term for quenches to both BCS and BEC final detunings at least for the values of the relevant parameters considered.

[81] Y. Dong, L. Dong, M. Gong, and H. Pu, Nat. Commun. **6**, 6103 (2015).

[82] T. Duyckaerts, C. Keni, and F. Merle, Cambridge J. Math. **1**, 75 (2013).

[83] P. Phillips, *Advanced Solid State Physics* (Westview, Boulder, CO, 2003).